

**Surface Modification of Silica Aerogels by
Hexamethyldisilazane-Carbon dioxide Mixtures and
Their Phase Behaviour**

by

Ayşe Meriç Kartal

**A Thesis Submitted to the
Graduate School of Engineering
in Partial Fulfillment of the Requirements for
the Degree of**

**Master of Science
in
Chemical and Biological Engineering**

Koc University

September 2009

Koc University

Koc University
Graduate School of Sciences and Engineering

This is to certify that I have examined this copy of a master's thesis by

Ayşe Meriç Kartal

and have found that it is complete and satisfactory in all respects,
and that any and all revisions required by the final
examining committee have been made.

Committee Members:

Prof. Dr. Can Erkey

Asst. Prof. Dr. Alper Kiraz

Asst. Prof. Dr. Seda Kızılel

Date:

ABSTRACT

There are several advantages to using supercritical CO₂ (scCO₂) as solvent in chemical modification of the metal oxide surfaces. In particular, the low viscosity and low surface tension of the super critical fluids (SCFs) leads to enhanced deposition kinetics over conventional solution methods. The application areas include polymer modification, construction of low-energy hydrophobic surfaces, preparation of stationary phases for reversed-phase chromatography, making biocompatible surfaces, and forming monolayers for lithography, micropatterning, and sensors where alkylsilanes are generally used as the modifying agent.

In this study, we rendered the surface of monolithic silica aerogels hydrophobic by hexamethyldisilazane (HMDS)-carbon dioxide mixtures. The silica aerogels were prepared by two step (acid-base) sol-gel method using 50 wt. % tetraethylorthosilicate (TEOS) and ethanol as solvent. The effects of HMDS concentration in the fluid phase and the reaction time were investigated at a fixed temperature of 333.15 K and a fixed pressure of 20.68 MPa. The treatment led to hydrophobic silica aerogels which are as transparent as untreated aerogels. The extent of hydrophobicity was determined by contact angle test and contact angle was found to be 130° at different conditions. FTIR spectra confirmed the hydrophobicity by indicating a reduction in hydrophilic surface silanol groups and the emergence of hydrophobic CH₃ groups.

The second part of the work deals with the vapor-liquid equilibria study of the binary mixture of HMDS-CO₂. The bubble point pressures of the HMDS-CO₂ system were obtained at temperatures 298.2 K, 313.2 K, 327.7 K and 342 K and at various concentrations. At a fixed temperature, the bubble point pressure decreased as the concentration of HMDS increased. At a fixed composition, bubble point pressure increased as the temperature increased. The bubble point pressures were modeled using the Peng-Robinson Stryjek-Vera equation of state (PRSV EOS) and compared well with the experimental data.

ÖZET

Metal oksit yüzeylerinin kimyasal modifikasyonunda süper kritik karbondioksitin (sk CO₂) çözücü olarak kullanılmasının pek çok avantajı bulunmaktadır. Özellikle, süper kritik akışkanların düşük viskozitesi ve düşük yüzey gerilimi geleneksel çözelti metotlarına göre depozisyon kinetiklerinin gelişmesini sağlar. Uygulanan alanları polimer modifikasyonu, düşük-enerjili hidrofobik yüzeylerin oluşturulması, ters-faz kromatografilerde kullanılmak üzere sabit fazların hazırlanışı, biyo-uyumlu yüzeylerin yapımı ve litografi, mikropatterning, sensörlerde monotabakaların oluşturulması gibi alkil-silanların modifikasyon ajanı olarak kullanıldığı alanlardır.

Bu çalışmada, monolitik silika aerogellerin yüzeylerini hexametildisilazan (HMDS)-karbon dioksit karışımları kullanarak hidrofobik olarak değiştirdik. Silika aerogeller iki aşamalı (asit-baz) sol-jel metodu kullanılarak, % 50 ağırlıklı tetraetilortosilikat ve çözücü etanolla hazırlanmıştır. Akışkan fazdaki HMDS yoğunluğunun etkileri ve reaksiyon süresi, 60 °C sabit sıcaklık ve 20.68 MPa sabit basınçta incelenmiştir. Uygulama sonucunda oluşan hidrofobik silika aerogeller, uygulamaya tabi tutulmamış aerogellerle aynı saydırlıktadır. Hidrofobiklik derecesi temas açısı testiyle belirlenmiş olup bu açı farklı şartlarda 130 ° olarak bulunmuştur. FTIR spektra hidrofobik yüzey silanol gruplarının azaldığını ve hidrofobik metil gruplarının oluştuğunu belirterek hidrofobikliği teyit etmiştir.

Bu tezin ikinci bölümü HMDS-CO₂'nin ikili karışımının buhar-sıvı denkleğiyle ilgilidir. HMDS-CO₂ sisteminin bubble point basınç değerleri 298,2 K, 313,2 K, 327,7 K ve 342 K'de ve çeşitli yoğunluklarda elde edilmiştir. Sabit sıcaklıkta, bubble point basınçları HMDS yoğunluğu arttıkça azalmıştır. Sabit yoğunlukta, bubble point basınçları sıcaklık arttıkça artmıştır. Bubble point basınçları Peng-Robinson Stryjek-Vera durum denklemi kullanılarak modellenmiş olup deneysel sonuçlarla uyum göstermiştir.

ACKNOWLEDGEMENTS

Firstly, I would like to thank my advisor, Professor Can Erkey for his kindness and support throughout my academic life in Koc University. He was not only my thesis advisor but my guide who had influenced the last three years of my life. He gave me the chance to experience an academic environment, take responsibility, participate in international symposiums and workshops, and write a journal article which will be published soon. Thanks to him, we had a lovely time eating at beautiful places in France and İstanbul with colleagues. It was a pleasure to work in his laboratory and learn from him.

I would also like to thank Professor Seda Kızılel and Professor Alper Kiraz for their support in my thesis work.

Then, I would like to thank my colleagues Seda Giray, Selmi Bozbağ, Erdal Uzunlar, and Nil Dinçer for their help in the laboratory. I would also thank Dr. Ayşe Bayrakçeken for her support and kind heart. I especially want to thank a former colleague Pınar Çetin who had helped me in great deal for gaining ground in my thesis subject. She was not only a colleague but a good friend. I specially thank my beloved and charming colleague Seda Yaşar who was beside me all the time during these two years. We shared the happiness and hard times together.

I also want to give my thanks to Müge Karaman and Gözde Kaynak for being the best home mates and Deniz Şanlı for being a good friend. I want to thank all of the friends whom I have met here. They made life enjoyable.

Special thanks to my family. I love them very much.

Finally, I want to thank TÜBİTAK for its financial support.

TABLE OF CONTENTS

List of Tables	ix
List of Figures	xi
Chapter 1: Introduction	1
Chapter 2: Literature Review	4
2.1 Overview.....	4
2.2 Properties and applications of silica aerogels.....	5
2.2.1 Mechanical characteristics.....	9
2.2.2 Thermal conductivity.....	10
2.2.3 Optical properties.....	10
2.3 Surface chemical modification.....	13
2.3.1 Modification of Silica Surfaces.....	13
2.3.2 Silation Agents.....	15
2.3.3 Modification methods for silica surfaces.....	17
2.3.3.1 Co-precursor method for modification of silica aerogels.....	17
2.3.3.2 Derivatization Method.....	18
2.4 Surface modification in scCO ₂ phase.....	23
2.4.1 Supercritical CO ₂	23
2.4.2 Advantages of SCF in surface modification as solvents.....	25
2.4.3 Literature examples of surface modification by deposition of metals and polymers in porous media.....	26
2.4.4 Literature examples of surface modification by silation in scCO ₂ phase.....	26

2.5	Characterization of Hydrophobic Silica Aerogels.....	28
2.5.1	Contact Angle Test.....	28
2.5.2	Fourier transform infrared spectra (FTIR) Analysis.....	30
2.5.3	Measurement of silane groups on the modified surface.....	32
2.6	Thermodynamic description of processes: Phase Equilibria.....	33
2.6.1	Gibbs phase rule and phase diagrams.....	34
2.6.2	Phase equilibria calculations.....	40
2.6.3	Thermodynamic principles of vapor-liquid phase equilibria.....	41
2.6.4	Equations of State.....	42
2.6.5	Experimental methods to determine V-L bubble-point pressure.....	44
Chapter 3:	Experimental	47
3.1	Synthesis.....	47
3.2	Modification of Hydrophilic Silica Aerogels.....	48
3.2.1	Apparatus and Procedure for Modification of Silica Aerogels.....	48
3.2.2	HMDS-CO ₂ Solutions in Modification Processes.....	50
3.3	Characterization of Treated Silica Aerogels.....	51
3.3.1	Contact Angle Determination.....	51
3.3.2	FTIR Analysis.....	51
3.4	Bubble point pressure measurements.....	51
3.4.1	Apparatus and Procedure for Bubble Point Pressure Measurements.....	51
3.4.2	HMDS-CO ₂ Solutions in Bubble Point Pressure Measurements.....	53
Chapter 4:	Results	55
4.1	Mold study results.....	55
4.1	Modification results.....	56
4.2	Vapor-liquid phase equilibria results.....	64
4.3.1	Phase diagram of CO ₂ -HMDS binary mixture.....	64
4.3.2	Testing the accuracy of the data obtained by the set-up.....	66

4.3.3 Modeling.....	67
Chapter 5: Conclusion	74
Bibliography	76
Appendix	81

LIST OF TABLES

Table 2.1	Summary of morphologic and macroscopic properties of silica aerogels	7
Table 2.2	Applications of Silica Aerogels	8
Table 2.3	Typical Thermal Conductivities of Various Materials	10
Table 2.4	Methyl silating agents	15
Table 2.5	Organofunctional silation agents	17
Table 2.6	Comparison of the physical properties of gases, liquids and SCFs	24
Table 2.7	Critical coordinates of usual pure fluid	25
Table 2.8	Phase equilibria in binary systems and their representations in P,T,x-space	37
Table 2.9	Parameters for cubic equation of state	43
Table 2.10	Parameters in equation 2.33 for three equations of state	43
Table 3.1	Compounds in the synthesis of silica aerogels	47
Table 4.1	Pure component properties used in PRSVEOS	64

Table 4.2	Experimental Data for Ethanol- Carbon dioxide Binary Mixture at 333 K	67
Table 4.3	κ_1 parameter regressed for the pure components in the PRSVEOS	70

LIST OF FIGURES

Figure 2.1	Number of publications per year containing the word “silica aerogels” in their title, abstract or the keywords until 2008	4
Figure 2.2	a) Representation of hemispherical (direct+diffuse) transmittance through aerogel samples, b) Optical transmittance spectra of silica aerogels in the UV-NIR region.	11
Figure 2.3	Silation of silica surface	13
Figure 2.4	Reaction mechanism of grafting alkoxysilanes on silica a) hydrolysis reaction of alkoxysilanes as a result of the reaction of adsorbed surface water with alkoxysilane b) condensation reaction of hydrolyzed species to form oligomers c) surface modification reaction of silica- reaction of hydrolyzed species with surface silanols	14
Figure 2.5	Modified aerogels prepared by co-precursor method	18
Figure 2.6	Surface modification reaction of silica aerogel with HMDS	21
Figure 2.7	a) modified silica aerogel by co-precursor method, b) derivatization method	22

Figure 2.8	States of the CO ₂ solvent; dotted lines refer to critical pressure and critical temperature, not the phase boundaries	23
Figure 2.9	Liquid behavior on solid	29
Figure 2.10	Calculation of the contact angle θ from the dimensions of the spherical water droplet, r is the radius, w is the base length and h is the height of the drop on the aerogel surface.	30
Figure 2.11	FTIR Analysis for unmodified (H1) and modified silica aerogels (increasing extent of hydrophobicity from H2 to H4)	32
Figure 2.12	Three cases where the compositions of the two phases of a two-phase equilibrium are equal: a) Pure component boiling points, b) azeotropic point c)critical point.	38
Figure 2.13	Figure 2.13 The six basic types of fluid phase behavior according to the classification of van Koynenburg and Scott	39
Figure 2.14	Variable volume static view cell	45
Figure 2.15	Recirculation method	46
Figure 3.1	The schematic representation of the procedure during silica aerogel synthesis by sol-gel method.	48

Figure 3.2	Apparatus for surface modification of hydrophilic silica aerogels	50
Figure 3.3	Apparatus for bubble point pressure measurements	53
Figure 3.4	Changes in phases as seen from the view cell. a) initially, b) at single phase (above bubble point) , c) at bubble point	53
Figure 4.1	Top view images of a) an un-modified silica aerogel, b) a water droplet on un-modified silica aerogel, c) a water droplet on a modified silica aerogel	56
Figure 4.2	The image of a drop of water on the modified silica aerogel surface	56
Figure 4.3	The image of a water droplet on the inside surface of the aerogels a) top view, b) side view	57
Figure 4.4	FTIR spectra of a) untreated silica aerogel, b) treated silica aerogel	58
Figure 4.5	Diffusion through the open pore structure of the silica aerogels	60
Figure 4.6	Surface modification of silica aerogel pores with HMDS loaded scCO ₂ .	61
Figure 4.7	Boundary conditions	63

Figure 4.8	a)HMDS-CO ₂ binary mixture presents a type II phase behavior, and P-x sections for type II b) $T < T_{UCEP}$, c) $T = T_{UCEP}$, d) $T_{UCEP} < T < T_C$	65
Figure 4.9	Comparison of bubble points for ethanol-carbon dioxide binary mixtures in the literature and obtained in this study	66
Figure 4.10	Algorithm for calculating bubble point pressure	69
Figure 4.11	Bubble point pressure data for various temperatures and mole fraction of CO ₂	71
Figure 4.12	The bubble point pressure results at 298.75K for various mole fractions of CO ₂	73
Figure 4.13	Molecular structures of a) CO ₂ and b) HMDS	73

Chapter 1

INTRODUCTION

The silica aerogels based on tetraethylorthosilicate (TEOS) are hydrophilic and absorb moisture which results in deterioration of the aerogels with time. The hydrophilicity is attributed to the presence of the hydroxyl groups (OH) within the silanol (Si-OH) groups of the aerogel because they promote the adsorption of water. By replacing the hydrogen (H) in the surface silanol groups by a hydrolytically stable organofunctional group (e.g. Si-CH₃), hydrophobic aerogels can be obtained. This can be accomplished by reacting the silanol groups with silylation agents (SAs) containing hydrophobic functional groups.

Surface chemical modification of silica surfaces by using SAs has been accomplished using two different methods which are classified as the co-precursor method [1, 2] and the derivatization method [1, 2, 3, 4, 5, 6, 7, 8]. In the co-precursor method, SAs are incorporated to the silica matrix during the standard procedure for the sol-gel synthesis of silica aerogels. This can be accomplished by mixing the SA and a hydrophilic precursor at a certain mole ratio in the sol. Hexamethyldisilazane (HMDS) or various other organosilanes such as monoalkyl, dialkyl, trialkyl, aryl, alkoxy and chloro silanes can be used as SAs in the co-precursor method. HMDS is a difunctional trialkyl (trimethyl) silyl silane which is known to be highly reactive with surface silanols due to the presence of highly reactive nitrogen atom within the compound [3]. High silylation power of HMDS has been demonstrated by various studies in literature [1, 2, 3, 4, 5]. Among various organosilanes, Rao et al. found that HMDS gave the highest contact angle (135°) for aerogels synthesized using TEOS and or tetramethylortho silicate (TMOS) [1]. However, the optical transmittance was as low as 5%. In another study, the mole ratio of HMDS to TEOS was varied from 0.1 to 0.6 which resulted in a decrease in optical transmittance from 65% to 5% and an increase in contact angle from 110° to 136° [2]. These studies indicate that the transmittance has to be sacrificed to

increase hydrophobicity for the co-precursor method. Furthermore, an increase in HMDS amount causes cracks in the monoliths.

Modification of silica aerogels by the derivatization method can be achieved through reactive deposition of SAs on the surface of the wet form of silica aerogel (alcogel surface) from liquid solvents prior to the extraction of the pore liquid from the gels [1, 2, 4]. The alcogels were immersed in a mixture of a solvent (ethanol, methanol [1, 2] and hexane [4]) and SA for more than 12 hours at a temperature above 45 °C before drying. According to one study, usage of HMDS as a derivatization agent yielded silica aerogels with improved transmittance up to 70% and 88% for TMOS based and TEOS based aerogels, respectively [1]. Similarly monolithic aerogels with a transparency of 85% and a contact angle of 109° [2], and aerogels with a transparency of 75% and a contact angle of 143° could be obtained [4]. The major drawbacks of this method are the possible effect of the side product ammonia and the difficulties associated with the removal of unreacted HMDS, ammonia and solvent by several heat treatments above 50 °C.

Conventional solution methods are not applicable for surface modification of dry silica aerogels because of the large capillary forces exerted on the pores of silica aerogels when contacted with a liquid solvent which leads to pore collapse and crumbling. Supercritical carbon dioxide (scCO₂) has been attracting increased attention in modification of a wide variety of inorganic surfaces including silica [6, 7, 8]. The low viscosity, and surface tension of scCO₂ coupled with adjustable properties with changes in temperature and pressure make scCO₂ an attractive medium for carrying out surface modification. Furthermore, scCO₂ is inert and leaves no residue on the treated surface.

Zemanian et al. reported that scCO₂ at 150°C and 7500 psi provided faster deposition (5 minutes vs. 10 hours of manipulation time and several days for drying), higher surface population of silanes (6.55 silanes/nm² vs. 4.97 silanes/nm²) and a better quality monolayer (complete coverage vs. defect density) on mesoporous silica over toluene at 110°C in the reaction of silica with mercaptopropyltrimethoxysilane [6]. This enhancement in scCO₂ was partially attributed to the temperature difference (150°C for scCO₂ and 110°C for toluene). In another study, the reaction of silica with HMDS in scCO₂ (at 50 °C and at 200 bar) yielded a side product, ammonia which then reacted

with CO₂ to form ammonium carbamate [7]. Ammonium carbamate blocked a portion of the surface silanol groups from participating in the reaction with HMDS. Ammonium carbamate could be removed easily by purging. It was also found that production of ammonium carbamate could be completely prevented by setting the CO₂ pressure lower than 90 bar since at such low pressures, ammonium carbamate formation was not favored. In another study, Chuntao et al. used (dimethylamino)octadimethylsilane as the derivatization agent in scCO₂ at 70°C and 7200 psi for the modification of porous silica [8]. The same temperature and derivatization agent concentration was used for the modification in toluene. They reported no differences in bonding densities at the same silation agent concentration and reaction temperature. It was concluded that scCO₂ was a viable reaction medium for this process. The promising results obtained in the studies mentioned above suggest that it may be possible to modify the surface of silica aerogels by contacting them with silation agents dissolved in scCO₂.

In this work, the modification of silica aerogel surfaces by the derivatization method using scCO₂ as the solvent and HMDS as the derivatization agent was studied for the first time. The hydrophobicity was characterized by contact angle tests and FTIR investigations. Furthermore, in order to develop these types of technologies for the surface modification of various matrices, there is need for thermodynamic data for mixtures of SAs with CO₂. Therefore, the phase behavior of HMDS and CO₂ was studied through determination of bubble point pressures for different mole fractions of HMDS and at different temperatures. The experimental data was correlated using PRSV equation of state model.

Chapter 2

LITERATURE REVIEW

2.1 Overview

Silica aerogel refers to sol-gel derived, low density silica with pores typically between 2 and 50nm in width. The increased attention of global markets to “nano” is a driving force to move silica aerogels into the focus of research interest recently. As can be seen in Figure 2.1, the number of publications per year on silica aerogels have been increasing since 2003.

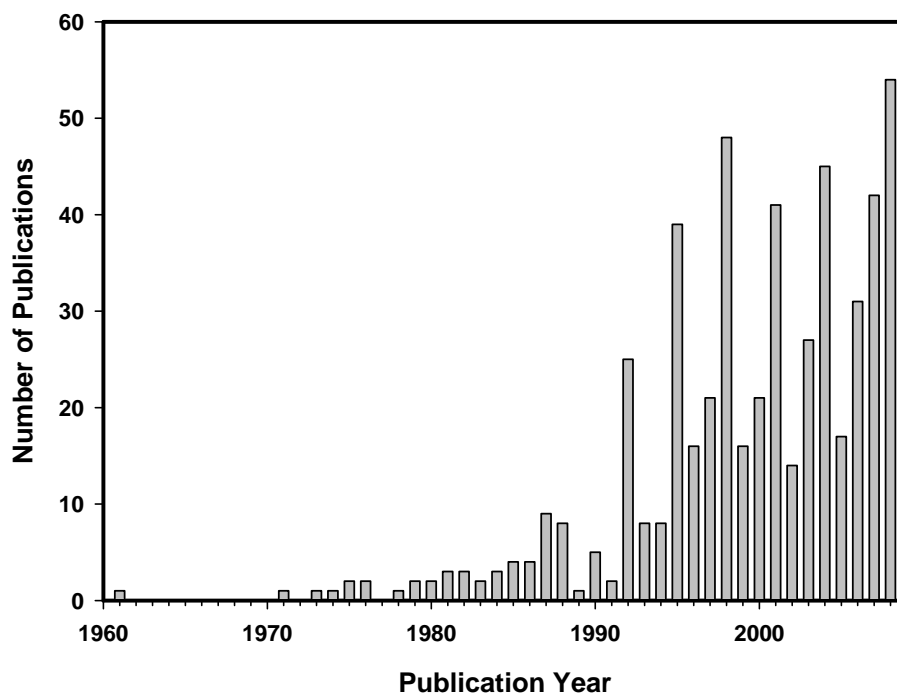


Figure 2.1 Number of publications per year containing the word “silica aerogels” in their title, abstract or the keywords until 2008 [9].

The properties of the silica aerogels, their dependence on the sol-gel parameters and the corresponding applications are explained in section 2.2. One of the most significant

applications of the silica aerogels is their usage as transparent thermal insulation materials. The necessary properties for such an application, mechanical strength, low thermal conductivity, and transparency are explained in the same section. Silica aerogels need to be resistant to moisture for such an application. Thus, hydrophobicity of the silica aerogels is also desirable. In order to achieve this, surface modification of silica aerogels is carried out by incorporating typically a silation agent in the sol prior to gelation or after the gel formation either to the wet or the dry forms of the gel. The modification of the silica or silica aerogels will be explained in section 2.3. Furthermore, some of the characterization methods for determining the extent of the hydrophobicity of the silica aerogels and the theory behind them will be explained in the same section. These sections comprise the first part of the literature review. In the second part, in section 2.4, the studies on the vapor-liquid equilibria of binary mixtures along with theoretical background will be explained. The determination of the phase behavior of the modification media and the modification agent is of great importance for designing efficient large scale surface modification processes of metal oxide surfaces such as silica.

2.2 Properties and applications of silica aerogels

Silica aerogels are interesting since they have appealing properties which are listed in Table 2.1. The unique properties of the silica aerogels are a result of the distribution and the layout of the two phases which are the solid backbone and the pore network. The pore phase properties such as the overall porosity, contribution of the micro-, meso- and macroporosity, pore size distribution, average pore size, the pore shape, pore connectivity and physical/chemical properties of the solid-pore interface effects the properties of the silica aerogels. The solid phase also has an impact on the silica aerogel properties through its composition, its connectivity and the size of the backbone segments such as length and diameter. The backbone characteristics are reflected in macroscopic quantities such as mechanical behavior, electrical or thermal transport along the solid phase.

The silica aerogel properties are under extensive investigation due to the possibility of adjusting the sol-gel parameters in the sol-gel route for the synthesis of silica

aerogels. In sol-gel synthesis, highly diluted reactants of a gel-precursor and solvents are mixed before a reaction is started. Therefore their miscibility is important in order to prevent inhomogeneous or partially precipitated gel formation. After the reactants are fully dissolved, the solution undergoes two major reactions on molecular level: (1) hydrolysis for creating or activating reactive sites) and (2) polycondensation (the condensation of monomers, oligomers, and clusters through cross-linking of the reactive sites). The kinetics of these reactions can be controlled by various parameters such as concentration of the reactants, the solvent, the catalyst used (acid catalyst or base catalyst-one step process or acid catalyst and base catalyst together-two step process), the catalyst concentration (pH value), the temperature, etc. The parameters which affect the kinetics along with the solubility effects determine the properties of the resulting gel applicable to various fields of science and industry. The properties along with corresponding applications are summarized in Table 2.2.

One of the most significant applications of silica aerogels is their usage as thermal insulation materials. The desirable properties of the silica aerogels for this application are mechanical strength (sufficient for preserving the monolithicity), transparency and low thermal conductivity and these will be explained in sections 2.2.1, 2.2.2 and 2.2.3 respectively.

Table 2.1 Summary of morphologic and macroscopic properties of silica aerogels

Property	Value	Comments
Density	0.003-0.35 g/cc	Most common density ~0.1 g/cc [10]
Porosity	85-99.87 %	Open pore structure
Specific Surface Area	600-1000 m ² /g	Related to meso- or macropores range
Average pore size	~20 nm	Mostly in mesopore range
Primary particle diameter	~2-5 nm	
Transmittance	$TR = 97.9 \%$	For an aerogel sample of thickness equal to 4 mm. [11]
Refractive index	1.0-1.08	In the visible range [10]
Dielectric constant	1.1	For a density of 0.1 g/cc
Thermal conductivity	0.015 W/m K in air 0.010 W / m K in vacuum	For a density of 0.15 g/cc [12]. This value compares with 0.35 W /m K (in air) for polyurethanes, mineral wool and expanded polystyrene.
Sound velocity	100 m/s	For a density of 0.07 g/cc [10]
Temperature stability	Up to 600 °C [13]	

Table 2.2 Property applications relationships for silica aerogels

Property	Features	Applications
Thermal conductivity	Best insulating solids Transparent High temperature lightweight	Architectural and appliance insulation, portable coolers, transport vehicles, pipes, cryogenic, skylights
Density/porosity	Lighest synthetic solid Homogeneous High specific surface area Multiple compositions	Catalysts, sorbers, sensors, fuel storage, ion exchange Targets for internal confinement fusion (ICF), x-ray lasers
optical	Low refractive index Transparent Multiple compositions	Cherenkov detectors, lightweight optics, lightguides, special effect optics
acoustic	Lowest sound speed	Impedence matchers for transducers, range finders, speakers
mechanical	Elastic lightweight	Energy absorber, hypervelocity particle trap
electrical	Lowest dielectric constant High dielectric strength High surface area	Dielectrics for ICs, spacers for vacuum electrodes, vacuum display spacers, capacitors

2.2.1 Mechanical Characteristics:

The ability to obtain porous materials not only as powders but also to mold them into any desired shape can increase their range of applications significantly. In addition, the advantages of each pore size regime, e.g. high flux for macropores and high selectivity for micropores, can be utilized independently and large surface area is provided by the combination of several pore sizes within one material. The possible applications can be seen in Table 2.2. Especially monolithic silica aerogels can be utilized as thermal insulation materials. Therefore, mechanical strength of the gels is of great importance.

The structural features of a highly porous oxide material prepared by sol-gel method depend to a great deal on the drying conditions. The wet network with a random distribution of pores are very sensitive to large capillary pressures exerted on the structure during drying, very often resulting in collapse of the gel body. One typical procedure to prevent collapse is drying with supercritical fluids (scf), e.g. carbon dioxide, since the building-up of a gas/liquid interface is avoided, and hence no capillary pressures evolve.

The monolithic aerogels can be obtained by supercritical extraction, but they are brittle and elastic materials like glasses or ceramics with a poor mechanical strength owing to their large pore volume [14]. In order to reduce the fragility of the silica aerogels, various methods have been proposed. One method is to perform aging to strengthen the gel backbone. Aging can be performed just after gelation when the weak branches of the gels are very flexible and can be brought in contact with each other by heat. The independent oligomers not yet linked to the gel backbone may aggregate as side branches and reinforce the network. Einarsud et al. achieved to increase the density of the silica gels in the wet form by immersing them in aging solutions (a certain volume % of mother precursor, solvent or water) at 70°C, for a certain period of time. The density increased from 0.168 g/cc to 0.4 g/cc and the corresponding increase in mechanical strength was from 5 MPa to 40 MPa [15].

2.2.2 Thermal Conductivity

Thermal conductivity is an intensive property of a material that measures its capacity to sustain heat flow. Aerogel materials are open cell, nanoporous materials that have a very high proportion of free void volume (see Table 2.1) compared to conventional solid materials. A comparison of thermal conductivities of silica aerogel products with other insulation materials are shown in Table 2.3. Their high pore volume, low solid content and their solid connectivity give rise to low values of thermal conductivity [16].

Table 2.3 Typical Thermal Conductivities of Various Materials [16]

Materials	Thermal Conductivity (W/(m K))
Air	0.025
CCl ₂ F ₂	0.012
CCl ₃ F	0.007
Dense polyurethane	0.15
polyurethane foam	0.04
polyurethane foam with CFC	0.021
dense silica glass	1.00
silica powder	0.025
silica powder (evacuated)	0.004
silica aerogel	0.008
silica aerogel (evacuated)	0.002

2.2.3 Optical Properties

Optical clarity of the aerogels are governed by light scattering resulting from inhomogeneities between air and solid matrix of the aerogel on a small length scale in the nanometer range. Transparency in silica aerogels are attainable since a silica aerogel microstructure has a scale small with respect to the wavelength of light, λ [10]. This

behavior can be described by Rayleigh scattering theory. Rayleigh scattering is the scattering effect observed by small dust particles in the atmosphere. The actual entity that causes scattering, called the scattering center, can be as small as a single large molecule (with an inherent inhomogeneity) or clusters of small molecules arranged in a non-uniform way. However, scattering becomes more effective when the size of the scattering center is similar to the wavelength of the incident light. This occurs in small particles (~400-700nm in diameter for visible light), or by larger, macroscopic, particles that have inherent irregularities. When scattering centers are smaller in size than the wavelength of the incident light, scattering is much less effective. In silica aerogels, the primary particles have a diameter of ~2-5 nm, and do not contribute significantly to the observed scattering. However, scattering does not necessarily arise from solid structures. In silica aerogels, a network of pores can act themselves as scattering centers [17]. Thus the small pore sizes in silica aerogels are also important for achieving transparency.

The transparency can be expressed by transparency ratio TR [18, 19]

$$TR = \frac{\tau_v^{nd}}{\tau_v^{nh}} \quad (2.1)$$

where τ_v^{nd} and τ_v^{nh} are normal/diffuse and normal/hemispherical transmittances respectively as shown in Figure 2.2.

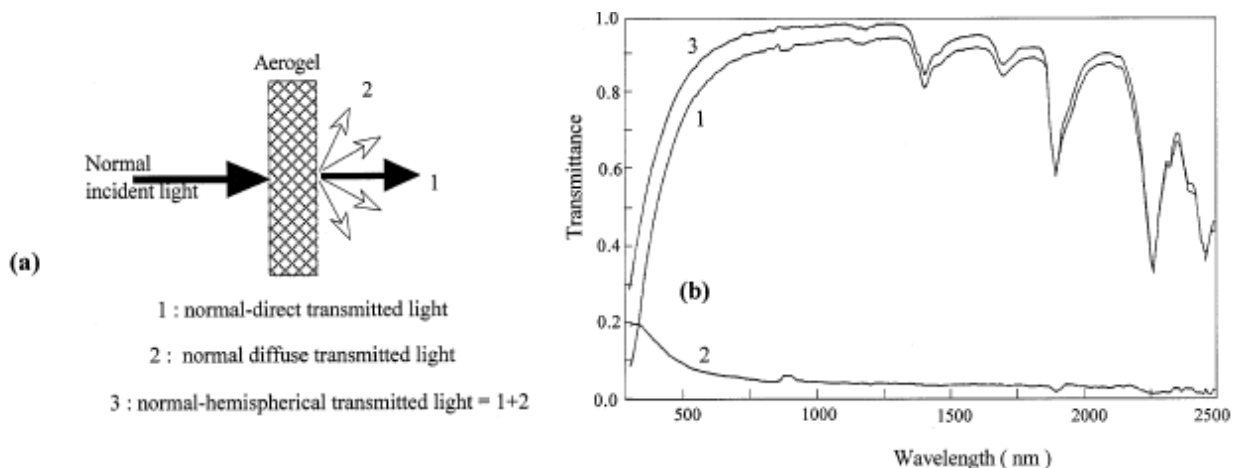


Figure 2.2 [12] a) Representation of hemispherical (direct+diffuse) transmittance through aerogel samples, b) Optical transmittance spectra of silica aerogels in the UV-NIR region.

The higher the value of TR , the better the transparency and clarity of the image seen through the material are. This ratio does not take into account the influence of light absorption. TR values represent the influence of diffuse light on the transparency. A sample must exhibit both a high τ_v^{nh} and high TR in order to obtain good imaging systems.

The transmission in aerogels can be calculated using (2.2) [20]

$$T = A \exp(B \cdot t / \lambda^4) \quad (2.2)$$

where A is the wavelength independent coefficient arising from scattering from the surface due to damage, large channels created from solvent flows, cracks, and damage with a characteristic size large compared to the wavelength of light. B describes the coefficient of the wavelength dependence (μ^4/cm) and t is the thickness of the sample (cm). This formula may be used to compare clarity of aerogels of various thickness, origin, and surface condition and to separate intrinsic and extrinsic qualities of the aerogel. It is also useful in separating effects of solvents, or impurities that effect the transmission in the short wavelength visible region.

Only a few general rules have been proposed to control transparency. One of them is the use of two-step sol-gel chemistry combined with scCO_2 drying. Scattering is theoretically entirely controllable at the chemical stage during the sol-gel reactions (hydrolysis and condensation) which affect the sizes of macroscopic particles, their inherent irregularities and surface roughness. Cao and Hunt report that two-step gels are more transparent than the one-step gels over the entire visible spectrum [21]. More important is that the former has a much higher transmittance in the short wavelength region where Rayleigh scattering dominates and is responsible for the blue haze of an aerogel. This is attributed to the morphological differences of the gels obtained by two different routes. As an example of one step gels, base catalyzed gels show a particle-like morphology consisting of fine silica particles that are loosely connected and a pore size distribution with a peak at 10-20 nm in pore diameter, some extending 100 nm. Two-step gels show a distinctive polymer-like morphology composed of linear chains 3-5 nm in size that are highly branched and linked to a silica network with average pore sizes which are smaller than one-step process, distributed over a narrow band between 4 and 20 nm and no pores larger than 50 nm. Considering the pore size distribution and the size of the solid network, the two-step process based gels demonstrate a better

homogeneity which results in less scattering, thus more transparency. In addition sc drying is important to preserve this structure.

Furthermore, the relationship between the adsorption of water as well as organic compounds on the surface silanol groups of the silica aerogel and the transparency of the silica aerogels has been investigated [22]. It is reported that as the aerogel is heated, their transparency is improved due to desorption of water and desorption of the organic groups.

2.3 Surface Chemical Modification

2.3.1 Modification of Silica Surfaces

Chemical modification of inorganic surfaces by covalent attachment of organosilanes has been utilized to improve adhesion of organic coatings to inorganic substrates, to protect metal surfaces from corrosive environments, to make water repellent surfaces, to enhance biocompatibility of solid surfaces, to tailor the chromatographic characteristics of solid supports, and to form monolayers for lithography.

Modification of silica surfaces can also be achieved by silation of silica with hydrophobic silation agents which results in silica surfaces with water repellent properties. This can be achieved by replacing the active hydrogen atom in the surface silanol by the hydrophobic (silyl) groups as shown in schematic in Figure 2.3.

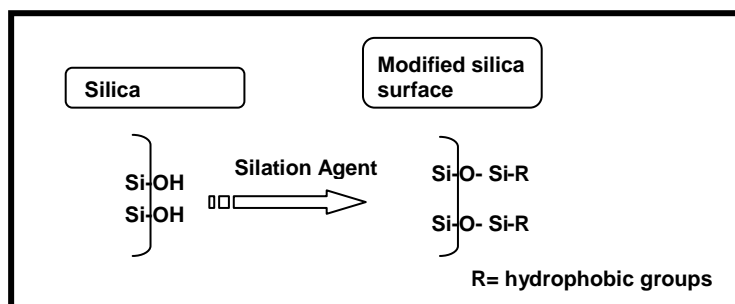


Figure 2.3 Silation of silica surface

Bringing the silating agent in contact with the silica surface can be carried out in vapor, liquid or supercritical fluid media depending on the phase of the solvent which contains the silating agent. The literature examples will be explained in section 2.3.3. After the silating agent is introduced to the silica surface, silation reaction mechanism of silica with a silation agent comprises two steps [23]. The first reaction is the hydrolysis of the silane through the presence of water on the silica surface (previously adsorbed surface water). The subsequent reactions are competitive and these are condensation of hydrolyzed species in solution leading to the formation of oligomers and the reaction of hydrolyzed species with the silanol groups of the silica surface leading to the grafting of the silane molecules (see Figure 2.4). It is the latter that causes the modification of the silica surfaces.

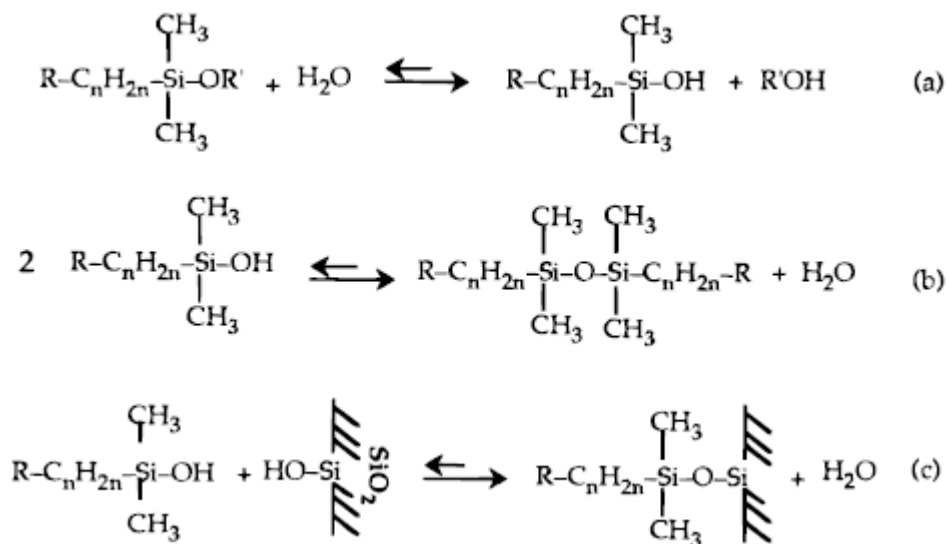




Figure 2.4 [23] Reaction mechanism of grafting alkoxy silanes on silica a) hydrolysis reaction of alkoxy silanes as a result of the reaction of adsorbed surface water with alkoxy silane b) condensation reaction of hydrolyzed species to form oligomers c) surface modification reaction of silica- reaction of hydrolyzed species with surface silanols

In the subsequent sections 2.3.2 and 2.3.3, the most commonly used silation agents and the methods for silating silica surfaces will be explained respectively. Furthermore, characterization methods for determining hydrophobicity will be explained in section 2.5.

2.3.2 Silation Agents

A silating agent is typically a trimethylsilyl halide, dimethylsilyl dihalide, or a trimethylsilyl nitrogen-functional compound. A mixture of silating agents (e.g. TMCS and HMDS) may also be used [24]. The mixture can be more reactive than the silating agents alone. The typical commercial silating agents are listed in Table 2.4.

Table 2.4 Methyl silating agents

Chemical name	Common abbreviation	Formula
trimethylchlorosilane	TMCS	$(\text{CH}_3)_3\text{SiCl}$
dimethyldichlorosilane	DMCS	$(\text{CH}_3)_2\text{SiCl}_2$
hexamethyldisilazane	HMDS	$(\text{CH}_3)_3\text{SiNHSi}(\text{CH}_3)_3$
chloromethyldimethylchlorosilane	CMDMS	$\text{ClCH}_2(\text{CH}_3)_2\text{SiCl}$
N,N'-bis(trimethylsilyl)-urea	BSU	$[(\text{CH}_3)_3\text{SiNH}]_2\text{CO}$
N-trimethylsilyldiethylamine	TMSDEA	$(\text{CH}_3)_3\text{SiNH}(\text{C}_2\text{H}_5)_2$
N-trimethylsilylimidazole	TSIM	
N,O-bis(trimethylsilyl)acetamide	BSA	$(\text{CH}_3)_3\text{SiN}-\text{C}(\text{CH}_3)\text{OSi}(\text{CH}_3)_3$
N,O-bis(trimethylsilyl)trifluoroacetamide	BSTFA	$(\text{CH}_3)_3\text{SiN}=\text{C}(\text{CF}_3)\text{OSi}(\text{CH}_3)_3$
N-methyl-N-trimethylsilyltrifluoroacetamide	MSTFA	$(\text{CH}_3)_3\text{SiN}(\text{CH}_3)\text{COCF}_3$
tert-butyl dimethylsilylimidazole	TBDMIM	
N-trimethylsilylacetamide	MTSA	$(\text{CH}_3)_3\text{SiNHCOCH}_3$
trimethylsilyltrifluoromethanesulfonate	TMS triflate	$(\text{CH}_3)_3\text{SiOSO}_2\text{CF}_3$
trimethylsilyliodide	TMSI	$(\text{CH}_3)_3\text{SiI}$

The first three are available in bulk quantities and are most suitable for large scale commercial silation. Chlorosilanes are generally used in combination with an acid. The chlorosilanes are clear liquids that should be treated as strong acids. They react readily with water to form corrosive HCl gas and liquid. The nitrogen-functional silanes have certain advantages for particular applications. The nitrogen-functional silanes react with water to form ammonia, amines, or amides. Fluorinated silating agents give enhanced rates of reaction and more volatile by-products. Trimethylsilyltrifluoromethanesulfonate and trimethylsilyliodide form very corrosive acidic products.

The most commonly used commercial silating agents for the silation of inorganic surfaces for applications in construction are octyltrimethoxysilane, octyltriethoxysilane, iso-butyltrimethoxysilane, and iso-butyltriethoxysilane. The silane is usually diluted in an alcoholic solvent and applied to the masonry surface where it bonds to the surface and gives long-lasting hydrophobicity. Treatment of brick, mortar, sandstone, concrete, and other masonry protects the surface from spalling, cracking, efflorescence, and other types of damage caused by water.

Silation can be applied to organic surfaces as well as inorganic surfaces. As an example of silation in organic synthesis, commercial synthesis of penicillins can be given. The aim of the silation process in this case is to protect 6-amino penicillanic acid (6-APA) by getting use of the blocking effect of the trimethylsilyl and dimethylsilyl.

Whereas alkylsilylating agents provide low energy surfaces designed for release, a series of organofunctional silylating agents (silane coupling agents) is offered commercially as adhesion promoters. Principal applications have been as coupling agents in glass- or mineral-reinforced organic resin composites and as adhesion promoters for paints, inks, coatings, and adhesives. Organofunctional silanes are also used to control orientation of liquid crystals, bind heavy-metal ions, immobilize enzymes and cell organelles, modify metal oxide electrodes, and to bind antimicrobial agents to surfaces. Representative commercial silane coupling agents are listed in Table 2.5. These compounds can also be used as chemical intermediates for preparing other more specialized organofunctional silanes.

2.5 Organofunctional silation agents

Chemical name	Formula
vinyltrimethoxysilane	$\text{CH}_2=\text{CHSi}(\text{OCH}_3)_3$
3-methacryloxypropyltrimethoxysilane	$\text{CH}_2=\text{C}(\text{CH}_3)\overset{\text{O}}{\parallel}\text{CO}(\text{CH}_2)_3\text{Si}(\text{OCH}_3)_3$
vinylbenzyl cationic silane	$\text{CH}_2=\text{CHC}_6\text{H}_4\text{CH}_2\text{NHCH}_2-\text{CH}_2\text{NH}(\text{CH}_2)_3\text{Si}(\text{OCH}_3)_3 \cdot \text{HCl}$
3-aminopropyltriethoxysilane	$\text{H}_2\text{NCH}_2\text{CH}_2\text{CH}_2\text{Si}(\text{OC}_2\text{H}_5)_3$
N-(2-aminoethyl)-3-aminopropyltrimethoxysilane	$\text{H}_2\text{NCH}_2\text{CH}_2\text{NH}(\text{CH}_2)_3-\text{Si}(\text{OCH}_3)_3$
3-glycidoxypropyltrimethoxysilane	$\text{CH}_2\overset{\text{O}}{\triangle}\text{CHCH}_2\text{O}(\text{CH}_2)_3\text{Si}(\text{OCH}_3)_3$
bis(3-triethoxysilylpropyl)tetrasulfide	$((\text{CH}_3\text{CH}_2\text{O})_3\text{SiCH}_2\text{CH}_2-\text{CH}_2\text{SS})_2$
3-mercaptopropyltrimethoxysilane	$\text{HSCH}_2\text{CH}_2\text{CH}_2\text{Si}(\text{OCH}_3)_3$
3-chloropropyltrimethoxysilane	$\text{ClCH}_2\text{CH}_2\text{CH}_2\text{Si}(\text{OCH}_3)_3$

2.3.3 Modification methods for silica surfaces

2.3.3.1 Co-precursor method for modification of silica aerogels

Silica aerogels must exhibit good hydrophobic properties for a long period of time for applications involving thermal insulation. One method to reach this goal is to co-gel some silicon precursor containing at least one non-polar chemical group such as Si-CH₃ bond (silating agent), with the normal silicon precursor (hydrophilic precursor). This can be accomplished by mixing the silating agent and a hydrophilic precursor at a certain mole ratio in the sol. Hexamethyldisilazane (HMDS) or various other organosilanes such as monoalkyl, dialkyl, trialkyl, aryl, alkoxy and chloro silanes can be applicable in co-precursor method as silating agents. HMDS is a difunctional trialkyl (trimethyl) silyl silane which is known to be highly reactive with surface silanols due to the presence of highly reactive nitrogen atom within the compound [3]. High silation power of HMDS has been demonstrated by various studies in literature [1, 2, 3, 4, 5].

Among various organosilanes, Rao et al. found that HMDS gave the highest contact angle (135°) for aerogels synthesized using TEOS and or tetramethylortho silicate (TMOS) [1]. However, the optical transmittance was as low as 5%. In another study, the mole ratio of HMDS to TEOS was varied from 0.1 to 0.6 which resulted in a decrease in optical transmittance from 65% to 5% and an increase in contact angle from 110° to 136° [2]. The decrease of transparency for a hydrophobic surface was also reported for another silating agent called methyltrimethoxysilane (MTMS) [25]. The transparency was decreased from 95% to 80% for an aerogel sample of thickness 1 cm. Poor optical property was principally attributed to the enlargement of the pore size. It is also worth noting that some silating agents can be used alone as a precursor without mixing it with other hydrophilic precursors. For example with MTMS and methyltriethoxysilane (MTES) could result in hydrophobicity up to 175° [1] and 163° [26] but again the obtained samples are opaque as shown in Figure 2.5. These studies indicate that the transmittance has to be sacrificed to increase hydrophobicity for the co-precursor method. Furthermore, an increase in HMDS amount causes cracks in the monoliths.

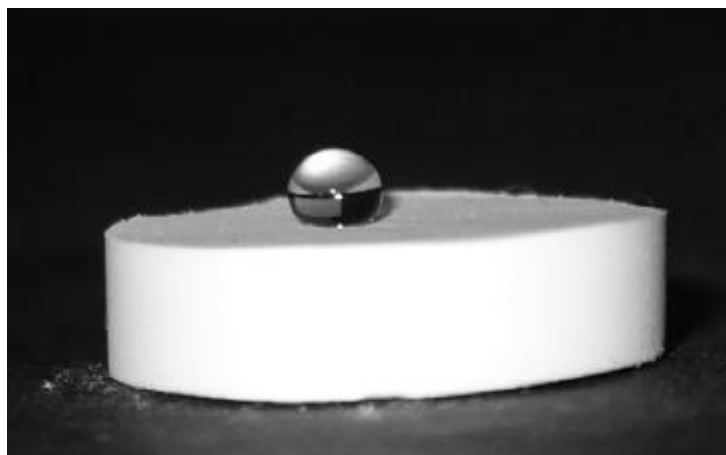


Figure 2.5 [26] Modified aerogels prepared by co-precursor method

2.3.3.2 Derivatization Method

The methods for derivatization of silica surfaces by silation agents can be classified according to the silation reaction medium. These are liquid media such as organic solvents which are used in the conventional solution methods and the gaseous

media such as N_2 . The procedure for conducting such processes involves the reaction of silica with silating agents through immersing the silica in the mixture of silating agent dissolved in a liquid solvent if the conventional process is carried out or bringing silica in contact with a silation agent in the gaseous phase. The realization of the surface modification reaction in gaseous media requires the usage of silating agents which have sufficient volatility. There is also a limitation for the usage of liquid solvent, such that the silating agent should be soluble in the liquid solvent. After the modification reaction is carried out for a certain period of time, the samples are washed and/or dried for removal of reaction products and obtaining modified silica.

The studies show that the ratio of the number of hydrophobic groups to Si of the silating agent is an important factor which effects the modification reactions. Gauthier et al. reported that silating agents with three hydrophobic groups demonstrate enhanced reactivity over silating agents with one hydrophobic group for grafting the silica. In fact no grafting was observed when monoethoxysilane is used [23]. In addition, the most important observation of this study was the necessity of the presence of surface water on silica for the hydrolysis of silanes that initiates the modification reaction. It was reported that the most efficient modification reaction was carried out with a trichlorosilane in non-aqueous media with surface water on the silica. However the resulting surface layer was very fragile. In addition, when trichlorosilane is used in aqueous media, it is seen that hydrolyzed trichlorosilanes react with each other in the aqueous media prior to grafting the surface. Thus, the grafting process is less efficient than the one with non-aqueous solution as well as triethoxysilane in aqueous media which resulted in more stable and reliable surface coverage. Thus, the type of the silation agent and the reaction media are effective parameters to be considered for obtaining materials with desired properties.

The critical effect of the surface water on the modification reaction was also investigated by Tripp and Hair by using different silation agents [27, 28]. The usage of octadecyltrichlorosilane (OTS) as silating agent required more than one layer of water on the surface of silica in gaseous media (N_2) [27]. No direct reaction of OTS with the surface $-OH$ groups or adsorption with the first water layer bound to the surface of silica was observed. The first layer of water was strongly bonded to the surface, acted more like bulk layer in character, and did not participate in direct hydrolysis of OTS. A

major increase in the kinetics of the reaction occurred when the coverage of water exceeded a monolayer. In another study, they investigated the reaction of trichloromethylsilane (TCMS) with a silica surface which contained varying amounts of adsorbed water at both gaseous and liquid media [28]. It was found that TCMS reacted with adsorbed water at the gaseous phase and formed methyltrisilanol which was adsorbed on the surface but did not polymerize or form a siloxane bond with the surface silanols. When the reaction was carried out in liquid media, TCMS reacted readily with water and the product methyltrisilanol was adsorbed on the silica surface where it condensed to a polymeric material. Once again, the type and the reaction media are found to be important parameters in surface chemical modification.

Yoshinda et al. demonstrated and quantified the effect of surface water on the multilayer silation [29]. They claim that silation coverage increase with the amount of surface coverage and reach a maximum at two layers of water coverage. Subsequent decline is attributed to the formation of bulk polysilanes and the decreased accessibility of the water-bearing surface to hydrophobic silation agent. There is low or non-existent silane coverage at low surface coverage while above maximum water coverage (two layers of water), silation agent condenses in the surface water layer to form polysilanes and these are only physically deposited and can be removed easily. Thus, depending on the amount of surface water, reproducible surface silation may be obtained.

Derivatization of silica aerogels

Solvent approaches described above have been used for the large scale production and processing of silica. However, the classical solvent approaches may sometimes be harmful, since the used liquids can easily destroy the functional surfaces they are helping to create. This is due to viscosity and surface tensions. For silica aerogels, the large capillary forces exerted on their pores when contacted with a liquid solvent leads to pore collapse and crumbling of aerogels.

One alternative is to modify the surface of the dry silica aerogels from the gaseous phase. In some studies, TMOS-based, supercritically dried silica aerogels were modified by methoxylation [30, 31]. Methoxylation process comprises of heating hydrophilic aerogel samples in methanol vapor at 240 °C for 10 h. This process

consumes not only energy and methanol in large amounts but also time. Alternatively, the sol-gel route provides a step where derivatization in liquid solvent is applicable. The modification of silica aerogels can be performed when the gel has still liquid in its pores prior to drying (when it is alcogel). Derivatization in alcogels have been widely studied in literature by using several different silating agents but here in this thesis, the focus will be on studies using HMDS [1, 2, 4]. As it was mentioned earlier (in section 2.4.3.1), HMDS is found to be highly reactive with surface silanols. The modification reaction is shown in Figure 2.6.

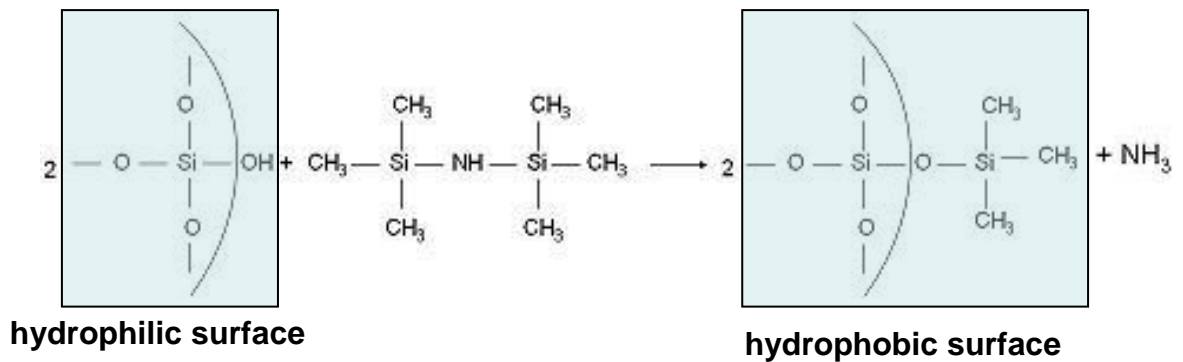


Figure 2.6 Surface modification reaction of silica aerogel with HMDS

The procedure for the derivatization method is as follows: the alcogels were immersed in a mixture of a solvent (ethanol, methanol [1,2] and hexane [4]) and SA for more than 12 hours at a temperature above 45 °C before drying. According to the previous studies, usage of HMDS as a derivatization agent yielded more transparent aerogels over co-precursor method [1, 2, 4]. The comparison of the silica aerogels obtained by the co-precursor and derivatization method can be seen in Figure 2.7.

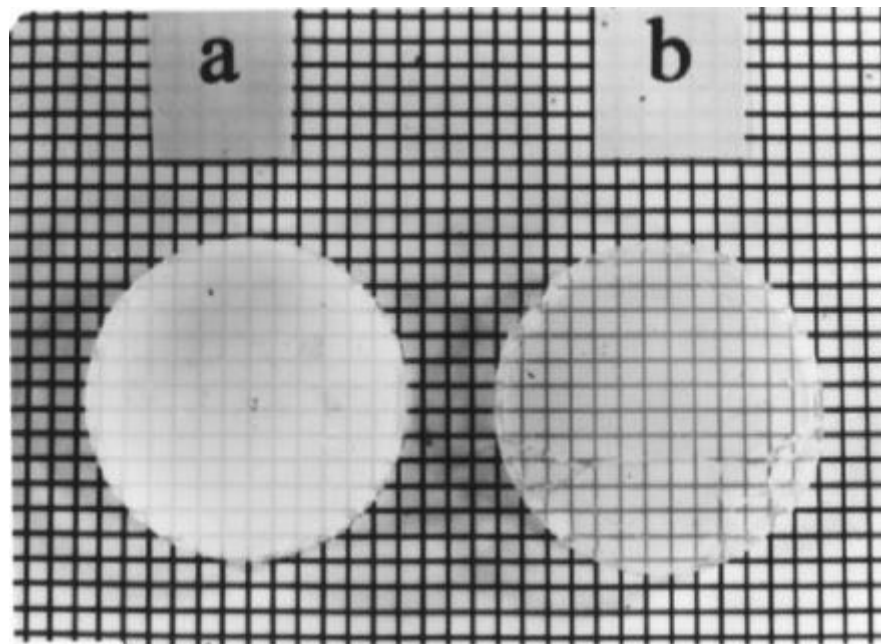


Figure 2.7 [2] a) modified silica aerogel by co-precursor method, b)derivatization method

In one study yielded transmittance improved up to 70% and 88% for TMOS based and TEOS based aerogels, respectively compared to 5% transmittance obtained from co-precursor method for aerogels with contact angle of 135° [1]. Similarly, monolithic aerogels with a transparency of 85% and a contact angle of 109° [2], and aerogels with a transparency of 75% and a contact angle of 143° could be obtained [4]. This improvement depends on the structural differences yielded by co-precursor method and derivatization method [2]. In the co-precursor method, the terminal methyl groups do not allow the structure to grow uniformly in all the directions and hence the aerogel consists of nonuniform and irregular shaped particles. Whereas in the derivatization method, the gels are treated with the hydrophobic reagent which react with the surface OH groups only, without affecting the growth and structure of the SiO_2 particles. Therefore, the aerogels obtained by the derivatization method have been found to have more uniform pore and particle sizes. On the other hand, the aerogels obtained by the co-precursor method have non-uniform and, large pore and particle sizes resulting in scattering of light. Since the scattered intensity is directly proportional to radius of pore per particle and inversely proportional to wavelength of light, the aerogels obtained by the co-precursor method are semi-transparent and opaque. The major drawbacks of this

method are the possible effect of the side product ammonia and the difficulties associated with the removal of unreacted HMDS, ammonia and solvent by several heat treatments above 50 °C.

Another important consideration is the environmental impact of both vapor and liquid processes and it must be minimized. Problems exist for liquid techniques since they use large quantities of organic solvents. Although vapor technique does not require large quantities of potentially harmful solvents, it can be environmentally dangerous because it requires considerable amounts of energy and reactive silanes with significant vapor pressure. In addition, the lengthiness of the process (silication time up to several days [6]) along with the environmental issues constitute the major drawbacks of the conventional methods.

2.4 Surface modification in scCO₂ phase

2.4.1 Supercritical CO₂

A substance is called a supercritical fluid when it is simultaneously heated and compressed above its critical temperature (T_c) and critical pressure (P_c) and is maintained there. General P-T diagram of a CO₂ which is given in Figure 2.8 can be used to demonstrate the supercritical region.

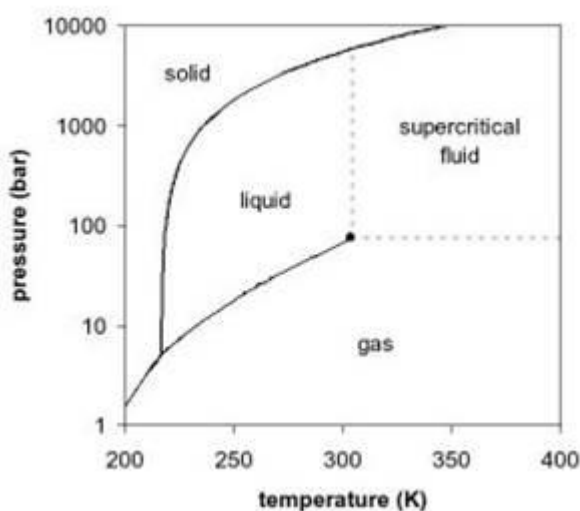


Figure 2.8 [32] States of the CO₂ solvent; dotted lines refer to critical pressure and critical temperature, not the phase boundaries

In the supercritical region, no phase boundaries exist, meaning that in the supercritical region, only a single homogeneous phase exists regardless of pressure and temperature. Therefore, it is possible for a substance to cross from a liquid state to the gas state without any phase transition (in this case boiling) by passing through the supercritical region.

The properties of a supercritical fluid are governed primarily by its density which is a strong function of both temperature and pressure. The density which defines the solvent power of a substance is very flexible in supercritical fluids with respect to pressure and temperature. Close to the critical point, a very little change in either pressure or temperature can result in large changes in density; hence this solvating power can be altered over a wide range. This feature is what makes a supercritical fluid unique from conventional liquid solvents. In the supercritical region, the thermophysical properties of a substance include liquid-like densities, gas-like viscosities and kinematic viscosities and much higher diffusivities than liquids [33]. A comparison of the properties of common supercritical fluids with that of liquids and gases are given in Table 2.6.

Table 2.6 Comparison of the physical properties of gases, liquids and SCFs [34]

Fluid	Liquid	Supercritical Fluid	Gas
Density (ρ) (kg/m ³)	1000	100-800	1
Viscosity (η) (Pa.s)	10 ⁻³	10 ⁻⁴ -10 ⁻⁵	10 ⁻⁵
Diffusion coefficient	10 ⁻⁹	10 ⁻⁸	10 ⁻⁵

The use of CO₂ as a solvent or raw material has been investigated somewhat continuously in academia and/or industry since 1950; interest in the use of CO₂ in these roles has intensified during the past 20 years as large-scale plants using CO₂ have been brought on line [35]. While supercritical fluids in general exhibit interesting physical properties as explained above, specific interest in CO₂ is magnified by its perceived

‘green’ properties—carbon dioxide is non-flammable, relatively non-toxic, and relatively inert. In addition, unlike water, the supercritical regime of CO₂ is readily accessible, given its critical temperature of only 304 K as shown in Table 2.7.

Table 2.7 Critical coordinates of usual pure fluids [36]

Fluid	T _c (°C)	P _c (MPa)	ρ _c (kg/m ³)
Carbon dioxide	31.2	7.38	468
Ammonia	132.4	11.29	235
Water	374.1	22.1	317
Ethylene	9.5	5.06	220
Ethane	32.5	4.91	212
Propane	96.8	4.26	225
n-Pentane	196.6	3.37	232
Cyclohexane	279.9	4.03	270
Methanol	240	7.95	275
Ethanol	243.1	6.39	280
Isopropanol	235.6	5.37	274
Acetone	235	4.76	273

2.4.2 Advantages of supercritical fluids in surface modification as solvents

Recently, scCO₂ has been attracting increased attention in modification of a wide variety of inorganic surfaces including silica [6, 7, 8, 37, 38]. The low viscosity, and surface tension of scCO₂ coupled with adjustable properties with changes in temperature and pressure make scCO₂ an attractive medium for carrying out surface modification. Furthermore, scCO₂ is inert and leaves no residue on the treated surface.

In the case of the modification of porous silica, solvents that will wet the pore structure efficiently are required [39]. Organic solvents are often too viscous to fill such small pores. Even gaseous species (when below critical temperature) can condense within small pores, thus forming a relatively viscous liquid “plug” that blocks the pore to further penetration. Since supercritical fluid solvents (e.g. scCO₂) have low surface

tensions and viscosities, they are good wetting agents and they do not condense into the liquid state within the small pores. Moreover, other potential advantages include rapid mass transfer, easy separations and ability to fill even small mesopores and micropores. The examples of surfaces modified by scCO₂ will be given in the following sections and the comparison of the results of the modification by silation with scCO₂ and other solvents will be given in section 2.4.4.

2.4.3 Literature examples of surface modification by deposition of metals and polymers in porous media

Fine control over solvent properties (e.g. by varying solvent density) may offer distinct advantages in this area. It is possible to synthesize metal nanoparticles within permanently porous structures [40], thereby exploiting wetting behavior, pore filling, and low viscosity. For example, silver nanoparticles have been introduced into the pore structure of porous cross-linked polystyrene beads and silica aerogels by scCO₂-assisted impregnation of silver followed by depressurization and subsequent addition of H₂ in order to reduce the complexes to metallic silver mass increases of 2-10 % were observed.

Furthermore, perfluorinated polyether coatings can be applied onto surfaces of marble, sandstone, and limestone by spraying from solutions in scCO₂ taking advantage of the solubility of perfluoropolyethers in CO₂ [41]. The penetration depth of the fluorinated coatings was found to strongly depend on the mean size and porosity of the stones. These results suggest that CO₂ can be used for the application of weather-proof fluorinated coatings for which there are no other viable, environmentally acceptable alternatives.

2.4.4 Literature examples of surface modification by silation in scCO₂ phase

Zemanian et al. reported that scCO₂ at 150°C and 7500 psi provided faster deposition (5 minutes vs. 10 hours of manipulation time and several days for drying), higher surface population of silanes (6.55 silanes/nm² vs. 4.97 silanes/nm²) and a better quality monolayer (complete coverage vs. defect density) on mesoporous silica over

toluene at 110°C in the reaction of silica with mercaptopropyltrimethoxysilane [6]. This enhancement in scCO₂ was partially attributed to the temperature difference (150°C for scCO₂ and 110°C for toluene). In another study, the reaction of silica with HMDS in scCO₂ (at 50 °C and at 200 bar) yielded a side product, ammonia which then reacted with CO₂ to form ammonium carbamate [7]. Ammonium carbamate blocked a portion of the surface silanol groups from participating in the reaction with HMDS. Ammonium carbamate could be removed easily by purging. It was also found that production of ammonium carbamate could be completely prevented by setting the CO₂ pressure lower than 90 bar since at such low pressures, ammonium carbamate formation was not favored.

In the studies of McCarthy and his group, fundamental research on trialkylsilane monolayers that are covalently attached to silicon surfaces under different reaction conditions: in the vapor phase, in toluene solution, and in scCO₂ were conducted [8, 42]. They have used alkyltrimethylchlorosilanes as the derivatization agents in scCO₂ at 70°C and 7200 psi for the modification of porous silica [8]. The same temperature and derivatization agent concentration was used for the modification in toluene [6]. They reported no differences in bonding densities at the same silation agent concentration and reaction temperature. The bonding density was 1.6 silane /nm² in both conditions. The contact angles of the obtained samples were also similar, around 100°. It was concluded that scCO₂ was a viable reaction medium for this process. Moreover, it was observed that modification reactions at solution-solid interface were slow in the later stages of the reaction and that long reaction times were necessary to achieve maximum bonding density. In comparison of toluene, vapor and scCO₂ media at the same temperature, the highest contact angles (indicating the densest monolayers) were obtained using vapor phase reactions, and the fastest reactions were found in supercritical CO₂.

Jia et al. has conducted modification of inorganic/organic buried interfaces between silicon wafers and polystyrene/polymethylmetacrylate with reagent (tridecafluoro-1,1,2,2-tetrahydrooctyl)dimethylchlorosilane using CO₂ at different conditions (1100 psi and 23°C, 1200 psi and 35°C and 2500 psi and 40°C) in order to improve the adhesion between organic solids (polymers) and inorganic silicon wafers [37]. It was found that liquid CO₂ (at 1100 psi and 23°C) was not an effective modification media while scCO₂ was able to yield modified interfaces. Moreover, contact angle increased

from 72° (moderate hydrophobicity) to 95° for 1200 psi and 35°C and 2500 psi and 40°C respectively. This was attributed to higher solubility of the modification agent in CO₂ and higher reaction kinetics at higher temperatures and pressures.

In another study, Higgings et al. demonstrated that the supercritical CO₂ deposition of octadecyldimethylchlorosilane (ODMCS) within the pores of a mesoporous silica (5 nm) membrane using supercritical CO₂ (at 200 atm and 50 °C, 15 minutes) is an effective and efficient method of preparation of hydrophobic membranes[38]. The usage of silane precursors resulted in covalent attachment of ODMCS to surface hydroxyl groups within the mesoporous membrane, in contrast to a polymerized silane layer normally found when using trichlorosilanes. Successful attachment was confirmed through infrared spectroscopic identification. The band due to isolated silanols disappeared and the bands due to methyl and methylene groups appeared. They also directly measured a 90% reduction in permeance of light gases through the modified membrane which also confirmed successful silane attachment and pore reduction. The synthesis process did not degrade the support membrane, was relatively efficient, and was free of organic solvents required for traditional synthesis.

2.5 Characterization of Hydrophobic Silica Aerogels

2.5.1 Contact Angle Test

The origin of the contact angle can be traced to the balance of the forces at the line of contact between the liquid and the solid when the solid is in contact with a liquid. The solid-vapor (γ_{sv}), solid-liquid (γ_{sl}) and liquid-vapor (γ_{lv}) surface tensions constitute the energy needed to create unit area of each of the interfaces (solid-vapor, solid-liquid, and liquid vapor interfaces). The necessary energy for the adhesion of the liquid to the solid surface can be expressed by (2.3) [43]

$$\Delta E = \gamma_{sv} + \gamma_{lv} - \gamma_{sl} \quad (2.3)$$

If $\Delta E < 0$, the liquid spreads spontaneously on the surface and forms a film. If on the other hand, $\Delta E > 0$, a droplet is formed since the liquid wants to minimize its energy (see Figure 2.9).

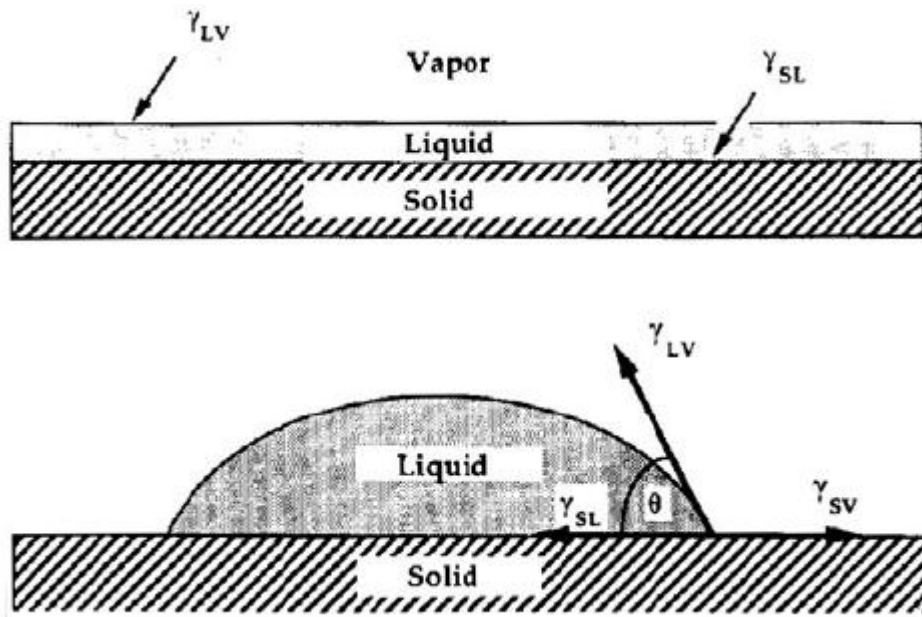


Figure 2.9 Liquid behavior on solid

The form of the liquid is characterized by the contact angle, θ . The balance of tensions are given by

$$\gamma_{SV} = \gamma_{SL} + \gamma_{LV} \cos\theta \quad (2.4)$$

This expression can be solved as:

$$\cos\theta = \frac{\gamma_{SV} - \gamma_{SL}}{\gamma_{LV}} \quad (2.5)$$

and 2.6 can be written by

$$\cos\theta = \frac{\Delta E}{\gamma_{LV}} - 1 \quad (2.6)$$

Now we can see that the liquid wets the surface (spreads over as shown in Figure 2.8 upper schematic) when $0 < \theta < 90^\circ$ and the liquid forms a droplet when $90 < \theta < 180^\circ$. Thus, in order to characterize the hydrophobicity, the behavior of water is observed on the modified silica aerogel surface. If it wets the surface, the sample is hydrophilic. If, on the other hand, it forms a droplet, the sample is hydrophobic. Subsequently, the extent of the hydrophobicity is determined by measuring or calculating the contact angle. The contact angle can be calculated by [1, 44]

$$\theta = 2 \tan^{-1} \left(\frac{2h}{w} \right) \quad (2.7)$$

where h is the height and w is the width of the droplet on the surface of the aerogel respectively. The construction of the formula can be seen in figure 2.10.

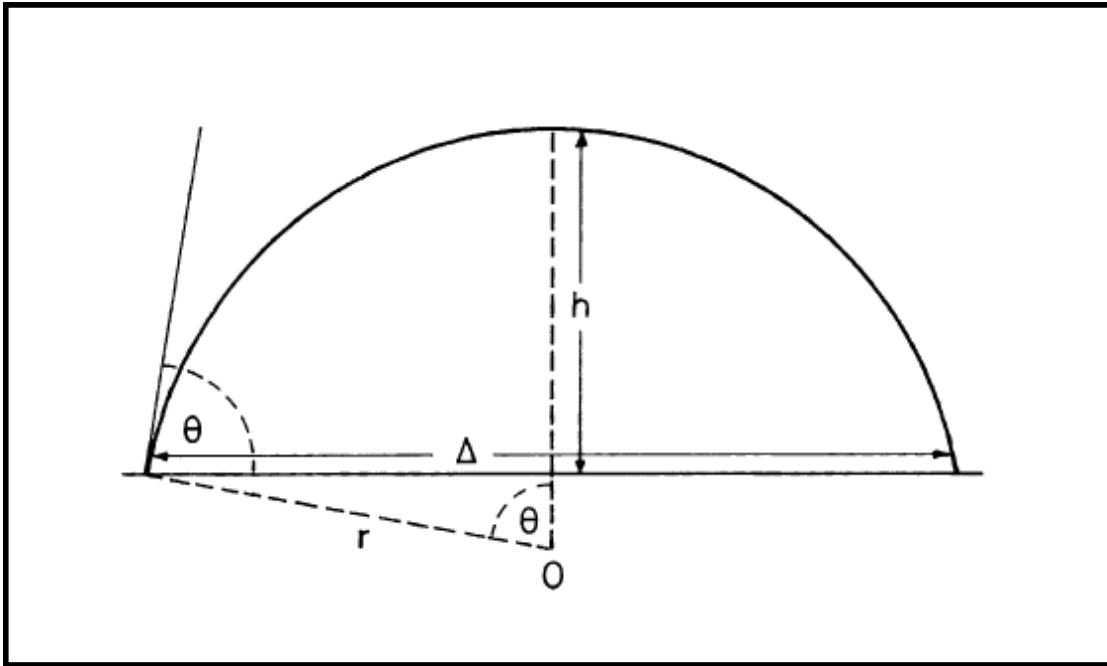


Figure 2.10[44] Calculation of the contact angle θ from the dimensions of the spherical water droplet, r is the radius, w is the base length and h is the height of the drop on the aerogel surface.

Furthermore, the hydrophobicity can also be determined by putting modified gels directly on water and measuring the amount of water adsorbed by the aerogels. If the weight of the adsorbed water is less than 2% of the sample weight, the sample is considered as hydrophobic. The sample is considered hydrophilic if the value is greater than 2% [25].

2.5.2 Fourier transform infrared spectra (FTIR) Analysis [45]

The most straightforward method for the acquisition of IR spectra of surface layers is standard transmission spectroscopy. This approach can only be used for samples that are partially IR transparent or that can be diluted with an IR transparent medium such as

KBr and pressed into a transmissive pellet. The extent to which the IR spectral region (typically, 600–4000 cm^{-1}) is available for study depends on the IR absorption characteristics of the solid support material. Transmission FTIR spectroscopy is most often used to study surface species on metal oxides such as silica. These solids leave reasonably large spectral windows within which the spectral behavior of the surface species can be viewed. Pellets of such oxides are usually prepared by mixing 5–10 wt% of the oxide with KBr and pressing a pellet that is several millimeters thick. Although the preparation of such systems is not difficult, often the pellet must be pressed for long periods of time to allow the KBr to fuse around the oxide particulates. Once prepared, IR spectra of these pellets can be acquired in standard KBr pellet holders.

The advantage of this approach for characterization of surface species is the ease of sample preparation and straightforward data interpretation. Spectra of such samples resemble normal transmission IR spectra and can be quantitated using conventional methods. In addition, this approach is reasonably sensitive with surface coverages down to ca 10% of a monolayer easily observed on oxides such as silica and alumina. One important point to note is the spectral interference that water adsorbed on an oxide surface can produce. In some cases, the spectrum from surface-confined water can swamp out the spectrum of other surface species of interest. In these cases, the transmission signal will not be strong enough to be of much use. This approach also does not work well for solids that are inherently strong IR absorbers for similar reasons. In these cases, approaches other than transmission FTIR spectroscopy must be used to acquire surface vibrational spectra.

FTIR is used in literature to confirm the hydrophobicity of the silica aerogel samples. The following images show the difference between the FTIR analysis results for the unmodified and hydrophobic silica aerogels in Figure 2.11 [46]. The major differences between the untreated and the treated aerogels is the emergence of methyl groups and the decrease of the surface silanol groups as seen at their corresponding bands.

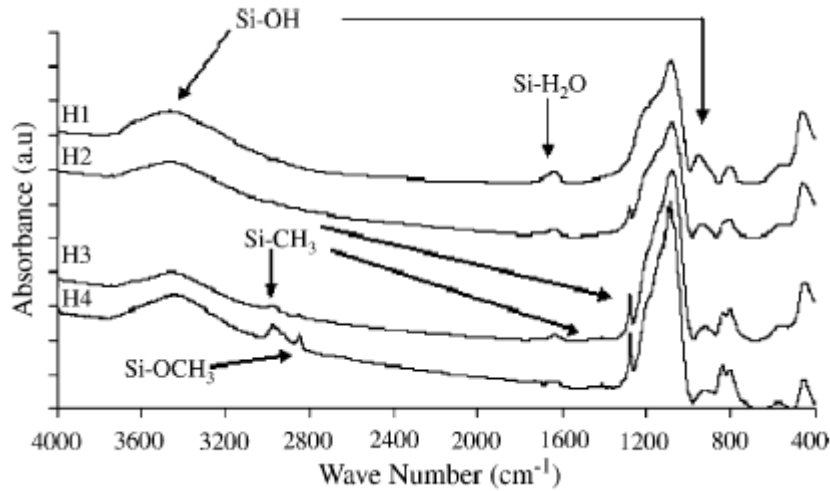


Figure 2.11 [46] FTIR Analysis for unmodified (H1) and modified silica aerogels (increasing extent of hydrophobicity from H2 to H4)

2.5.3 Measurement of silane groups on the modified surface

Different methods can be used in the determination of surface coverage. One of them is Si NMR spectroscopy [6]. It requires prior knowledge of the surface area of the starting material (which can be available from BET analysis). Modified samples are spiked with carefully weighed amounts of silation agent. The Si spectra are recorded using suitably long recycle times to permit quantitative determination of integrated silicon regions by comparison of the integral of the internal standard peak with the total silane integral. From the total number of moles of silation agent and the ratio of silation agent to the mass of modified samples, the integral ratio reveal the total number of moles of surface-bound silane in the sample. Dividing the number of moles of surface-bound silane by the surface area of the original silica provides an estimate of the population density at the silica interface. Because of the signal-to-noise limitations of solid-state Si NMR spectroscopy, this method of estimating population density is felt to be accurate to within (15 %). Deconvolution of the silane portion of the spectrum also allows for the determination of silane speciation within the monolayer.

Another method is the gravimetric method which also requires prior knowledge of the surface area also. The change in mass between the starting silica and the modified silica can be correlated to the silane component added to the porous substrate. It is

important to recognize that this analysis does not distinguish between monolayer siloxane and adventitious byproducts (e.g. residual polysiloxanes) trapped within the mesoporous matrix.

Also, a thermogravimetric analysis can also be performed in order to determine the methyl groups on silica surface [25]. In this method, modified aerogels can be heated from the room temperature to 425 °C. Wagh and Ingale determined that from 200 °C to 210 °C, a weight loss is determined to be 3.3% of the initial mass (10-20 mg) as a function of temperature (thermogravimetric analysis). This weight loss is due to thermal decomposition of the organic groups (–CH₃ groups). Thus, the number of surface methyl groups can be determined.

Surface coverage or grafting densities ($\mu\text{mol}/\text{m}^2$) of silica could be calculated from carbon elementary analysis also by using a sample of mass 0.8-1.2mg. Supposing that the grafted reagent forms a molecular monolayer on the surface of silica support, the overall grafting density, τ can be estimated using the following equation [47]

$$\tau = \frac{\%C \times 10^6}{12.011 \times n_C \times S_{BET} \left(\frac{\%C}{12.011 \times n_C} \right) (M - M_{Lgroups})} \quad (2.10)$$

where %C is the carbon percentage in the sample, 12.011 is the molecular weight of carbon (g/mol), n_C is the number of carbon atoms in the grafted molecule, S_{BET} is the specific surface area of the silica powder determined using nitrogen adsorption by BET, M is the molecular weight of the organosilane reagent and M_{Lgroup} is the molecular weight of the leaving group (in the case of surface modification of silica aerogel by HMDS, the leaving group is NH).

2.6 Thermodynamic description of processes: Phase Equilibria

For the description of the chemical processes such as silation processes, the knowledge of thermodynamic properties is essential especially when the pressure is relatively high and close to the critical one of some components in the mixture. Near critical or at critical conditions, the fluids exhibit properties similar to those of the liquids, leading to high loading of solutes, high molecular diffusivity and low viscosity. The solubility of a given solute appears to be practically exponential in density: as a

consequence very small pressure variations result in large changes of solubility. The enhanced solubility can be explained only with the high non-ideal thermodynamic behavior of mixtures. The presence of small amount of a non-critical compound can also have large effects on the solubility of a heavy compound in the high dense fluid.

Other phenomena can be simply explained by the fact that the critical pressure and temperature for a given mixture is not, as it happens for a pure fluid, the maximum temperature and pressure that allows the coexistence of a vapor and liquid phase in equilibrium.

In the case of silation process using mixtures of HMDS and CO₂, it is essential to determine the conditions at which the mixture is at single phase in order to perform efficient surface modification. Thus, the knowledge of the pressure, the temperature and the composition of the mixture when it exhibits vapor-liquid equilibria is required. Moreover, the accurate calculation of such data is important in order to estimate the process conditions without performing several experiments on vapor-liquid equilibria.

In this basic overview, firstly the construction of the phase diagrams of fluid mixtures in the guidance of Gibbs phase rule will be explained. Subsequently, types of phase equilibria calculations will be defined. Then, the equations of state which are used in the phase equilibria calculations will be presented. Finally the experimental methods to determine vapor-liquid equilibria will be explained.

2.6.1 Gibbs phase rule and phase diagrams

The equilibrium conditions for phase equilibria can be derived using Gibbs energy, G . According to the second law of thermodynamics, the total Gibbs energy of a closed system at constant temperature and pressure is minimum at equilibrium. If this condition is combined with the condition that the total number of moles of component i is constant in a closed system

$$\sum_{\alpha} n_i^{\alpha} \quad (2.11)$$

Where n_i^{α} is number of moles of component i in phase α , it can easily be derived that for a system of Π phases and N components the equilibrium conditions are:

$$\mu_i^{\alpha} = \mu_i^{\beta} = \dots = \mu_i^{\pi} \quad \text{for } i = 1, 2, \dots, N \quad (2.12)$$

μ_i^α is the chemical potential of component i in phase α and can be expressed by

$$\mu_i^\alpha = \left(\frac{\partial \sum_i n_i^\alpha g^\alpha}{\partial n_i^\alpha} \right)_{P, T, n_{i \neq j}} \quad (2.13)$$

where g is the molar Gibbs energy. Since μ_i^α is a function of pressure (P), temperature (T) and $(N-1)$ components (the additional condition $\sum_i x_i^\alpha = 1$ makes one of the mole fractions a dependent variable), Therefore the number of degrees of freedom F is

$$F = 2 - \Pi + N \quad (2.14)$$

(2.14) is the phase rule of Gibbs. The phase rule can be used to classify the different types of systems and equilibrium. A system with one component is called unary system, a system with two components is called a binary system and a system with three components is called a ternary system, etc. The minimum number of phases is $\Pi=1$, so the maximum value of F is given by:

$$F_{\max} = N + 1 \quad (2.15)$$

Equation (2.15) gives the dimension of the space needed to represent the complete phase behavior of a N component system. For a unary system, $F_{\max}=2$ and the phase behavior of such a system can be represented in a two-dimensional P, T plane. For $N=2$, $F_{\max}=3$ and we need a three dimensional P, T, x_1 -space to represent the system. For a ternary system, we need four dimensional P, T, x_1, x_2 -space etc. An equilibrium with $F=0$ is called nonvariant, an equilibrium with $F=1$ monovariant, an equilibrium with $F=2$ bivariant, etc. Since the minimum value of $F=0$, it can be concluded from 2.14 that the maximum number of phases that can co-exist in a system with N components is:

$$\Pi_{\max} = N + 2 \quad (2.16)$$

Using the guidance of Gibbs phase rule, one can figure out the representation of the system under investigation. For a unary system, the phase rule gives $F=3-\Pi$, and $\Pi_{\max} = 3$. According to the degrees of freedom, a three-phase equilibrium is represented by a point in the P, T -plane, the triple point solid-liquid-vapor (SLV). Another triple point is possible, and this is solid1-solid2-liquid (S1S2L). S1 and S2 are different modification of the same solid compound. Two phase equilibria are represented by a curve in the P, T -plane. Examples are the melting curve (SL), the sublimation curve

(SV), and the vapor pressure curve (LV). Equilibria of one homogeneous phase (S, L or V) are represented by a region in the P,T-plane. The regions of homogeneous phases are separated by the corresponding two-phase curves and a triple point is found at the intersection of three two-phase curves. So the vapor pressure curve starts in the triple point SLV and ends at the critical point L=V, which is nonvariant.

The phase rule for a binary system is given by $F=4-\Pi$ and in this case, the maximum number of phases that can coexist is $\Pi_{\max} = 4$. The phase behavior is not only more complicated because one needs three dimensions to represent the equilibria (P,T,x-space), but also because many more phases are possible. Solids cannot only form many different solid modifications, but solids of different compounds can also form one phase (mixed crystals) or do not mix at all or only mix partially. Also one needs to deal with more fluid phases. For instance two liquid phases (L1 and L2) can be formed due to composition difference of the components in binary mixture in these two phases. In extreme cases, the liquids are almost pure components or if the mutual solubility of the two liquids increases, for instance, with increasing temperature at constant pressure, the two liquid components can become miscible in all proportions and the region of liquid-liquid immiscibility is bordered by a liquid-liquid critical point (L2=L1). For binary systems, the different types of phase equilibria and their representation in P,T,x-space are given in Table 2.8.

Table 2.8 Phase equilibria in binary systems and their representations in P,T,x-space

Π	F	Representation in P,T,x	Examples
1	3	Region	S1/S2/L/V/L1/L2/S
2	2	Two surfaces: $x^\alpha(P,T), x^\beta(P,T)$	LV/S1L/L2L1
3	1	Three curves: $x^\alpha[P(T)], x^\beta[P(T)], x^\gamma[P(T)]$	S1LV/S2S1L/L2L1V
Critical curve	1	$x^c[P(T)]$	L=V/L2=L
Azeotropic curve	1	$x^{az}[P(T)]$	S2S1LV/S2L2L1V
4	0	Four points at one P and T	L2=L1V/L2L1=V/SL=V
Critical end point	0	Two points at one P and T	
Critical azeotrope	0	One point	

In a critical endpoint, two phases of a three-phase equilibrium become identical and the two corresponding curves in the P,T,x-space merge in one point. From this point, also a critical curve emerges. A critical azeotrope is an end point of the azeotropic curve. At this point the azeotropic curve is tangent to the critical curve $L=V$.

In practice mainly two-dimensional diagrams are used to represent phase equilibria and not the multi-dimensional P,T,x-space representations. The compositions of phases in α and β become equal in three different ways as shown in Figure 2.12. The curves can intersect at $x=0$ or $x=1$ (Figure 2.12 a). This is liquid-vapor equilibrium, LV where the curve that represents the composition of phase L which intersects the curve for phase V in the boiling points of both pure components. Also two curves can have a common horizontal tangent (Figure 2.12 b). In this case, the compositions of the two phases are equal. An example is an azeotropic point. A third possibility is that the two curves can merge in a horizontal tangent point $(\partial T/\partial x)_p = 0$ or $(\partial P/\partial x)_T = 0$. This type of point is a critical point, where not only the compositions but all the thermodynamic properties of the two phases become identical.

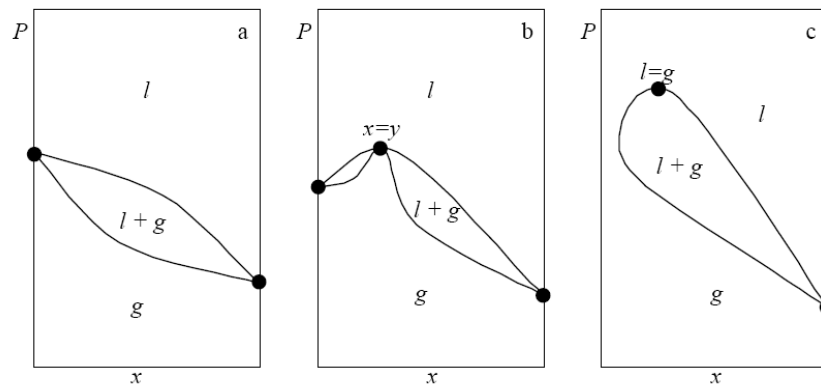


Figure 2.12 Three cases where the compositions of the two phases of a two-phase equilibrium are equal: a) Pure component boiling points, b) azeotropic point c) critical point.

According to the classification of van Konynenburg and Scott, one can distinguish between six main types of fluid phase behavior, which all have been confirmed experimentally. With exception of type VI, the existence of these types of phase behavior can be predicted with a simple equation of state such as van der Waals equation and for type VI, other equations of states can be used to represent the diagram. The schematic diagrams of the six types are shown below in Figure 2.13. In Figure 2.13, the curves lg are the vapor pressure curves of the pure components which end in a critical point $l=g$. The curves $l=g$, $l_1=g$ and $l_2=g$ are vapor-liquid critical curves and the curves $l_1=l_2$ are curves on which two liquid phases become critical. The points of intersection of a critical curve with a three-phase curve l_2l_1g is a critical endpoint. Distinction can be made between upper critical endpoints (UCEP) and lower critical endpoints (LCEP). The UCEP is highest temperature of a three-phase curve, the LCEP is the lowest temperature of a three-phase curve. The point of intersection of the l_2l_1g curve with a $l_1=g$ curve is a critical endpoint in which the l_1 liquid phase and the vapor phase are critical in the presence of a non-critical l_2 phase ($l_2+(l_1=g)$) and the point of intersection of the l_2l_1g curve with a $l_2=l_1$ curve is a critical endpoint in which the two liquid phases l_2 and l_1 are critical in the presence of a non-critical vapor phase ($(l_2=l_1)+g$).

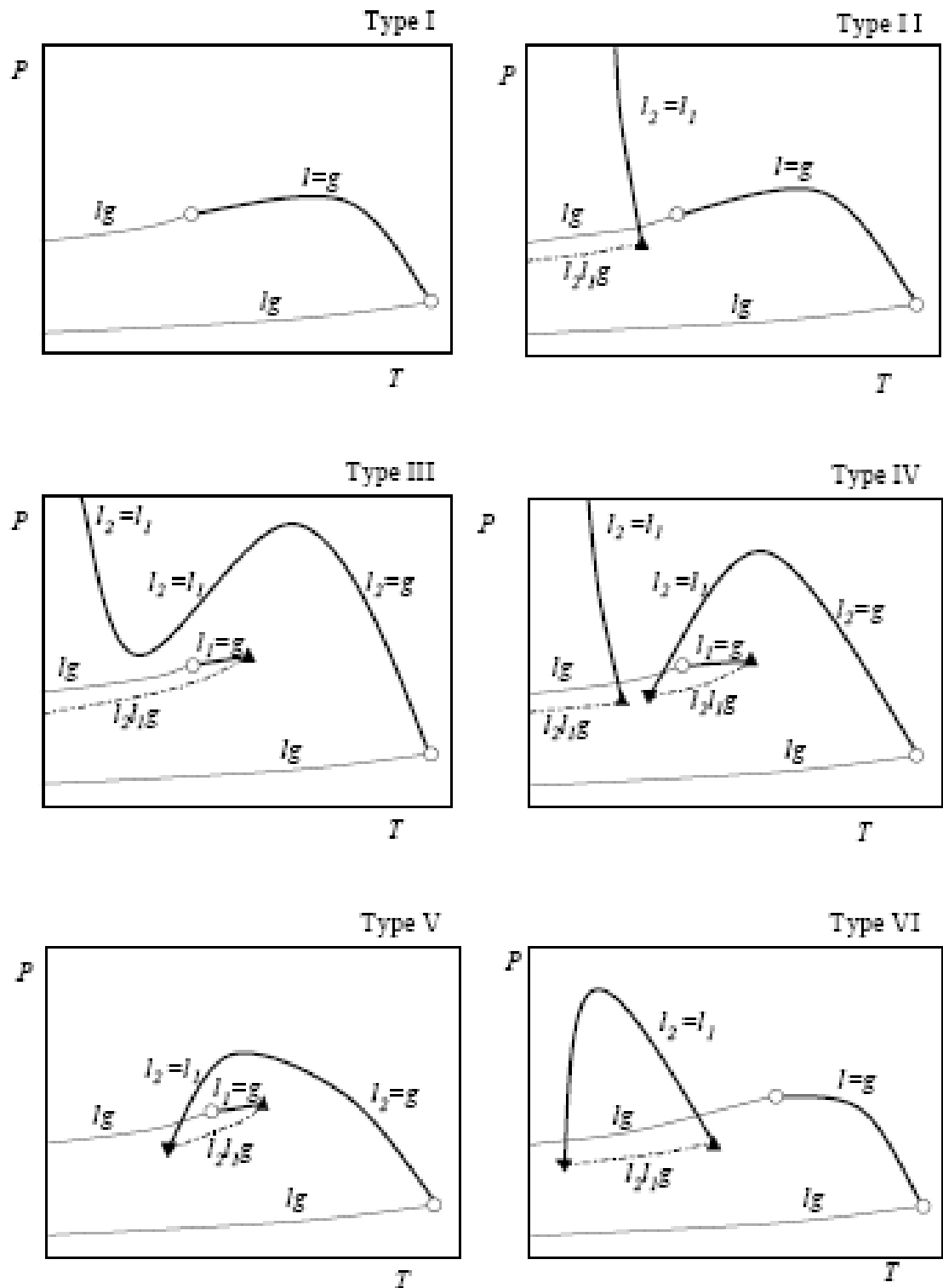


Figure 2.13 The six basic types of fluid phase behavior according to the classification of van Koynenburg and Scott

2.6.2 Phase equilibria calculations

The purpose of phase equilibria calculations is to predict the thermodynamic properties of mixtures, avoiding direct experimental determinations, or to extrapolate the existing data to different temperatures and pressures. The basic requirements for performing any thermodynamic calculation are the choice of the appropriate thermodynamic model and knowledge of the parameters required by the model. In phase equilibria calculations different combinations of input variables are possible but in general, the following choices are the most commonly used in order to solve typical problems:

- For a liquid mixture of given composition and at a given temperature (or pressure) the pressure (or temperature) at which the first bubble of vapor phase appears and its composition is calculated (bubble point calculation).
- For a vapor mixture of given composition and at a given temperature (or pressure) the pressure (or temperature) at which the first drop of liquid phase appears and its composition is calculated (dew point problem).
- For a mixture of given composition at given conditions of temperature and pressure, it can be determined if the mixture is a stable homogeneous liquid or vapor or that the mixture is heterogeneous and splits in a vapor phase and a liquid phase with different composition. If the mixture is heterogeneous the composition and the amount of the vapor phase and of the liquid phase are calculated. This calculation is known as flash calculation.

Bubble point calculations and dew point calculations can be considered as particular cases of the general flash calculation. All these calculations with an equation of state are iterative and performed by computer simulations. In the following sections (section 2.6.3 and 2.6.4), the approaches used in such simulations will be described.

2.6.3 Thermodynamic principles of vapor-liquid phase equilibria

The introduction of auxiliary functions

In the thermodynamic treatment of phase equilibria, auxiliary thermodynamic functions such as fugacity coefficient and the activity coefficient are often used. These functions are closely related to the Gibbs free energy. The fugacity of component i in a mixture, \hat{f}_i , is defined by

$$d\mu_i = RT \ln \hat{f}_i \quad \text{at constant T} \quad (2.17)$$

with

$$\lim_{P \rightarrow 0} \frac{\hat{f}_i}{P_i} = 1 \quad (2.18)$$

According to this definition, \hat{f}_i is equal to the partial pressure P_i in the case of an ideal gas.

The fugacity coefficient, $\hat{\phi}_i$ is defined by

$$\hat{\phi}_i = \frac{\hat{f}_i}{P_i} \quad (2.19)$$

and is a measure of the deviation from ideal gas behavior.

The activity a_i is defined as the ratio of \hat{f}_i and the fugacity of component i in the standard state at the same P and T:

$$a_i \equiv \frac{\hat{f}_i(P, T, x)}{f_i^0(P, T, x^0)} \quad (2.20)$$

An activity coefficient is defined by

$$\gamma_i \equiv \frac{a_i}{a_i^{id}} \quad (2.21)$$

So the fugacity of a non-ideal solid or liquid solution can be written as

$$\hat{f}_i = x_i \gamma_i f_i^0 \quad (2.22)$$

In the next section, the description of vapor-liquid phase equilibria calculation will be on equation of state model instead of activity coefficient model. Thus the usage of

activity coefficient is limited with this introduction of the activity coefficient described above.

2.6.4 Equations of State

In phase equilibria calculations, the thermodynamic model used is generally an equation of state which is able to describe the properties of the both phases. In order to best fit the equation of state model to experimentally determined bubble point pressure values, the choice of the type of the equation of state is important. The models used to predict equilibria in the supercritical region can be divided into the following groups:

- the van der Waals family of cubic equations of state;
- the virial family of equations of state;
- the group contribution equations of state;
- equations of state for associating and polar fluids;
- equations of state from theory and computer simulation

As it is mentioned earlier in this section, the cubic equations of state are able to represent the different types of the vapor-liquid equilibria except one (type VI) and they are (especially Peng-Robinson (PR) and the Soave-Redlich-Kwong (SRK)) most commonly used since they require little input information (only critical properties and an acentric factor to calculate the generalized parameters) and require little computer time. Van der Waals family of cubic equations of state will be explained below. The generalized cubic equation of state is

$$P = \frac{RT}{V-b} - \frac{(V-\eta)\theta}{(V-b)(V^2 + \delta V + \varepsilon)} \quad (2.23)$$

The parameters in Equation 2.23 can be seen in Table 2.9 for different equations of state.

Table 2.9 Parameters for cubic equation of state

Author	Year	θ	η	δ	ε	$P = \frac{RT}{V-b} - \Delta$ Δ
Van der Waals	1873	a	b	0	0	$\frac{a}{V^2}$
Clasius	1880	a/T	b	2c	c ²	$\frac{a/T}{(V+c)^2}$
Berthelot	1899	a/T	b	0	0	$\frac{a/T}{V^2}$
Redlich-Kwong	1949	a/ \sqrt{T}	b	B	0	$\frac{a/\sqrt{T}}{V(V+b)}$
Soave	1972	$\theta_S(T)$	b	B	0	$\frac{\theta_S(T)}{V(V+b)}$
Lee-Erbar-Edmister	1973	$\theta_L(T)$	$\eta(T)$	B	0	$\frac{\theta_L(T)[V-\eta(T)]}{(V-b)(V+b)}$
Peng-Robinson	1976	$\theta_{PR}(T)$	b	2b	-b ²	$\frac{\theta_{PR}(T)}{V(V+b)+b(V-b)}$
Patel-Teja	1981	$\theta_{PT}(T)$	b	b+c	-cb	$\frac{\theta_{PT}(T)}{V(V+b)+c(V-b)}$

Each of the equation of state discussed here can be written in the cubic form

$$Z^3 - \alpha Z^2 + \beta Z + \gamma = 0 \quad (2.24)$$

Where $Z = PV/RT$ is compressibility factor, and the parameters α , β and γ for some representative equations of state are given in Table 2.10.

Table 2.10 Parameters in equation 2.33 for three equations of state

parameter	Van der Waals	Redlich-Kwong and Soave	Peng-Robinson
α	-1-B	-1	-1+B
B	A	A-B-B ²	A-3B ² -2B
Γ	-AB	-AB	-AB+B ² +B ³

B in Table 2.10 is

$$B = \frac{bP}{RT} \quad (2.25)$$

and A is

$$A = aP/(RT)^2 \quad \text{for van der Waals, Soave and Peng-Robinson EOS} \quad (2.26)$$

$$A = aP/(RT)^2 \sqrt{T} \quad \text{for Redlich-Kwong EOS} \quad (2.27)$$

a and b in equations (2.25-2.27) are evaluated using the conditions for critical point (2.28)

$$\left(\frac{\partial P}{\partial V}\right)_{T_c} = 0 \quad \text{and} \quad \left(\frac{\partial^2 P}{\partial V^2}\right)_{T_c} = 0 \quad \text{at } P_c \text{ and } V_c \quad (2.28)$$

where P_c , V_c and T_c are critical pressure, critical volume and critical temperature respectively.

2.6.5 Experimental methods to determine vapor-liquid bubble-point pressure

For a mixture, the highest pressure at which the first bubble forms is called the bubble point pressure of the system. Different types of apparatus have been developed in the literature, which enable the measurement of the temperature, the pressure and the composition of coexisting vapor and liquid phases. The methods can be classified as static and dynamic methods.

The bubble point pressure data are measured in a constant composition expansion experiment using a temperature controlled pressure-volume-temperature (PVT) visual cell by static methods as shown in Figure 2.14. The mixture is placed into an evacuated cell, which is placed in a constant temperature bath (usually a liquid or air bath, although also metal-block thermostats have been used). The contents of the cell which are separated into two or more phases of different densities are brought to equilibrium by shaking, stirring, or agitation (e.g. by placing a magnetic stirrer in the cell and placing the cell on a magnetic stirrer plate). The sample remains enclosed in the cell, and no phase or part of the system is subject to flow with respect to the others. Because we are dealing with a closed system, this method requires careful evacuation of the cell and tubing and degassing of the materials, in order to avoid errors in the reading of the equilibrium pressure, although this problem is not as crucial as at low pressures.

The pressure of the system can be changed by the movable piston, and the phase change can be observed so that the pressure at which the first bubble formed can be determined.

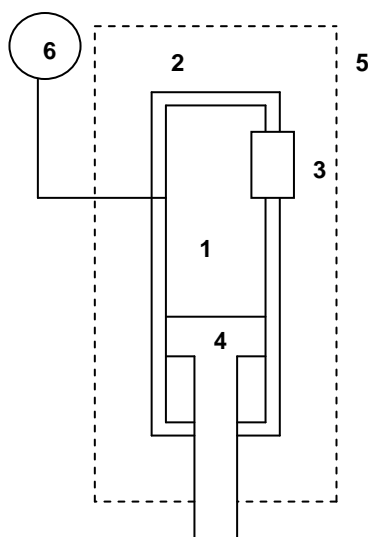


Figure 2.14 Variable volume static view cell

- | | |
|----------------------|-------------------|
| 1, mixture; | 4, free piston; |
| 2, equilibrium cell; | 5, thermostat; |
| 3, window; | 6, pressure gauge |

Two methods are generally used to determine the composition of the equilibrium phases. In the first method, known amounts of the pure substances are introduced into the cell, so that the overall composition of the mixture contained in the cell is known. The compositions of the co-existing equilibrium phases may be recalculated by an iterative procedure from the predetermined overall composition, and equilibrium temperature and pressure data. It is necessary to know the pressure volume temperature (PVT) behavior, for all the phases present at the experimental conditions, as a function of the composition in the form of a mathematical model (EOS) with a sufficient accuracy.

The second method is the recirculation method which was developed from the static methods. The apparatus for recirculation method is shown in Figure 2.15. The main part of the apparatus is a thermostated equilibrium cell. The equilibrium cell has facilities for mechanically driven circulation through external loop(s) of either the

lighter (i.e., the top) phase or the heavier (the bottom) phase, or of both phases. Magnetically operated high pressure pumps usually achieve the circulation. The purpose of introducing the external circulation of phases is to achieve their more efficient equilibration through stirring and contacting, and thereby to improve the contact of both phases and thus to reduce the time required to reach equilibrium. After equilibrium has been achieved in a steady-state regime, the phases which circulate through an external loop already represent a separated equilibrium phase. A portion of such a phase may be trapped in a sampling cell, which may be removed for analysis, or the phase may be temporarily circulated through an in-line sampling loop such as an injection valve, and then analyzed. The principle parts of the recirculating method are demonstrated in the schematic in 2.15.

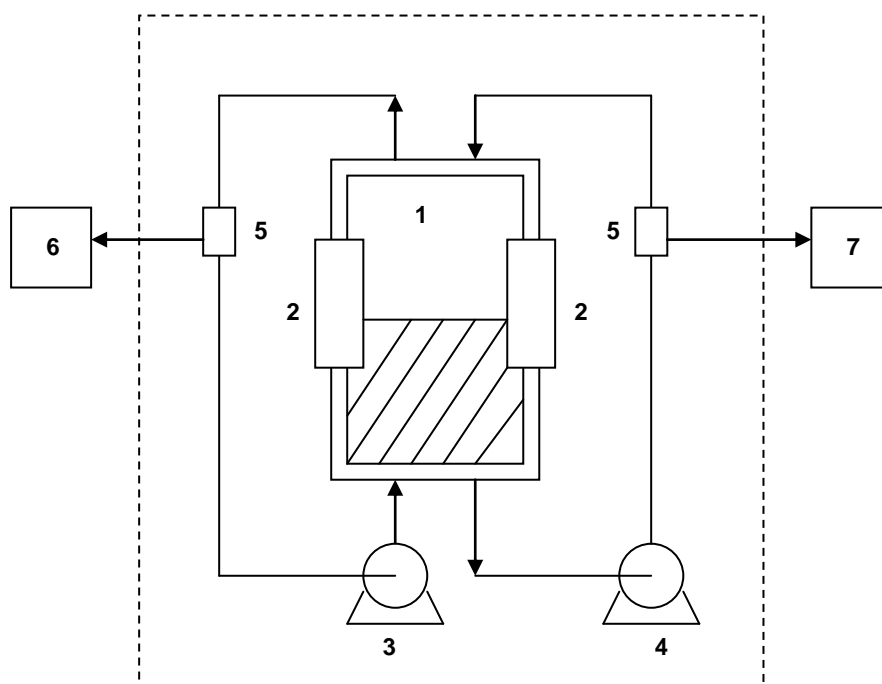


Figure 2.15 Recirculation method

- | | |
|-----------------------------------|------------------------|
| 1, equilibrium cell; | 5, sampler; |
| 2, window; | 6, analysis for vapor; |
| 3, recirculation pump for vapor; | 7, analysis for liquid |
| 4, recirculation pump for liquid; | |

These experimental methods, extensively used for the study of binary mixtures, are seldomly used for the determination of phase equilibria of complex multicomponent mixtures, mainly owing to analytical difficulties.

Chapter 3

EXPERIMENTAL

3.1 Synthesis

The schematic representation of the steps involved in the synthesis of silica aerogels can be seen in figure 3.1. Silica aerogels in this study were synthesized by a two-step procedure using TEOS (from Aldrich with 98.0% purity) as the precursor, HCl (from Riedel-de Haen with 37% purity) as the hydrolysis catalyst and NH_4OH (from Aldrich 2.0 M in ethanol) as the condensation catalyst. A 50 wt. % solution of TEOS in ethanol (from Merck with 99.9% purity) was prepared. Subsequently, water and acid catalyst were added to start hydrolysis under continuous stirring. Condensation started with the addition of the base catalyst and the sol was taken into cylindrical molds with a diameter of 10 mm for complete gelation. The overall mole ratio of TEOS to water was 1:4, TEOS to HCl was 500:1, and NH_4OH to TEOS was 2.6. The typical amounts of each compound for synthesis of a sample of silica aerogel are shown in Table 3.1

Table 3.1 Compounds in the synthesis of silica aerogels

Compound	Amount added in sol	Remarks
TEOS	1 g	Correspond to 0.0048 moles
ethanol	1 g	50 wt. % solution of TEOS and ethanol is obtained
Distilled water	0.34 g	Correspond to 0.0189 moles
0.05 M HCl/Ethanol solution	0.2 ml	Correspond to $9.78 \cdot 10^{-6}$ moles of HCl And 0.003 moles of ethanol The sol consisting of TEOS, ethanol, HCl and NH_4OH is left for hydrolysis for 40 minutes
0.1 M NH_4OH /Ethanol solution	0.6 ml	Correspond to $6.0 \cdot 10^{-5}$ moles of NH_4OH

After gelation was finished, the alcogels were taken out from the mold and placed in an aging solution which was 50 vol. % ethanol and water, and left in furnace at 323.2K for 20 hours. The aim of the aging step was to improve the mechanical strength of the alcogels. After the aging step was completed, the aging solution was replaced with pure ethanol and the alcogels were kept for two more days in pure ethanol in order to remove all the impurities other than ethanol. In order to extract ethanol from the pores of the alcogel, drying with supercritical CO_2 was used. This was conducted at 313.2K and 8.27 MPa. The aerogels that were obtained this way were hydrophilic.

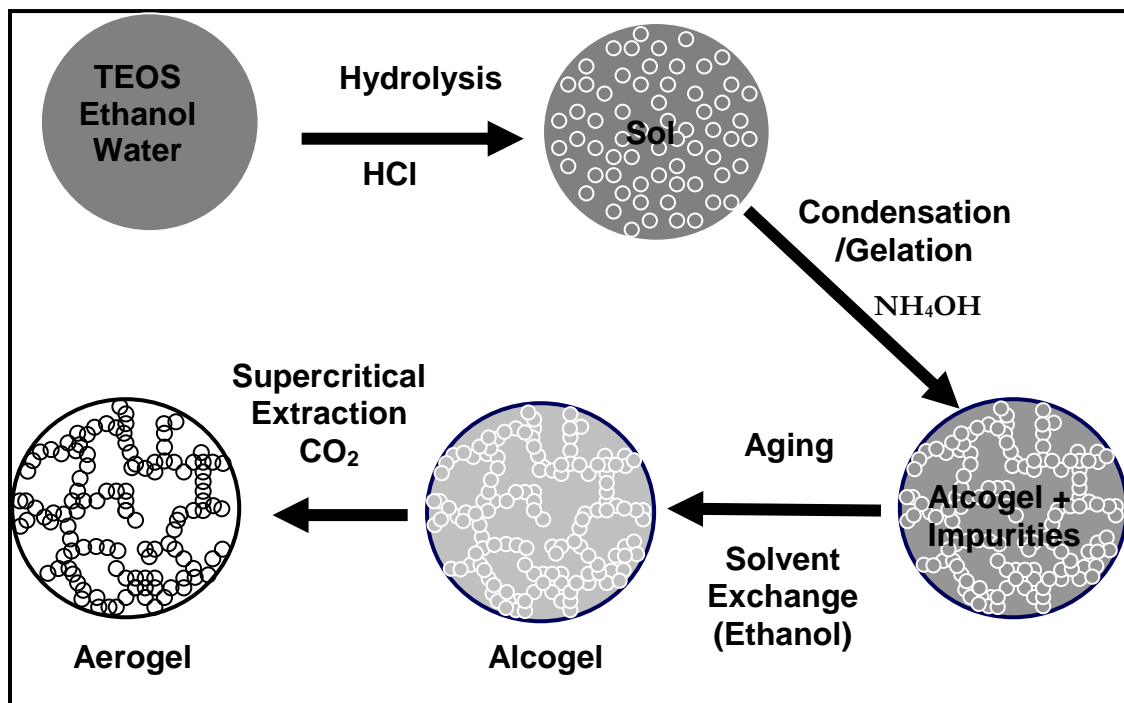


Figure 3.1 The schematic representation of the procedure during silica aerogel synthesis by sol-gel method.

3.2 Modification of Hydrophilic Silica Aerogels

3.2.1 Apparatus and Procedure for Modification of Silica Aerogels

The experimental apparatus for the surface modification of hydrophilic silica aerogels can be seen in Figure 3.2. Two high pressure vessels were used for conducting the experiments. One of them was used as the reaction vessel. It had an internal volume

of 54 ml and two sapphire windows for viewing the contents. The other one with a volume of 25 ml was used for mixing HMDS with CO₂. For a typical experiment, a certain amount of hydrophilic silica aerogel sample was placed in the reaction vessel and the vessel was brought to a temperature of 333.2 K by circulating water using a circulating heater (Cole-Parmer polystat temperature controller). The vessel was then charged to 10.34 MPa with CO₂ using a syringe pump (Teledyne ISCO model: 260D) and isolated at these conditions. The mixing vessel was prepared by placing a known amount of HMDS into the vessel within a glass vial along with glass beads which kept the glass vial intact and the vessel was charged with CO₂. This vessel was also kept at 10.34 MPa and at ambient temperature for 24 hours until all the HMDS was dissolved in CO₂. The surface modification of the hydrophilic aerogels was achieved by the injection of the HMDS solution from the mixing vessel to the reaction vessel. This was realized by pressurizing the mixing vessel up to 20.68 MPa by charging with CO₂ from the syringe pump. The CO₂ – HMDS mixture at 20.68 MPa and at room temperature was injected into the main vessel by opening the valve between the reaction vessel and the mixing vessel. This procedure was repeated until the pressure in the reaction vessel reached also 20.68 MPa. The vessel was isolated at 20.68 MPa and at 333.2K for the reaction of silica aerogel surface with HMDS for a certain period of time. After the reaction, the extraction of excess HMDS and other reaction byproducts was carried out at 10.34 MPa and at the reaction temperature. Then the vessel was depressurized at the same temperature and modified samples were obtained after the vessel was cooled. The surface modification reactions were carried out by changing mass fraction of HMDS in HMDS-CO₂ mixture and the time for reaction at the main vessel.

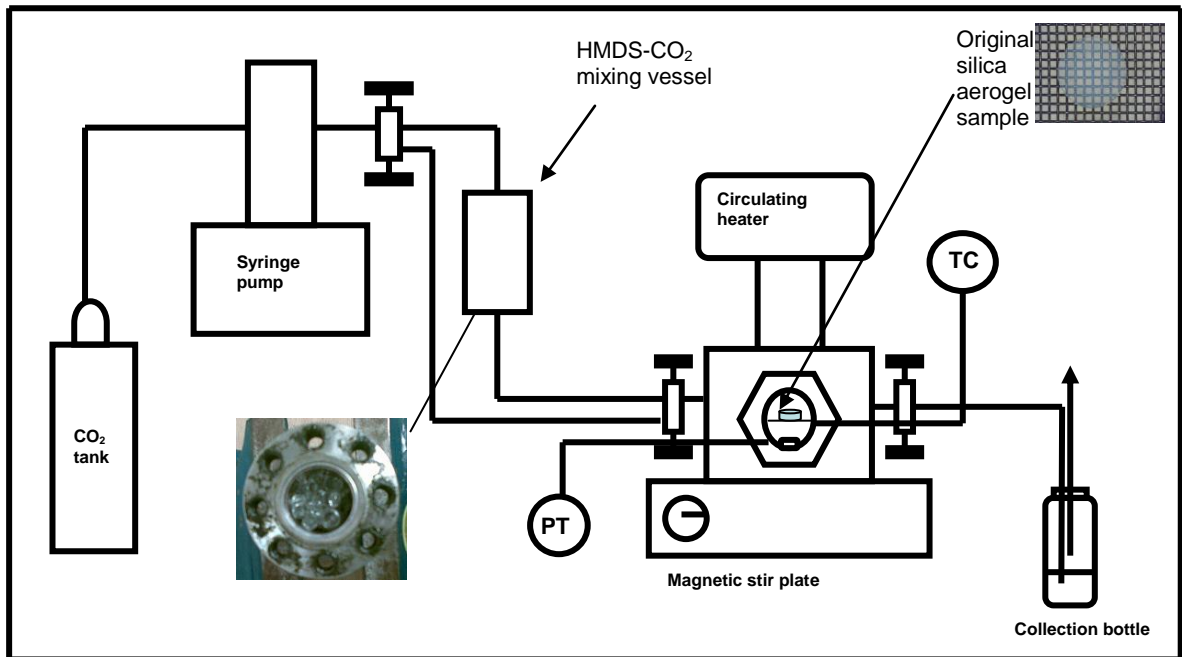


Figure 3.2. Apparatus for surface modification of hydrophilic silica aerogels

3.2.2 HMDS-CO₂ Solutions in Modification Process

The mass fraction of HMDS could be calculated by finding the ratio of HMDS mass in the mixing vessel to the overall mass of HMDS-CO₂ mixture which is used for modification of silica aerogels. In order to determine the mass of CO₂, the volume delivered by the pump and the density of CO₂ at the pressure and the temperature (298.2K) of the pump were used. For example, in order to determine the amount of CO₂ charged to the mixing vessel, firstly, the line until the mixing vessel inlet valve (see Figure 3.2) was charged to 10.34 MPa using the syringe pump and the pump volume was recorded. Then the inlet valve of the mixing vessel was opened and (see Figure 2.2) the vessel was charged to 10.34 MPa and the final volume of the pump was recorded. The resulting volume reduction of the pump indicated the volume of the CO₂ which entered to the mixing vessel. Using the density of CO₂ at 10.34 MPa and 298.2K, and the calculated volume of CO₂, the mass of CO₂ could be determined. Similar calculations were performed for determining the amount of CO₂ for the preparation of the reaction vessel, for pressurizing the mixing vessel to 20.68 MPa and for pressurizing the reaction vessel to 20.68 MPa. The total amount of CO₂ was found by the summation of the calculated CO₂ amounts. The amount of HMDS in the mixing vessel was

measured gravimetrically before it was put into the mixing vessel. Hence, the mass fraction of each compound in the mixture was calculated. For our experiments, HMDS mass fractions were 0.007 and 0.013.

3.3 Characterization of Treated Silica Aerogels

The characterization of the treated silica aerogels were done in order to measure and verify the hydrophobicity by contact angle test and FTIR analysis. In determining the surface contact angles of the modified gels, the degree of the contact angle was calculated from the photographic image of the water droplet at the surface of the modified aerogels as described in following section, 2.5.1. FTIR analysis was done to confirm the modification reaction by observing the changes in the surface molecular composition as described in section 2.5.2.

3.3.1 Contact Angle Determination

The contact angle of the treated aerogels was calculated using the formula 2.7 which was used elsewhere [1,44] from its photographic image.

3.3.2 FTIR Analysis

Infrared data of the treated and untreated silica aerogels were obtained by the transmittance method on a FT/IR-660 Plus model Jasco FTIR spectrometer. The samples were prepared using KBr pellets containing aerogel powder of around 0.0075% in weight (3mg of aerogel powder in around 400mg of KBr powder.)

3.4 Bubble point pressure measurements

3.4.1 Apparatus and Procedure for Bubble Point Pressure Measurements

The set-up for measuring bubble point pressures can be seen in Figure 3.4. A static method was followed for the bubble point measurements of the binary mixture of

HMDS and CO₂. The experiments were conducted in a high pressure vessel with a sapphire window which was kept at constant temperature using a circulating heater. A syringe pump was used to pressurize the vessel by charging it with CO₂. The conditions inside the vessel were determined by a thermocouple (Omega Engineering Inc. model: GTMQSS-062G-6 along with the meter of model: DP462) and a pressure transducer (Omega Engineering Inc. model: PX4100-6KGV along with a strain meter of model: DP25B-S-230).

For a typical experiment, a certain amount of HMDS was weighed and placed in the high pressure vessel (see Figure 3.5.a). The vessel was pressurized by charging with CO₂ to a pressure above the bubble point pressure where a single phase existed (see Figure 3.5.b). The magnetic stirrer within the vessel was used to mix CO₂ and HMDS within the vessel continuously during the experiment. Then the vessel was depressurized slowly in order to detect the emergence of the phase separation at a unique pressure for a certain composition at constant temperature. This pressure was recorded as the bubble point pressure (see Figure 3.5.c). This procedure was repeated for various compositions (the determination of the compositions are described in the following section 3.4.2.) at four different temperatures which were 298.8K, 313.5K, 327.7K and 342K. Finally, pressure-mole fraction of CO₂ (P-x) diagram was constructed for different temperatures.

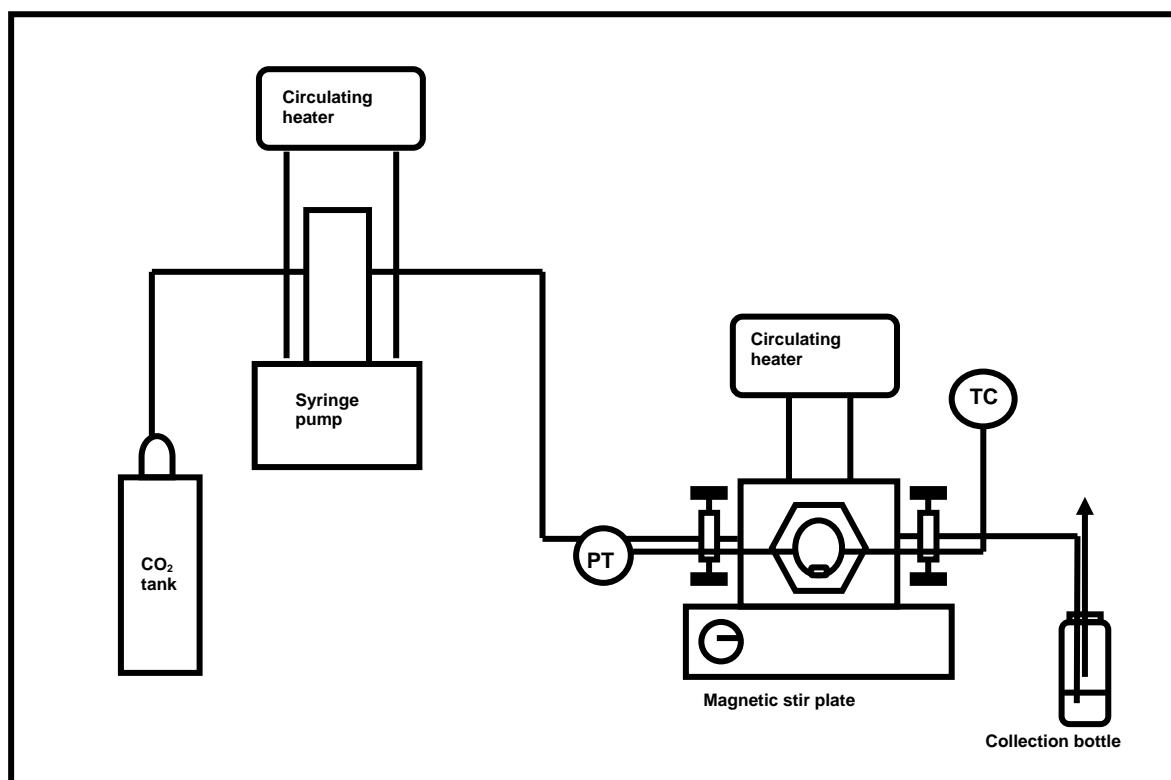


Figure 3.3 Apparatus for bubble point pressure measurements

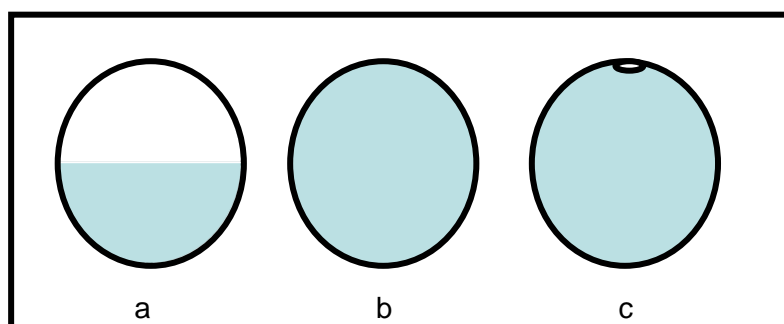


Figure 3.4 Changes in phases as seen from the view cell. a) initially, b) at single phase (above bubble point) , c) at bubble point

3.4.2 HMDS-CO₂ Solutions in Bubble Point Pressure Measurements

The concentration in terms of mole fraction of HMDS and CO₂ can be determined using the mass of HMDS which was put into the vessel and the mass of the CO₂ that entered the vessel. Mass of CO₂ could be found analogously using the procedure described in section 3.2.2. First, by using the syringe pump, the line to the view vessel was charged to a pressure which was estimated to be above the bubble point

pressure of the mixture. The pump volume at this step was recorded as the initial value. Then the inlet valve to the view vessel was opened and the vessel was also charged to the same pressure. This pump volume was recorded as the final pump volume. The reduction of the initial pump volume indicated the amount of CO₂ which was delivered into the vessel. Using the density of CO₂ at this pressure and at the temperature of the pump, mass of CO₂ in the vessel could be calculated. The temperature of the cylinder of the pump was kept constant at 298.2 K using a circulating bath (Cole-Parmer Polystat Circulating Bath).

Chapter 4

RESULTS

4.1 Mold study results

The choice of the mold material is critical for obtaining monolithic silica aerogels, because alcogel tends to stick to the mold material and may crack into pieces when taken out of the mold. At first, a glass test tube was used as a mold and the mouth of the test tube was closed by a stopper. It was not possible to take the gel out of the test tube after gelation was reached because the gel was squeezed in the test tube. When the tube was broken in order to get the gel out, the gel was broken too. Another technique was to fill the tube with the sol and seal the mouth with the stopper followed by turning the tube upside down before gelation. After the gelation point and 1 hour aging in the tube, the bottom of the test tube was broken and the stopper at the mouth was removed. Then the gel was like in a glass tube open from both ends. It was possible to push the gel from one side and take out from other side but the gel was already broken during the removal of the stopper. These experiments suggested that wet gels can be taken out by pushing them; this gave the idea to use a syringe as a mold. The 5 ml syringes were chosen when the vessel dimensions, which will be used in the drying step, were taken into consideration. The inner diameter of a 5ml syringe is 10 mm. The sol could be easily taken into the syringe and was sealed easily. After gelation, the syringe was cut from the sealed part and easily pushed into the aging solution. By this way we were able to produce cylindrical crack free monoliths. All of the monolithic silica aerogels that are used in the surface modification were prepared by using plastic syringes. The diameter of the monolithic aerogels was 10 mm and their thickness ranged from 1.8 to 4.25 mm depending on the volume of the sol put into the molds.

The next study was conducted in order to produce monoliths larger in size. If the same idea in syringes was used in larger molds, a monolith would not be obtained since in larger molds, it is difficult to exert the same force per unit area of the alcogel in

contact with the movable part, thus the alcogels are expected to stick to the sides of the molds while some of it cracked and pushed forward out of the mold. Thus, it is required to find a material to which the silica alcogel would not stick. Molds in the shape of rectangular prisms with one open side which are made of teflon, aluminum and a wrapping paper resistant to oil or grease were tested. It was found that except the wrapping paper, silica alcogel stuck to other materials. In the case of the wrapping paper molds, monoliths were easily obtained by peeling off the wrapping paper. Furthermore, the usage of such a cheap material is also advantageous.

4.2 Modification results

The concentration of HMDS in the vessel, HMDS uptake time and modification reaction temperature was investigated. The effect of HMDS concentration was tested by keeping the uptake time constant at 30 minutes and changing the HMDS mass fraction from 0.007 to 0.013. In addition to this, the effect of HMDS uptake time was observed by keeping the HMDS mass fraction at 0.007 and changing the uptake time from 30 minutes to 22 hours. Both of the treatments rendered the surface of the aerogels hydrophobic as indicated by a contact angle test. In the top view images of a water droplet on the silica aerogels (figure 4.1b and figure 4.1c), the effect of water on the hydrophilic and treated silica aerogels is clearly seen. In Figure 4.1b, the water deteriorates the surface of the untreated aerogel while in Figure 4.1c, the treated surface repels the water.

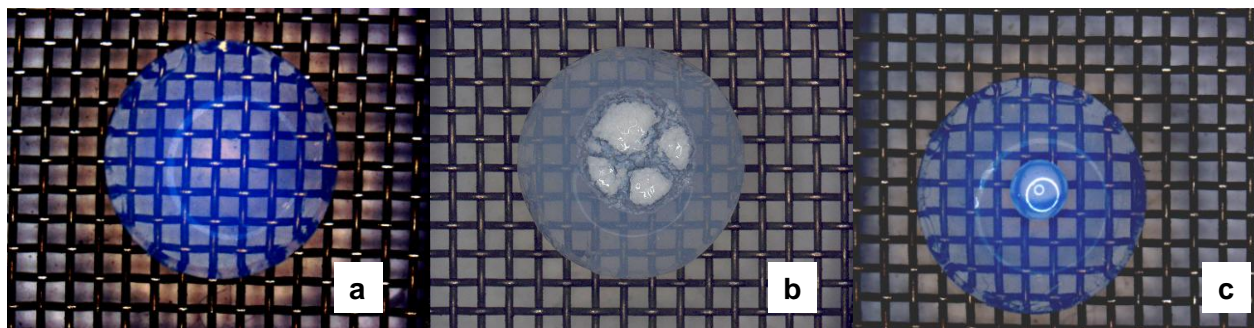


Figure 4.1 Top view images of a) an un-modified silica aerogel, b) a water droplet on un-modified silica aerogel, c) a water droplet on a modified silica aerogel

Furthermore, the contact angle of the treated aerogels was calculated using the formula 2.7. Two gels did not show any difference in their extent of modification in terms of contact angle values. The contact angles of the two modified aerogels were both calculated to be 130° (see Figure 4.2).



Figure 4.2 The image of a drop of water on the modified silica aerogel surface

The hydrophobicity was not restricted to the surface only. When the silica aerogel disks are cracked into two, the internal surface of the samples demonstrated the same hydrophobicity (see Figure 4.3a for top view image and 4.3b for side view image).

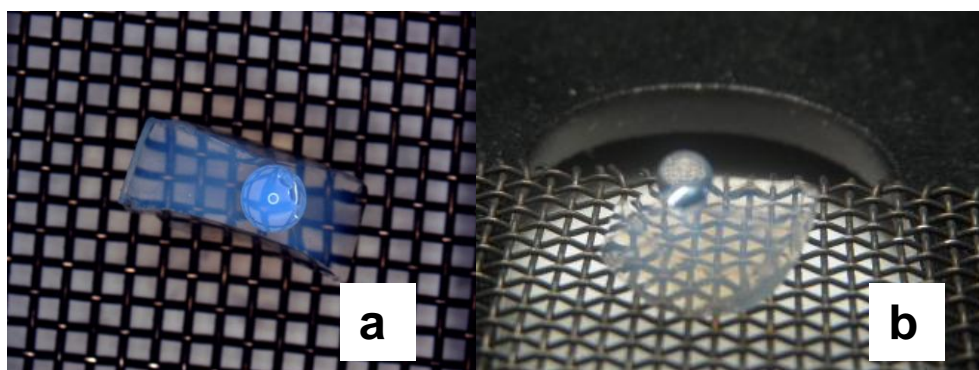


Figure 4.3 The image of a water droplet on the inside surface of the aerogels a) top view, b) side view

In addition to the contact angle test, treated and untreated samples were studied by infrared spectroscopy in order to confirm the existence of hydrophobic groups on the surface of the treated samples. The obtained absorption bands were interpreted by

referring to previous publications [2, 4, 46]. Figure 4.4 presents the infrared transmittance spectra for the two aerogels.

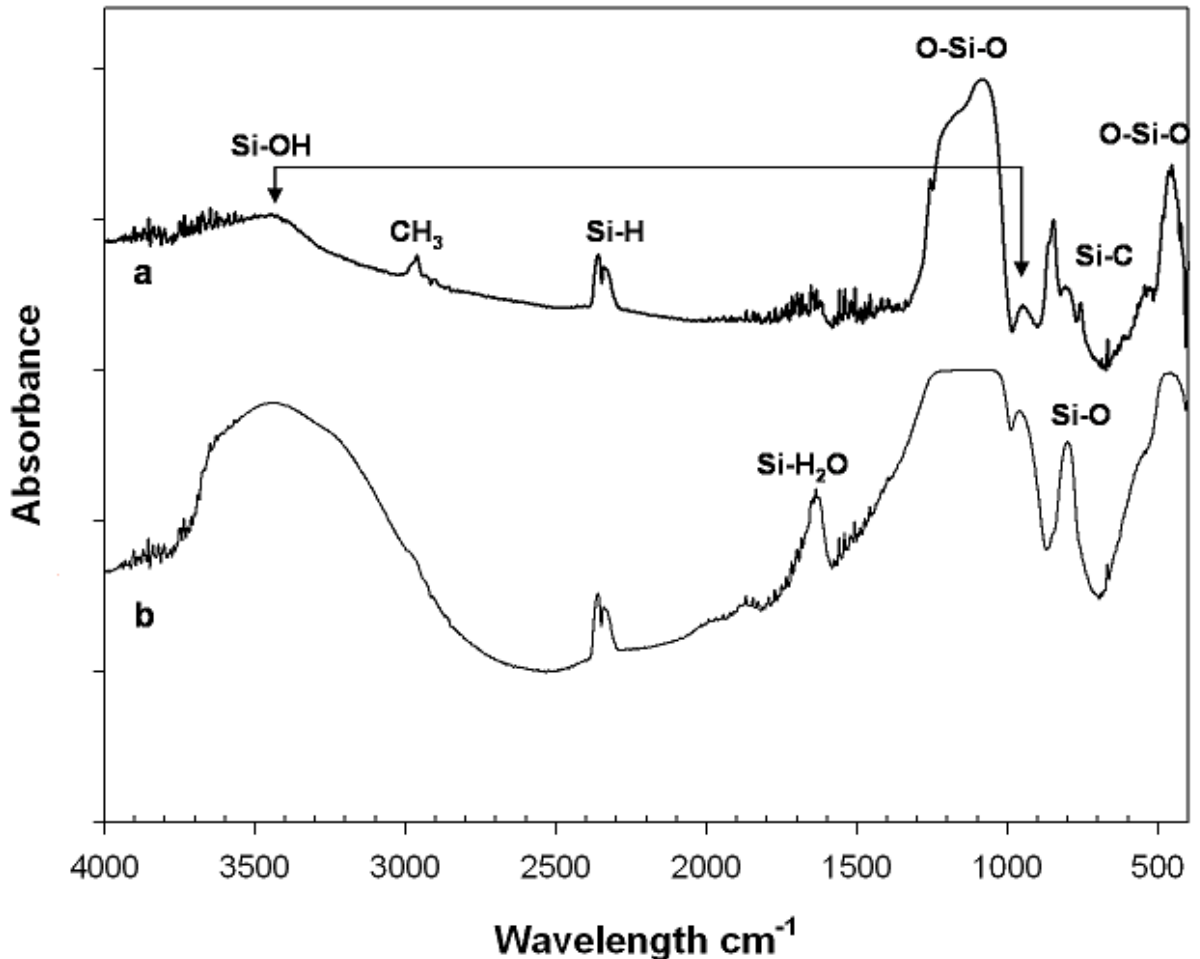


Figure 4.4 FTIR spectra of a) treated silica aerogel, b) untreated silica aerogel

FTIR investigations on treated samples (Figure 4.4b) clearly indicate that the surface of the aerogels were modified due to the reduction of the intensity of the broad Si-OH band around 3500 cm⁻¹ the other Si-OH peak around 1000 cm⁻¹. In addition, the presence of sharp Si-CH₃ peak around 2900 cm⁻¹ in the treated samples, confirmed the presence of hydrophobic groups on the surface.

Also, in each case, the treatment did not result in a reduction in the transparency as well. The extent of transparency of the untreated and treated silica aerogel can be seen clearly in Figures 4.1a and 4.1c, respectively. Thus, HMDS concentration and uptake time at 333.2K did not have a significant effect on modification reaction within the

range of given experimental parameter values. Similarly, the treatments did not cause a significant weight change in the modified aerogels which may be attributed to the formation of a single layer silation on the surface of the treated aerogels. This assumption can be based on a simple calculation. During the modification reaction, the hydrogen atom of a hydroxyl group is replaced by a silyl tri-methyl group ($\text{Si}(\text{CH}_3)_3$). Therefore, 1 g of hydrogen is replaced by 73 g per silyl tri-methyl group and this would correspond to replacement of $1.66 \cdot 10^{-24}$ g per H atom by $1.21 \cdot 10^{-22}$ g per $\text{Si}(\text{CH}_3)_3$ molecule. Therefore, the mass increase by the chemical modification reaction is $1.2 \cdot 10^{-22}$ g per bond. The determined weight of the aerogel sample is 0.04 g and assuming that the surface area is $1000 \text{ m}^2/\text{g}$, and there is 1 bond per nm^2 , the weight increase should be 0.005g. When there is more than a monolayer, then the weight change would have been much more apparent.

Furthermore, it was found that not all of the silation agents were applicable for modifying the surfaces of silica aerogels in scCO_2 media. For example, a silation agent, methyltrimethoxysilane (MTMS) which was used in co-precursor method and derivatization method in liquid solvent in previous studies [1, 2, 44], was not able to yield modified surfaces in scCO_2 media in our study. The same procedure explained in section 3.2.1 was conducted by replacing HMDS with MTMS. The resulting aerogel gave the same response to a water droplet of the unmodified gel as shown in Figure 4.1b. This is due to either very low extent of reaction or no reaction of MTMS with surface of silica aerogels. MTMS contains three hydrolysable groups and one non-hydrolysable organic group while HMDS have three non-hydrolysable organic groups and one hydrolysable group bonded to its Si atoms. This might have an influence on lower silation power of MTMS compared to HMDS and more reaction time or higher concentration of MTMS might be required.

Silation mechanism

The extent of the reaction at silica aerogel pores depend on several factors: the diffusivity of the silane reagent in the pores, the accessibility of the silanol groups on the surface, and the reaction kinetics of the silation agent. Here, the diffusivity of the silating agent in the pores will be discussed.

According to the modification results, we see that the silation of the silica surface was not restricted to the surfaces of the monolith which are directly in contact with the silation agent. Inner silica aerogel surface was also modified (see Figure 4.3 a, 4.3 b). This is attributed to the open pore structure of the silica aerogels as mentioned in section 2.2. It is assumed that the reaction starts at the surfaces in direct contact with the silating agent and proceeds with diffusion of the silating agent in the pores. In Figure 4.5, the diffusion through the open pore structure is schematized.



Figure 4.5 [12] Diffusion through the open pore structure of the silica aerogels

The modification reaction can be thought of as the opposite of the extraction of the pore fluid from the alcogel pores in drying. In extraction, ethanol mixes with CO_2 and leaves the pores by venting ethanol loaded CO_2 whereas the silating agent loaded scCO_2 diffuses into the pores in modification process as shown in Figure 4.6.

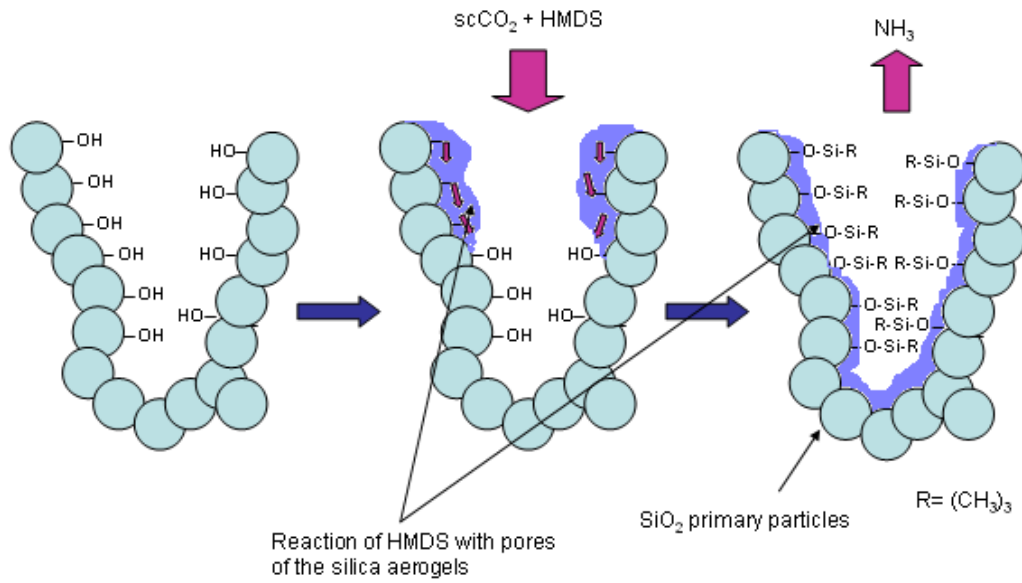


Figure 4.6 Surface modification of silica aerogel pores with HMDS loaded scCO₂.

When the pores were assumed to be cylindrical, the extraction of ethanol from the pores of the aerogels and the diffusion of HMDS to the pores of the aerogels which are filled with CO₂ can be treated as diffusion through capillary, flux is given by Fick's first law of diffusion,

$$N_A = D_{AB} \left[\frac{dC_A}{dz} \right] \quad (4.1)$$

Where N_A is the flux, D_{AB} is the binary diffusion coefficient of either ethanol and carbon dioxide or HMDS and carbon dioxide. C_A is the concentration of ethanol in CO₂ or concentration of HMDS in CO₂ (in terms of mol/m³).

The binary diffusion coefficient of ethanol/HMDS and carbon dioxide can be calculated at the extraction or modification reaction conditions using Schmidt number correlation proposed by Funazukuri and Wakao [48];

$$Sc^+ = \frac{Sc}{Sc^*} = 1 + \exp \left[\sum_{i=0}^5 a_i \left(\frac{v_0}{v} \right)^i \right] \quad (4.2)$$

$$Sc^* = \frac{5}{6} \left[\frac{\sigma_1 + \sigma_2}{2\sigma_2} \right]^2 \left[\frac{2M_1}{M_1 + M_2} \right]^{1/2} \quad (4.3)$$

Where Sc is Schmidt number at high pressure and Sc^* is at atmospheric pressure at the same temperature, v is the molar volume, σ_1 and σ_2 are the hard sphere diameters of

solute and solvent respectively. v_0 is the hard sphere closest packed volume of solvent molecules which can be calculated for carbon dioxide as;

$$v_0 = \frac{1}{1.384} \left(\sum_{i=0}^4 c_i T^i \right) \quad (4.4)$$

Then D_{AB} is calculated using the formula;

$$D_{AB} = \frac{\mu}{\rho \cdot Sc} \quad (4.5)$$

Where μ is the viscosity of CO_2 . The constants a_i and c_i used in 4.2 and 4.4 can be found in Appendix 1. Next effective diffusion coefficient, $D_{e,p}$ is found. Effective diffusion coefficient is a modified form of D_{AB} which takes into account the porosity (ε_p) and tortuosity (τ) of the silica aerogel. Tortuosity can be adjusted varying from less than unity to more than 6 depending on experimental data. Tortuosity is defined as the ratio of the actual distance of a molecule that travels between two molecules to the shortest distance between those two points. The equation for effective diffusion coefficient is given below.

$$D_{e,p} = \frac{F(\lambda) \varepsilon_p D_{AB}}{\tau} \quad (4.6)$$

$D_{e,p}$ values are used instead of D_{AB} in 4.1 for time determination. The time varies with aerogels of different volumes.

In the case of diffusion of HMDS to CO_2 in the pores of the aerogel, Fick's first law of diffusion is also used. Using the boundary conditions and $D_{e,p}$ value which is found to be $2.5 \cdot 10^{-9} \text{ m}^2/\text{s}$ by using the excel simulation (uses equations 4.2-4.6) shown in appendix 1, time needed for diffusion of HMDS to CO_2 in the pores of the aerogel can be calculated. The boundary conditions can be shown in Figure 4.7 for the modification of the silica aerogel sample with thickness of 0.0017 m using a mass fraction of 0.0013 HMDS (corresponding to 88 mol of HMDS / m^3).

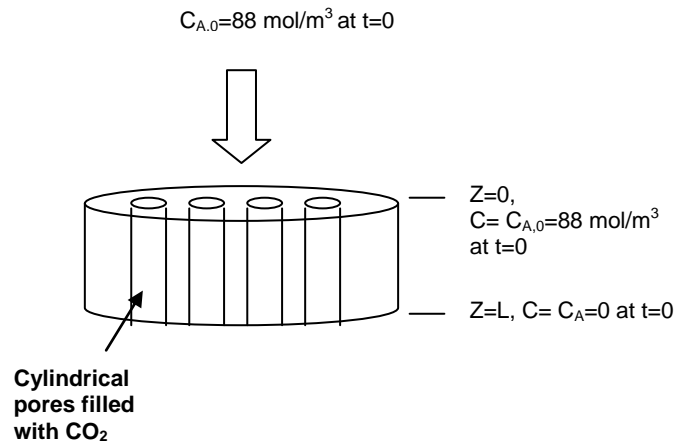


Figure 4.7 Boundary conditions

Assuming that the system is at steady state and N_A is found by

$$N_A = \frac{D_{e,p} \cdot (C_{A,0} - 0)}{L} \quad (4.9)$$

Time can be found by dividing the length of the sample by the diffusion velocity, V

$$t = \frac{L}{V} \quad (4.10)$$

Diffusion velocity is the ratio between the flux and the concentration of HMDS.

$$V = N_A / C_{A,0} \quad (4.11)$$

After performing the calculations, time required for the diffusion of HMDS was found as 20 minutes.

Also an analytical method can be followed in order to determine the time for unsteady-state diffusion into the aerogel pores. The mass transferred at any time is abbreviated as M_t and the maximum uptake as time, t becomes infinitely large is abbreviated as M_∞ . From the graphic [49] shown in Appendix 1, a relationship between

M_t / M_∞ and $\sqrt{D_{e,p} \cdot t} / L^2$ can be read. For $M_t = M_\infty$, the value of $\sqrt{D_{e,p} \cdot t} / L^2$ is found to be 1.6. Using this value, t is determined as 50 minutes for a sample of length, L equal to 0.0017 m and the same $D_{e,p}$ value in the above calculation which is $2.5 \cdot 10^{-9} \text{ m}^2/\text{s}$.

According to the results of the calculations, it is determined that 30 minutes is an efficient time for conducting surface modification reaction. Furthermore, the reaction in the pores should be taken into consideration. Since there is a reaction, there is a depletion of HMDS which would result in a high concentration gradient in the pore. As

a result, the time for diffusion through the thickness of the aerogels is relatively short (30 minutes vs. 10 hours at similar flow rates of CO₂, around 50 ml/h, in both processes).

4.3 Vapor-liquid phase equilibria results

4.3.1 Phase diagram of CO₂-HMDS binary mixture

The P-T phase diagram for CO₂-HMDS binary mixture could be obtained by using global phase equilibria calculations (GPEC) which uses pure component properties (T_c , P_c and ω are the critical temperature, critical pressure and acentric factor of the pure components, respectively) obtainable in the literature [50].

Table 4.1 Pure component properties used in PRSVEOS

Substance	Critical temperature (K)	Critical pressure (bar)	Acentric factor
CO ₂	304.19	73.82	0.23
HMDS	544	19.2	0.51

It was found that CO₂-HMDS binary mixture presents a type II phase behavior as shown in Figure 4.8 a in P-T section. The result of GPEC program is included in Appendix 2.

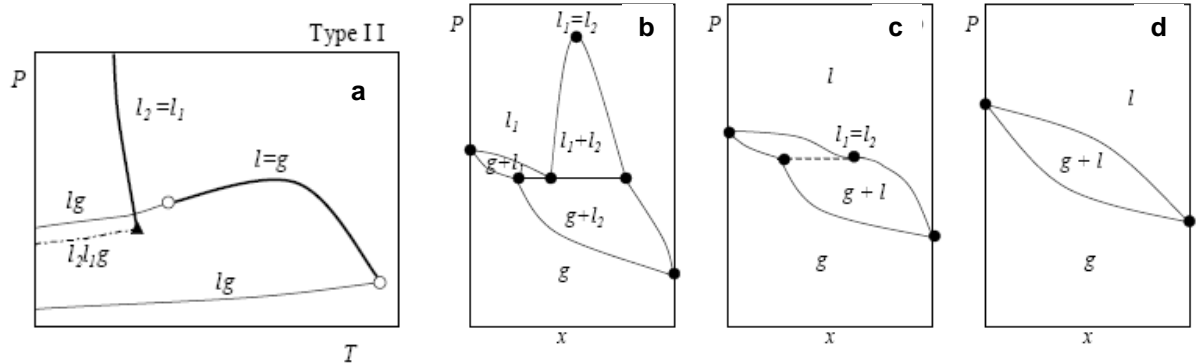


Figure 4.8 a) HMDS-CO₂ binary mixture presents a type II phase behavior, and P-x sections for type II b) $T < T_{UCEP}$, c) $T = T_{UCEP}$, d) $T_{UCEP} < T < T_c$

In type II fluid phase behavior, next to a continuous $l=g$ critical curve at low temperature also a $l_2=l_1$ critical curve and a three-phase curve l_2l_1g is found, which intersect in a UCEP $(l_2=l_1)+g$. This critical curve runs steeply to high pressure and represents upper critical solution temperatures. In P,T,x -space a two phase (l_2+l_1) region is found at temperatures lower than the $l_2=l_1$ critical curve and pressures higher than the three-phase curve. Figure 4.8 shows three P,x -sections for a type II system. Figure 4.8b is at $T < T_{UCEP}$, Figure 4.8c is at $T = T_{UCEP}$ and Figure 4.7c is at $T_{UCEP} < T < T_c$. In Figure 4.8c the bubble-point curve shows a horizontal point of inflection at the $l_2=l_1$ critical point. At higher temperatures the P,x -sections are similar to type I where there is only one critical curve, the $l=g$ critical curve, which runs continuously from the critical point of component A (CO₂) to the critical point of component B (HMDS) (see figure. 2.13). The P-x section of type I is as P-x section of type II shown in 4.7c where the upper line represents the bubble point curve and the lower curve represents the dew point curve.

4.3.2 Testing the accuracy of the data obtained by the bubble pressure measurement set-up (figure3.3)

The phase behavior of the HMDS-CO₂ binary mixture was studied by determining bubble point pressures at various HMDS concentrations and temperatures. Before conducting the experiments for this system, the accuracy of the experimental technique was tested by determining the bubble point pressures of the widely studied ethanol-CO₂ binary mixture at 333K. As seen in the isothermal P-x plot in Figure 4.9, the data are in good agreement with the results in literature [51, 52, 53]. The data in Figure 4.9 is given in Table 4.2.

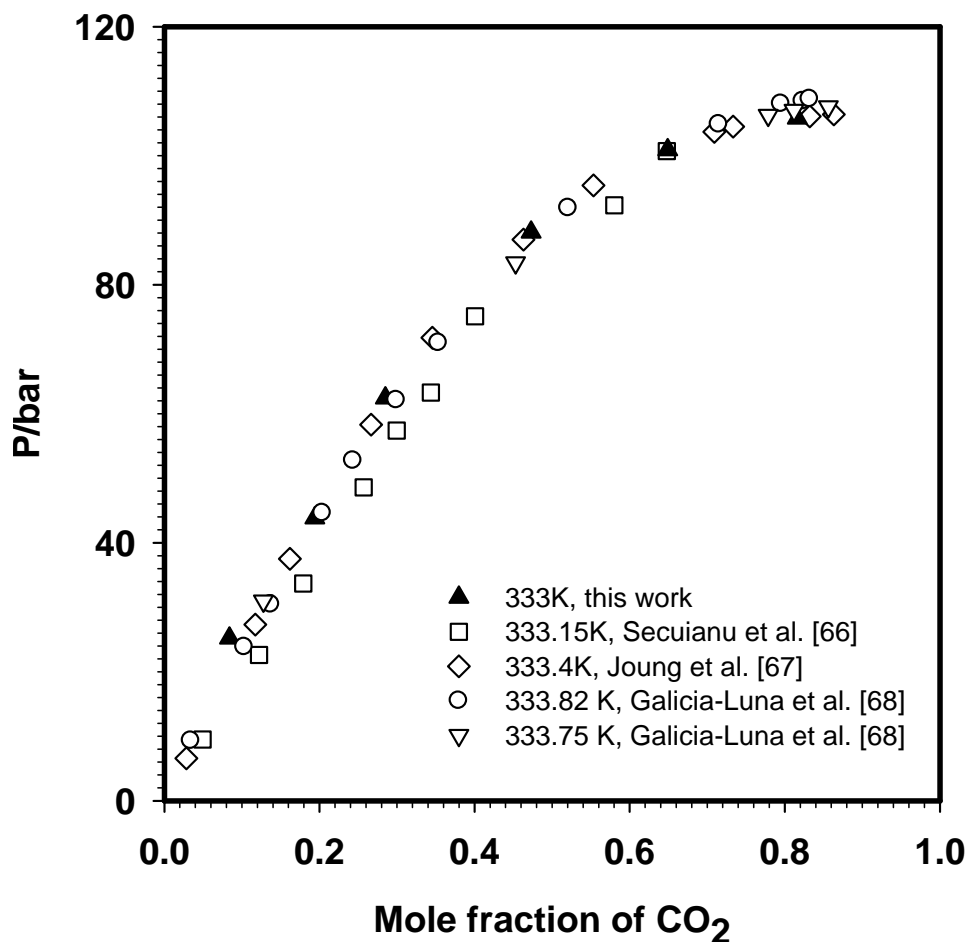


Figure 4.9 Comparison of bubble points for ethanol-carbon dioxide binary mixtures in the literature and obtained in this study

Table 4.2 Experimental Data for Ethanol- Carbon dioxide Binary Mixture at 333 K

Mole fraction of Carbon dioxide	Bubble point Pressure (bar)
0.084	24
0.194	43
0.285	62
0.473	87
0.649	100
0.816	106

Thus bubble points of HMDS-CO₂ system were obtained for various compositions and temperatures using this set-up. The experimental results are shown in Figure 4.9. At fixed temperature, as the mole fraction of CO₂ increased, the bubble point pressure of the mixture increased and at fixed composition, as the temperature increased the bubble point pressures also increased.

4.3.3 Modeling

The starting point for any phase equilibrium calculations is the equality criterion which states that fugacities of each species in each phase at the same temperature and pressure

$$\hat{f}_i^L(T, P, x_i) = \hat{f}_i^V(T, P, y_i) \quad (4.12)$$

where subscripts L and V refers to vapor and liquid phases respectively. Equation 4.1 can also be written as

$$\hat{\phi}_i^L x_i = \hat{\phi}_i^V y_i \quad (4.13)$$

by introducing the fugacity coefficients, $\hat{\phi}_i^L = \frac{\hat{f}_i^L}{P_i}$ and $\hat{\phi}_i^V = \frac{\hat{f}_i^V}{P_i}$,

Since $\sum_i y_i = 1$ ($y_1 + y_2 = 1$ for a binary mixture), the following equation should hold

for a binary mixture at equilibrium

$$\frac{\hat{\phi}_1^L}{\hat{\phi}_1^V} x_1 + \frac{\hat{\phi}_2^L}{\hat{\phi}_2^V} x_2 = 1 \quad (4.14)$$

The fugacity coefficient of component i for vapor phase can be calculated by [54]

$$\ln \hat{\phi}_i^V = \frac{1}{RT} \int_{\infty}^V \left[\frac{RT}{V} - N \left(\frac{\partial P}{\partial N_i} \right)_{T,V,N_{j \neq i}} \right] dV - \ln \frac{PV}{RT} \quad (4.15)$$

and the fugacity coefficient for the component i for liquid phase can be calculated analogously for the liquid phase by changing the subscript to L. The ratio of fugacity coefficients for L to V in 4.14 for component 1 and 2 can also be abbreviated by K_1 and K_2 respectively and 4.14 can also be written as

$$K_1 x_1 + K_2 x_2 = 1 \quad (4.16)$$

Algorithm for bubble point pressure calculations

The algorithm for calculating bubble point pressure is shown in Figure 4.10. For starting the bubble point pressure calculation, the liquid composition, x_i , and the temperature, T , are known and the vapor phase composition, y_i , and the pressure, P , must be calculated. For the iterative calculations, an initial guess for the bubble point pressure and the vapor-phase composition is needed. Furthermore, equation of state parameters are included for estimating fugacity coefficients. An initial guess for the pressure is assumed and the fugacity coefficient of each component in the liquid phase can be calculated. The fugacity coefficients of each component can be calculated for the vapor phase by using the assumed vapor composition of component i also. Consequently a first estimate of the vapor composition is evaluated. Using this vapor composition value, the fugacity coefficients of each species in the vapor phase are reevaluated. If $\sum_i K_i x_i$ changes, the vapor composition of component i is reevaluated using the value of $\sum_i K_i x_i$. This is repeated until the two successive values of $\sum_i K_i x_i$ are equal to each other. When this condition is established, the criterion of equilibrium which is shown in equation 4.16 is questioned. If equilibrium is achieved, the assumed P is concluded as the bubble point pressure. If not, a new pressure is assumed until the bubble point pressure is found.

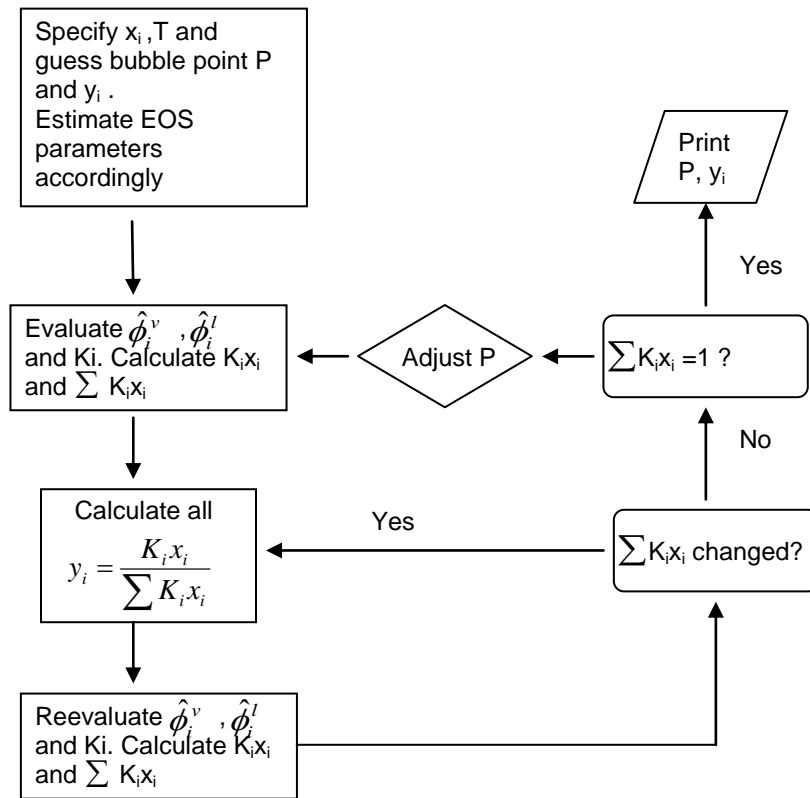


Figure 4.10 Algorithm for calculating bubble point pressure

In our model, we have used Peng-Robinson Stryjek-Vera EOS (PRSVEOS) [55]. PRSVEOS is a modified form of Peng-Robinson EOS and expressed in generalized form as:

$$P = \frac{RT}{V-b} - \frac{a(T)}{V(V+b)+b(V-b)} \quad (4.17)$$

Now defining a reduced temperature Tr ($Tr = T/T_c$), equation of state parameters can be found by using the pure component properties listed in Table 4.1. The constants a and b are determined using the following equations from 4.18 to 4.22

$$a(T) = 0.45724 \frac{R^2 T_c^2}{P_c} \alpha(T_r) \quad (4.18)$$

$$b = 0.07780 \frac{RT_c}{P_c} \quad (4.19)$$

where

$$\alpha(T_r) = \left[1 + \kappa (1 - \sqrt{T_r}) \right]^2 \quad (4.20)$$

κ in 4.20 is expressed by

$$\kappa = \kappa_0 + \kappa_1(1 + \sqrt{T_r})(0.7 - T_r) \quad (4.21)$$

where

$$\kappa_0 = 0.378893 + 1.4897153\omega - 0.17131848\omega^2 + 0.0196554\omega^3 \quad (4.22)$$

and κ_1 is found by fitting the vapor pressure curve for each compound by a computer program (see Appendix 2). κ_1 values for the components are given in Table 4.3.

Table 4.3 κ_1 parameter regressed for the pure components in the PRSVEOS

Substance	κ_1
CO ₂	0.0807
HMDS	0.0517

Furthermore, mixing rules are used to represent a and b for mixtures. We have used 1-parameter van derWaals mixing rules which are given by

$$a = \sum_i \sum_j x_i x_j a_{ij} \quad (4.23)$$

$$b = \sum_i x_i b_i \quad (4.24)$$

where x_i and x_j and the liquid mole fractions for pure components i . For vapor phase a and b , liquid mole fractions are replaced by vapor mole fractions and

$$a_{ij} = \sqrt{a_{ii}a_{jj}}(1 - k_{ij}) = a_{ji} \quad (4.25)$$

Here a new parameter k_{ij} , known as the binary interaction parameter, has been introduced to obtain better agreement in mixture EOS calculations. This parameter is found by fitting the EOS data by using the software provided in Orbey and Sandler (see Appendix 3) [56]. The software uses the fugacity coefficient calculation shown in 4.26

$$\ln \hat{\phi}_i^V = \frac{b_i}{b}(Z^V - 1) - \ln(Z^V - B) - \frac{A}{2.828B} \left(\frac{2 \sum y_j a_{ij}}{a} - \frac{b_i}{b} \right) \ln \left(\frac{Z^V + 2.414B}{Z^V - 0.414B} \right) \quad (4.26)$$

where V is replaced by L for liquid phase fugacity. Then, the algorithm for determining the bubble point pressure is followed.

The correlation results using the EOS model are shown in Figure 4.11 along with the experimental results. With the optimally fit k_{12} , satisfactory accuracy for the

calculated bubble point pressure was observed by the EOS model with an absolute average deviation (AAD) 2.45 % (0.555% for 298.8K, 3.332% for 313.5K, 2.877% for 327.7K and 3.018% for 342K). The calculation of AAD values can be seen in Appendix 4. It should be noted that, at the highest temperature, the model shows a big variation compared to the experimental data near the critical point which is above the AAD calculated for this set of data.

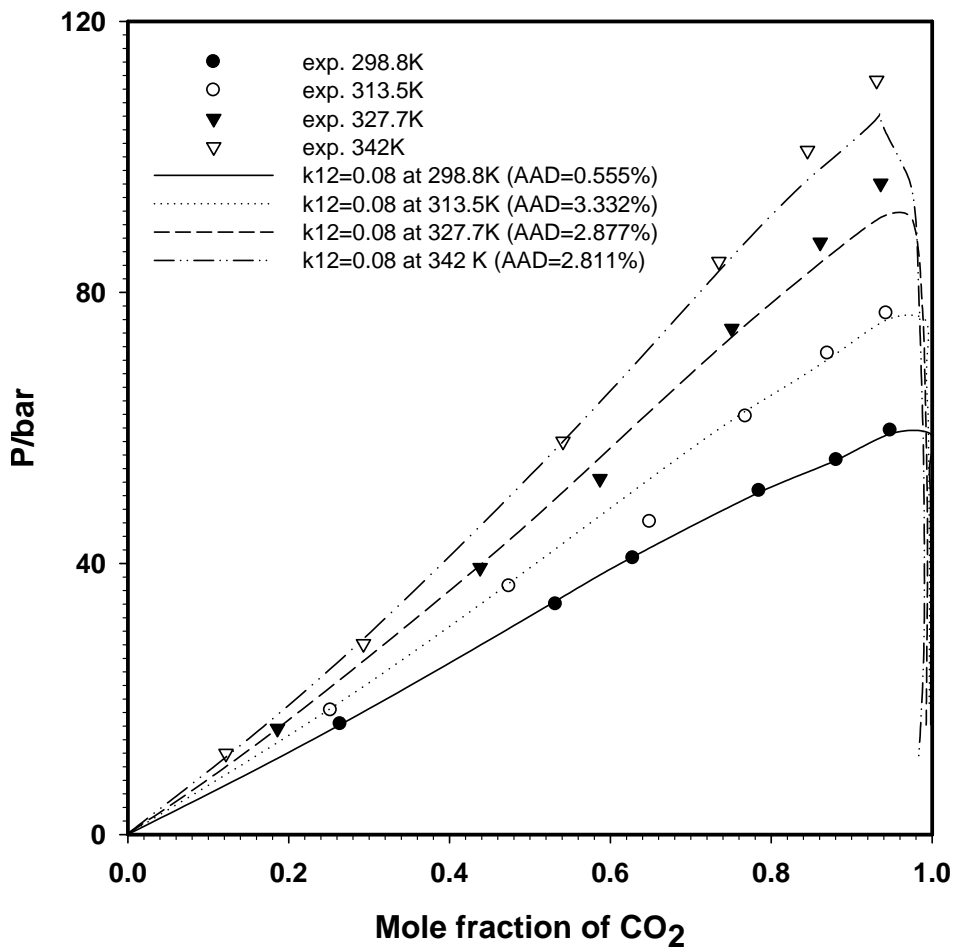


Figure 4.11 Bubble point pressure data for various temperatures and mole fraction of CO_2

Ideal solution model

A less complicated model, ideal solution model using Raoult's law for a binary mixture was also tested. Raoult's law uses the pure component vapor pressure values,

thus the model is derived for a temperature where each component has vapor pressures (below components critical temperature). The starting equation for Raoult's law is

$$y_i P = x_i P_i^{sat} \quad (4.15)$$

where P_i^{sat} is the vapor pressure of component i . Since $y_1 + y_2 = 1$, bubble point pressure P is be found easily using the vapor pressures of pure components and their mole fractions by reducing (4.15) to

$$P = x_1 P_1^{sat} + x_2 P_2^{sat} \quad (4.16)$$

The vapor mole fractions were also determined by rearranging (4.15) and solving for y_i

$$y_i = \frac{x_i P_i^{sat}}{P} \quad (4.17)$$

Using these values, a bubble point pressure vs. mole fraction of one of the components can be constructed. The vapor pressure of CO₂ and HMDS which are used in these equations are 64.83 bar and 0.026 bar respectively. The results are presented in Figure 4.12

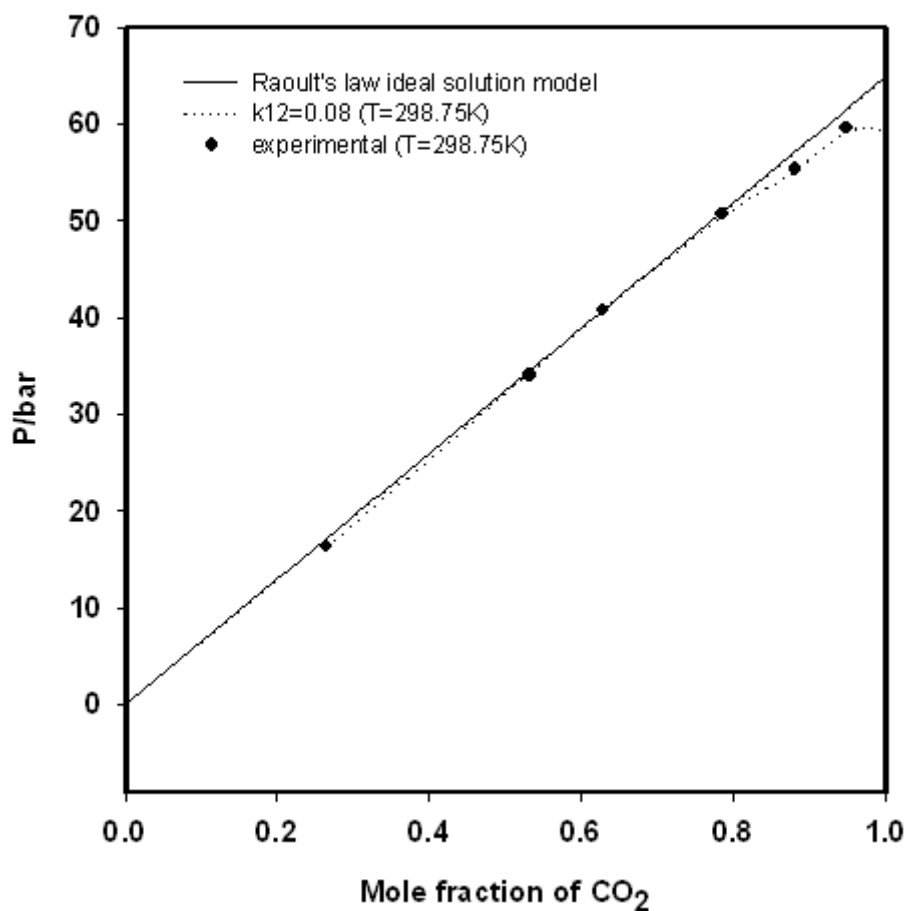


Figure 4.12 The bubble point pressure results at 298.75K for various mole fractions of CO₂

It is interesting to see that a mixture of such dissimilar molecules of CO₂ and HMDS (see figure 4.13) behave close to an ideal mixture. Furthermore, EOS model also agrees with ideal mixture model and experimental results since the AAD in pressure is only 0.555%.

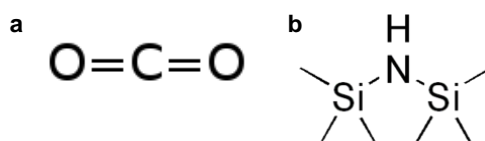


Figure 4.13 Molecular structures of a) CO₂ and b) HMDS

Chapter 5

CONCLUSIONS

We have demonstrated the surface chemical modification of silica aerogels by using HMDS in CO₂ at a pressure of 20.68MPa and at a temperature of 333.2K. The hydrophobicity of the silica aerogels were analyzed by the contact angle test and the values of 130° could be achieved. Also FTIR investigations on treated samples clearly indicated the hydrophobicity of the treated aerogels by the reduction of the silanol bands and the emergence of the methyl bands. The modified aerogels which are as transparent as their initial state can be obtained. Moreover, the modified aerogels showed no significant weight change compared to their initial state. This was attributed to the formation of a monolayer of silanes. A simple calculation for determining the weight of the silane monolayer on the modified sample showed that the weight change was 1% of the initial weight of the sample (0.005 g). Thus we have concluded that there would have been an apparent weight increase if more than monolayer was formed.

In addition, silation mechanism was also investigated by studying the diffusivity of HMDS to CO₂ which filled the pores of the silica aerogels. The diffusion of HMDS into the pores was compared to the opposite of extraction of ethanol from the pores of the aerogel for drying. It was concluded that the CO₂ was a good solvent for HMDS treatment and an efficient silation reaction can be carried out in a relatively short time such as 30 minutes. Calculations based on Fick's first law of diffusion and analytical methods were also performed to find the time for diffusion of HMDS. These were 20 minutes and 50 minutes respectively.

Furthermore, we have determined the bubble point data of binary mixture HMDS and CO₂ for various mole fractions and temperatures. The bubble point pressure decreases as the mole fraction of CO₂ decreases for a fixed temperature and it increases as the temperature increases. PRSVEOS was found to represent the data successfully with an average absolute deviation of 2.45 % for a constant binary interaction parameter which is determined by a computer simulation.

In addition, it was seen that at 278.8K, the binary mixture HMDS and CO₂ showed a closed resemblance to ideal solution model despite the large difference in the molecular structures of HMDS and CO₂.

BIBLIOGRAPHY

-
- [1] A. V. Rao, G. M. Pajonk, S. D. Bhagat, P. Barboux, Comparative studies on surface chemical modification of silica aerogels based on various organosilane compounds of the type R_nX_{4-n} , *J. Non-Cryst. Solids*, 350 (2004) 216
- [2] A. V. Rao, R. R. Kalesh, Organic surface modification of TEOS based silica aerogels synthesized by co-precursor and derivatization method, *J. Sol-gel Sci. Technol.*, 30 (2004) 141
- [3] V. M. Gun'ko, M. S. Vedamuthu, G. L. Henderson, J. P. Blitz, Mechanism and kinetics of hexamethyldisilazane reaction with fumed silica surface, *J. Colloid Interface Sci.* 228 (2000) 157
- [4] P. M. Shewale, A.V. Rao, A. P. Rao, Effect of different trimethyl silylating agents on the hydrophobic and physical properties of silica aerogels, *Appl. Surf. Sci.*, 254 (2008) 6902
- [5] S.V. Slavov, A. R. Sanger, K. T. Chuang, Mechanism of silation of silica with hexamethyldisilazane, *J. Phys. Chem. B.*, 104 (2000) 983
- [6] T. S. Zemanian, G. E. Fryxell, J. Liu, S. Mattigod, J. A. Franz, Z. Nie, Deposition of self assembled monolayers in mesoporous silica from supercritical fluids, *Langmuir* 17 (2001) 8172.
- [7] J. R. Combes, L. D. White, C. P. Tripp, Chemical modification of metal oxide surfaces in supercritical CO₂: In situ infrared studies of the adsorption and reaction of organosilanes on silica, *Langmuir* 15 (1999) 7870
- [8] C. Cao, A.Y. Fadeev, T. J. McCarthy, Reactions of organosilanes with silica surfaces in carbon dioxide, *Langmuir* 17 (2001) 757
- [9] (2009) <http://www.sciencedirect.com> [August, 2009]
- [10] A. S. Dorcheh, M. H. Abbasi, Silica aerogel; synthesis, properties and characterization, *Journal of Materials Processing Technology* 199 (2008) 10-26
- [11] G. M. Pajonk, Transparent silica aerogels, *J. Non-Cryst. Solids*, 225 (1998) 307-314.
- [12] A.C. Pierre, G. M. Pajonk, Chemistry of aerogels and their applications, *Chem. Rev.* 102 (2002) 4243-4265
- [13] M. Schmidt, F. Schwertfeger, Applications for silica aerogel products, *J. Non-Cryst. Solids*, 225 (1998) 364-368

-
- [14] T. Woignier, J. Phalippou, Mechanical Strength of Silica Aerogels, *Journal of Non-Crystalline Solids*, 100 (1988) 404-408
- [15] M. A. Einarsud, E. Nilsen, A. Rigacci, G. M. Pajonk, S. Buathier, D. Valette, M. Durant, B. Chevalier, P. Nitz, F. E. Dolle, Strengthening of silica gels and aerogels by washing and aging, *J. Non-Cryst. Solids*, 285 (2001) 1-7
- [16] B.E. Yoldas, M. J. Annen, J. Bostaph, Chemical Engineering of Aerogel Morphology Formed under Nonsupercritical Conditions for Thermal Insulation, *Chem. Mater.* 12 (2000) 2475-2484
- [17] W. C. Ackerman, M. Vlachos, S. Rouanet, J. Fruendt. Use of surface treated aerogels derived from various silica precursors in translucent insulation panels. *J. Non-Cryst. Solids*, 285 (2001) 264-271
- [18] G. M. Pajonk, E. Elaloui, B. Chevalier, R. Begag, Optical transmission properties of silica aerogels prepared from polyethoxidisiloxanes, *J. Non-Cryst. Solids*, 210 (1997) 224-231
- [19] G. M. Pajonk, Transparent silica aerogels, *J. Non-Cryst. Solids*, 225 (1998) 307-314.
- [20] A. J. Hunt, Light scattering for aerogel characterization, *J. Non-Cryst. Solids*, 225 (1998) 303-306.
- [21] W. Cao, A. J. Hunt, Improving the visible transparency of silica aerogels, *J. Non-Cryst. Solids*, 176 (1994) 18-25
- [22] A. R. Buzykaev, A. F. Danilyuk, S. F. Ganzhur, E. A. Kravchenko and A. P. Onuchin, Measurement of optical parameters of aerogel, *Nuclear Instruments and Methods in Physics Research Section A: Accelerators, Spectrometers, Detectors and Associated Equipment*, 433 (1999) 398-400.
- [23] S. Gauthier, J. P. Aime, T. Bouhacina, A. J. Attias, B. Desbat. Study of grafted silane molecules on silica surfaces with an atomic force microscopy, *Langmuir*, 12 (1996) 5126-5137
- [24] P.G. Pape, (2008). Silylating agents. In *Kirk-Othmer Encyclopedia of Chemical Technology* [e-book]. John Wiley & Sons, Inc. Available at Koç University Library/ e-books <http://0mrw.interscience.wiley.com.libunix.ku.edu.tr/emrw/9780471238966/kirk/article/aeroko.a01/current/pdf> [Accessed 4 August, 2009]
- [25] P. B. Wagh, S. V. Ingale, Comparison of some physico-chemical properties of hydrophilic and hydrophobic silica aerogels, *Ceramics International*, 28 (2002) 43-50
- [26] D. Y. Nadagi, A. V. Rao, Methyltriethoxysilane: New precursor for synthesizing silica aerogels, *Journal of Alloys and Compounds* 467 (2009) 397-404

-
- [27] C. P. Tripp, M. L. Hair, An infrared study of the reaction of octadecyltrichlorosilane with silica, *Langmuir*, 8 (1992) 1120-1126
- [28] C. P. Tripp, M. L. Hair, Reaction of alkylchlorosilanes with silica at the solid/gas and solid/liquid interface, *Langmuir*, 8 (1992) 1961-1967
- [29] W. Yoshinda, R.P. Castro, J. Jou, Y. Cohen, Multilayer alkoxy silane silylation of oxide surfaces, *Langmuir*, 17 (2001) 5882-5888
- [30] K. H. Lee, S. Y. Kim, K. P. Kim, K. P. Yoo, Low-density, hydrophobic aerogels, *J. Non-Cryst. Solids*, 186 (1995) 18
- [31] H. Yokogawa, M. Yokogawa, Hydrophobic Aerogels, *J. Non-Cryst. Solids*, 186 (1995) 23
- [32] (2009) alchemy.chem.uwm.edu/research/dietz/ [September, 2009]
- [33] F. Cansell, C. Aymonier, A. Loppinet-Serani, Review on materials science and supercritical fluids, *Current Opinion in Solid State and Materials Science*, 7, (2003), 331-340.
- [34] F. Cansell, B. Chevalier, A. Demourgues, J. Etourneau, C. Even, Y. Garrabos, V. Pessey, S. Petit, A. Tressaud and F Weill, Supercritical fluid processing: a new route for materials synthesis, *J. Mater. Chem.*, 9, (1999), 67-75
- [35] E.J. Beckman, Supercritical and near critical CO₂ in green chemical synthesis and processing, *Journal of Supercritical Fluids*, 28 (2004) 121-191
- [36] F. Cansell, B. Chevalier, A. Demourgues, J. Etourneau, C. Even, Y. Garrabos, V. Pessey, S. Petit, A. Tressaud and F Weill, Supercritical fluid processing: a new route for materials synthesis, *J. Mater. Chem.*, 9, (1999), 67-75
- [37] X. Jia, T. J. McCarthy, Buried interface modification using supercritical carbon dioxide, *Langmuir*, 18 (2002) 683-687
- [38] S. Higgings, B. A. McCool, C.P. Tripp, D. M. Ruthven, W. J. DeSisto, Covalent attachment of monochlorosilanes to mesoporous silica membranes using super critical fluid deposition, *Separation Science and Technology*, 43 (2008) 4113-4128
- [39] A. I. Cooper, Porous materials and supercritical fluids, *Advanced Materials*, 15 (2003) 1049-1059
- [40] K.S. Morley, P.C. Marr, P.B. Webb, A.R. Berry, F.J. Allison, G. Moldovan, P.D. Brown, S.M. Howdle, Clean preparation of nanoparticulate metals in porous supports: a supercritical route, *J. Mater. Chem.* 12 (2002) 1898.

-
- [41] F. E. Henon, R. G. Carbonell, J. M. Desimone, Effect of polymer coatings from CO₂ on water-vapor transport in porous media. *AICHE Journal*, 48 (2002) 941-952
- [42] A. Y. Fadeev, T. J. McCarthy, Trialkyl monolayers covalently attached to silicon surfaces: wettability studies indicating that molecular topography contributes to contact angle hysteresis, 15 (1999) 3759
- [43] P. Atkins, J. de Paula, *Atkins' Physical Chemistry*. Seventh edition. Oxford University Press Inc. New York, 2002
- [44] A.V. Rao, M.M. Kulkarni, Hydrophobic properties of TMOS/TMES-based silica aerogels, *Materials Research Bulletin*, 37 (2002) 1667-1677
- [45] S. Hofmann, (2008). Surface and interface analysis. In *Kirk-Othmer Encyclopedia of Chemical Technology* [e-book]. John Wiley & Sons, Inc. Available at Koç University Library/e-books <http://Omrw.interscience.wiley.com.libunix.ku.edu.tr/emrw/9780471238966/kirk/article/aeroko.a01/current/pdf> [Accessed 4 August, 2009]
- [46] H. El Rassy, A. C. Pierre, NMR and IR spectroscopy of silica aerogels with different hydrophobic characteristics, *J. Non-Cryst. Solids* 351 (2005) 1603
- [47] M. Lazghab, K. Saleh, P. Guigon, A new solventless process to hydrophobic silica powders in fluidized beds, *AICHE Journal*, 54 (2005) 897
- [48] T. Funazukuri, C.Y. Kong, S.Kagei, Impulse response techniques to measure binary diffusion coefficients under supercritical conditions, *J. Chromatogr. A*, 1037, (2004), 411-429.
- [49] A. L. Hines, R. N. Maddox, *Mass Transfer Fundamentals and Applications*, Prantice-Hall, Inc., New Jersey, 1985
- [50] C. L. Yaws *Handbook of Thermodynamic Diagrams*, Gulf Pub. Co. 1996
- [51] C. Secuianu, V. Feroiu, D. Geana. Phase behaviour for carbon dioxide + ethanol system: Experimental measurement and modeling with a cubic equation of state. 47 (2008) 109.
- [52] S.N. Joung, C.W. Yoo, H.Y. Shin, S.Y. Kim, K.-P. Yoo, C.S. Lee, W.S. Huh, Measurements and correlation of high-pressure VLE of binary CO₂-alcohol systems (methanol, ethanol, 2-methoxyethanol and 2-ethoxyethanol), *Fluid Phase Equilib.* 185 (2001) 219-230.
- [53] L.A. Galicia-Luna, A. Ortega-Rodriguez, D. Richon, New apparatus for the fast determination of high-pressure vapor-liquid equilibria of mixtures and of accurate critical pressures, *J. Chem. Eng. Data* 45 (2000) 265-271.

[54] S. I. Sandler, *Chemical and Engineering Thermodynamics*, second edition, John Wiley and Sons, Inc., 1989

[55] R. Stryjek, J. H. Vera. PRSV: An improved Peng-Robinson equation of state for pure compounds. *Can. J. Chem. Eng.* 64 (1986) 323

[56] H. Orbey, S. I. Sandler, *Modelling vapor-liquid equilibria cubic equations of state and their mixing rules*, Cambridge University Pres. 1998.

Appendix 1

DIFFUSION

- 1.1 Constants for Schmidt number correlation by Funazukuri and Wakao [48]**
- 1.2 Effective diffusion coefficient calculation by excel simulation**
- 1.3 Graphic for mass transfer into a slab with constant surface concentration**

1.1 Constants for Schmidt number correlation by Funazukuri and Wakao [48]**Table A1.1** Constants in correlation of Schmidt number with solvent molar volume (a_i) and effective hard-sphere packed volume (c_i) [48]

i	a_i	c_i
0	-4.92519817	4.452×10^{-5}
1	54.5529385	-1.152×10^{-7}
2	-245.231443	2.749×10^{-10}
3	607.893924	-3.073×10^{-13}
4	-708.884016	1.290×10^{-16}
5	329.611433	-

1.2 Effective diffusion coefficient calculation by excel simulation

A	B	C	D	E	F	G	H	I	J	K	L	M
1	i	Ci	T ^a i	Ci ^T ^a i	V0	V	(V0/V) ^a i	Ai ^T (V0/V) ^a i	Sc+	sigma1 (solute) (nm)	sigma2 (solvent) (nm)	
2	0	-4.92519817	4.452E-05	1	4.452E-05	1.942E-05	5.98E-05	1	-4.92519817	3.867873	1.0	0.4
3	1	5.45529386E+01	-1.152E-07	333	-3.836E-05	1.942E-05	5.98E-05	0.32479	17.71824031	M1 (solute)	M2 (solvent)	Sc*
4	2	-2.45231443E+02	2.749E-10	110889	3.048E-05	1.942E-05	5.98E-05	-25.86905282		161		44
5	3	6.07893924E+02	-3.073E-13	36926037	-1.135E-05	1.942E-05	5.98E-05	20.82740292				Sc
6	4	-7.08884016E+02	1.290E-16	12296370321	1.586E-06	1.942E-05	5.98E-05	-7.88832761				12.37138
7	5	3.29611433E+02			1.942E-05	5.98E-05	0.003612	1.190535844				
8												
9				SUM (Ci ^T ^a i)				SUM Ai ^T (V0/V) ^a i		p (scCO2) (kg/m3)	viscosity (cP) (60.3000 psi)	
10				2.688E-05				1.053570477		736.1	viscosity (kg/ms)	0.065
11											DAB	7.14E-09
12												
13												
14										porosity (εp)	tortuosity (τ)	
15										0.77	1.1929	
16										ds(solute diameter) (nm)	dp(pore diameter)(nm)	
17										1	7	
18										Λ (ds/dp)	F(Λ)	De,p
19										0.142857143	0.541561665	2.50E-09

1.4 Graphic for mass transfer into a slab with constant surface concentration

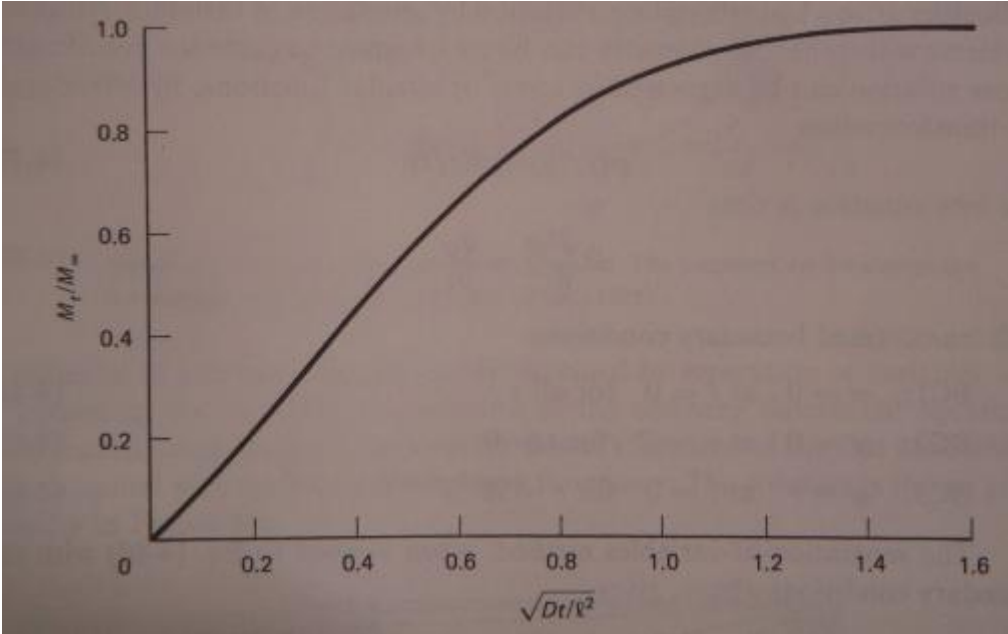


Figure A1.1 Mass transfer into a slab with constant surface concentration

Appendix 2

GLOBAL PHASE EQUILIBRIA CALCULATIONS (GPEC)

- 2.1 Program Input Window for System Carbon Dioxide Hexamethyldisilazane Calculation**
- 2.2 Program Output: Pressure-Temperature Diagram of System Carbon Dioxide Hexamethyldisilazane**
- 2.3 Type II Regions in Output Pressure-Temperature Diagram of System Carbon Dioxide Hexamethyldisilazane**
- 2.4 Excel Pressure-Temperature Diagram of System Carbon Dioxide Hexamethyldisilazane**
- 2.5 Excel Tables of Program Output Results**

2.1 Program Input Window for System Carbon Dioxide Hexamethyldisilazane Calculation

Maximum pressure for liquid - liquid critical line 2000 [Bar]

Binary System:

CARBON DIOXIDE
 CARBON DIOXIDE
 ETHANOL
 HEXAMETHYLDISILAZANE
 METHANE
 METHANOL
 n-BUTANE
 n-DECANE
 n-HEXANE
 n-TETRADECANE
 n-TRIDEDECANE
 PROPANE

Choose Model

Soave-Redlich-Kwong RK-PR
 Peng-Robinson PC-SAFT
 SPHCT GC-EOS

Choose Combining Rule

van der Waals
 Lorentz-Berthelot

Binary Interactions Parameters

K12 0.08 L12 0.0000

Fugacity vs. Composition (at specified T and P)
 Pressure vs. Density or Volume (at specified T and X1)

T [K] x1 min 0
 P [Bar] x1 max 1
 Composition Step 0.01

Plot

Component Constants and Model Parameters for CARBON DIOXIDE

Tc [K] 304.21 Pc [bar] 73.83 Vc [lt/mol] 0.094
 T_c^{EOS} [K] 304.21 P_c^{EOS} [bar] 73.83 V_c^{EOS} [lt/mol] 0.105313 ω 0.2236
 a_c [bar.m⁶/Kmol²] 3.96208 b [lt/mol] 0.026652 m 0.705994

Calculate Parameters Modify database

Added in 10-Dec-06 by No User available

Component Constants and Model Parameters for HEXAMETHYLDISILAZANE

Tc [K] 544 Pc [bar] 19.2 Vc [lt/mol] 0.613
 T_c^{EOS} [K] 544 P_c^{EOS} [bar] 19.2 V_c^{EOS} [lt/mol] 0.724166 ω 0.5101
 a_c [bar.m⁶/Kmol²] 48.71984 b [lt/mol] 0.183269 m 1.091113

Calculate Parameters Modify database

Added in 22-Jul-09 by No User available

NO GLOBAL DIAGRAM
 JUST A TWO-PHASE REGION

T [K] P [Bar]
 Po [Bar] To [K]
 ΔP_1 0.1 [Bar] ΔT_1 0.2 [K]
 Plot Plot

Estimation at Po
 X1
 Y2

Estimation at To
 X1
 Y2

Figure A2.1 GPEC Program Input Window

2.2 Program Output: P-T Diagram of CO₂-HMDS System

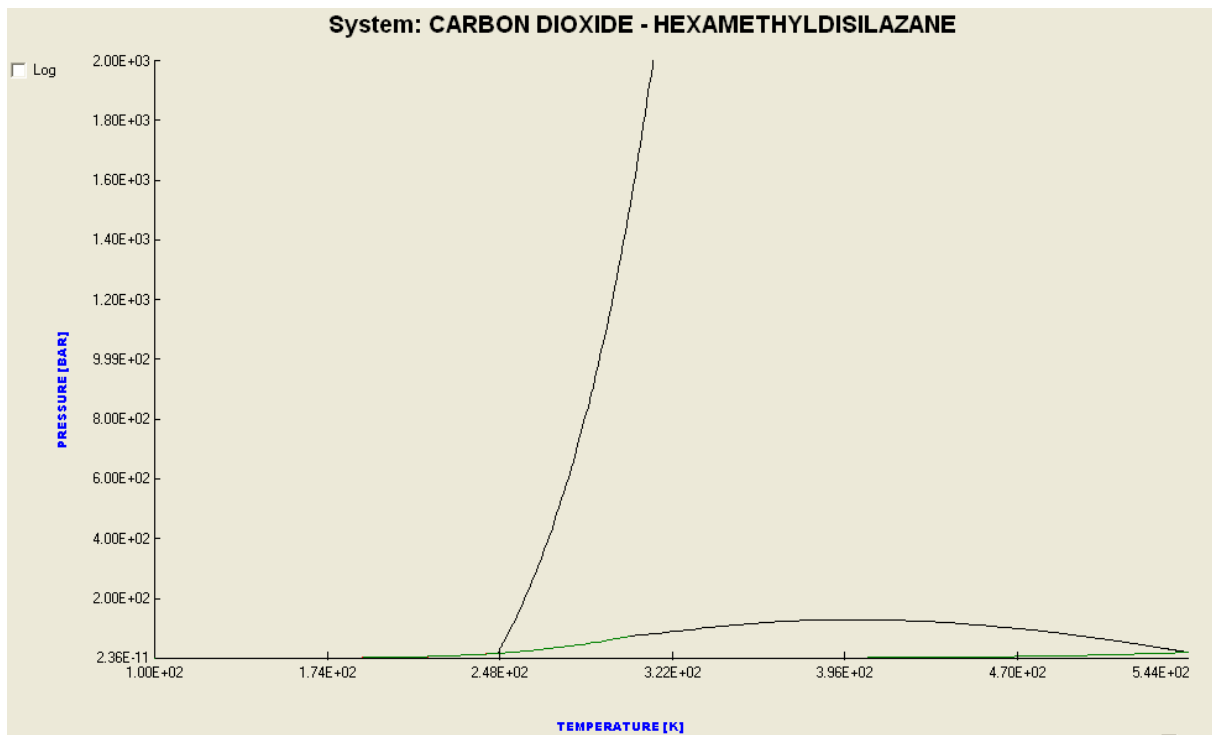


Figure A2.2 PT Diagram of all Regions

2.3 Type II Regions in : P-T Diagram of CO₂-HMDS System

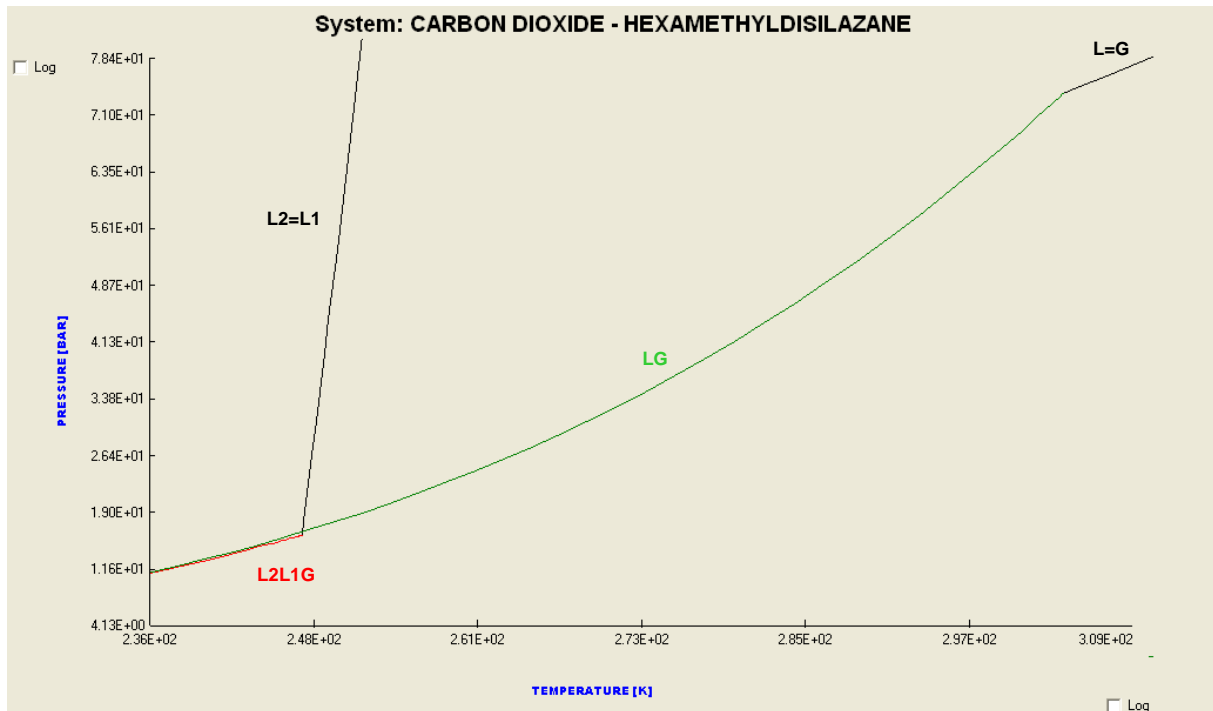


Figure A2.3 PT Diagram zoom in vapor pressure curve (LG), vapor-liquid critical curve (L=G), liquid1-liquid2 critical curve (L1=L2), three phase curve (L2L1G)

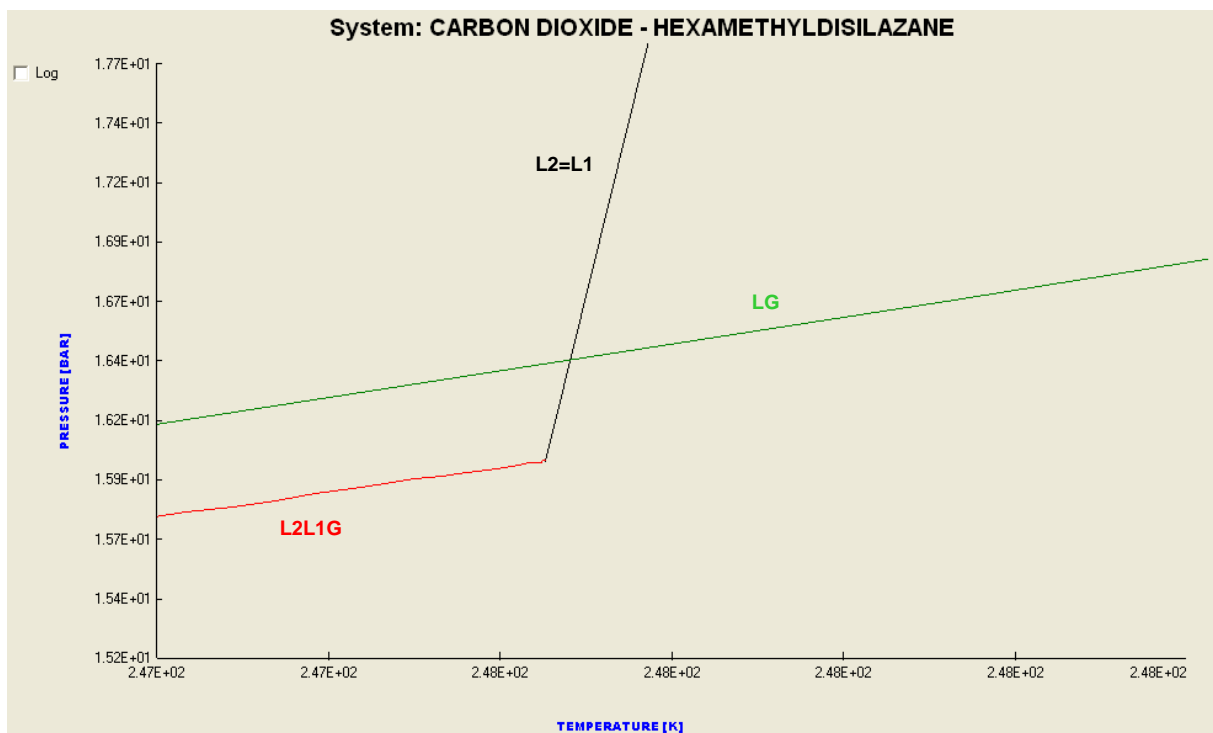


Figure A2.4 PT Diagram zoom in vapor pressure curve (LG), liquid1-liquid2 critical curve (L1=L2), three phase curve (L2L1G)

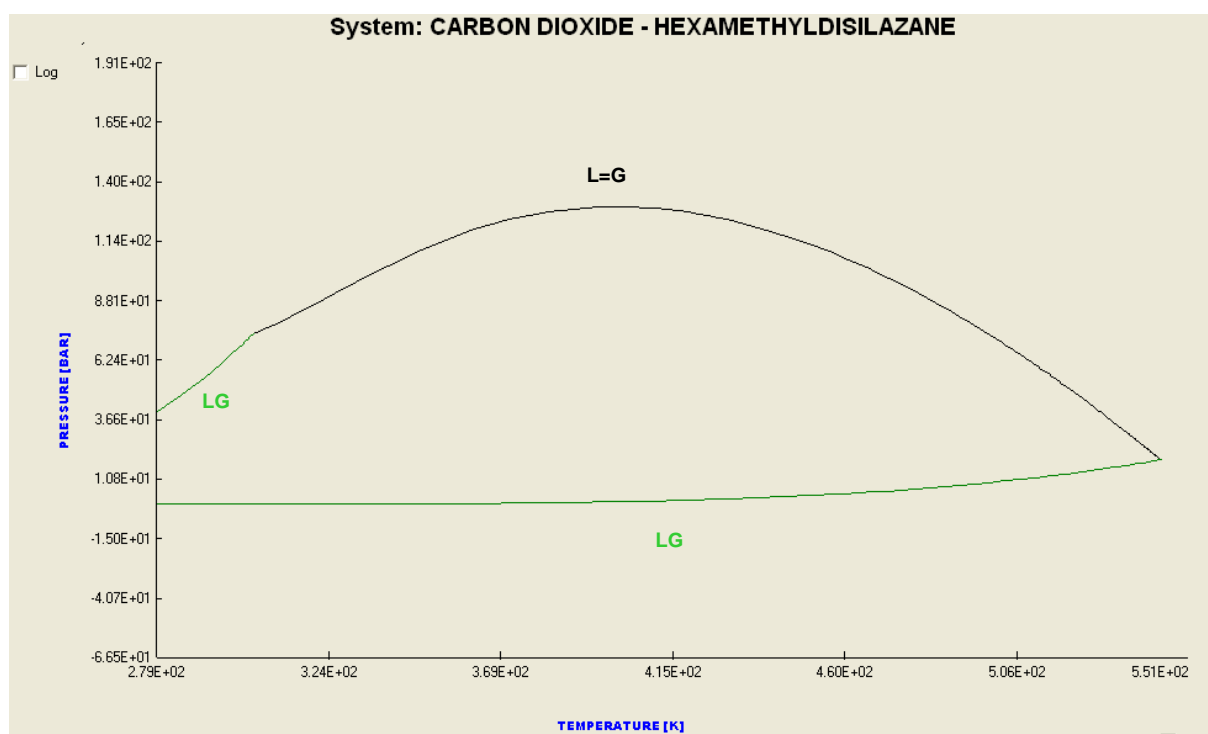


Figure A2.5 PT Diagram zoom in vapor pressure curve (LG), vapor-liquid critical curve (L=G)

2.4 Excel Pressure-Temperature Diagram of System Carbon Dioxide Hexamethyldisilazane

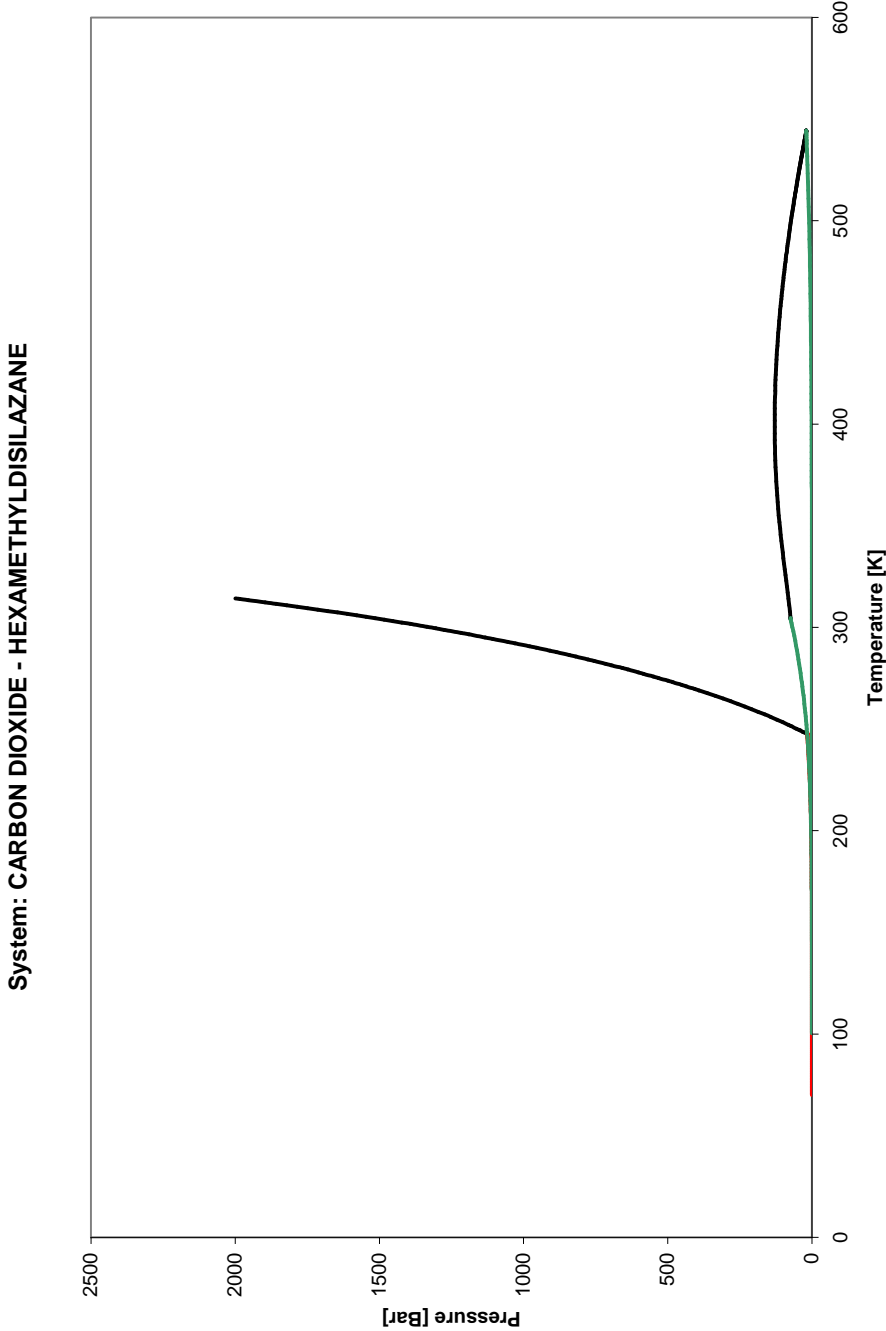


Figure A2.6 Excel P-T Daigram of Figure A2.1.

Table A2.1 Data of Diagram shown in Figure A1.2 and Figure A1.6

Critical Line 1		Critical Line 2		L-L-V Line 1		V- Pressure Line 1		V-Pressure Line 2	
T [K]	P [BAR]	T [K]	P [BAR]	T [K]	P [BAR]	T [K]	P [BAR]	T [K]	P [BAR]
544	19.2	314.31	1999	247.62	15.99	304.21	73.83	544	19.2
544	19.2027	314.04	1984	247.62	15.99	304.187	73.79	543.965	19.19
544	19.2063	313.49	1954.3	247.62	15.99	303.937	73.39	543.601	19.09
543.99	19.2134	312.41	1896.1	247.62	15.99	303.467	72.62	542.915	18.89
543.98	19.2276	311.68	1858.2	247.62	15.99	302.88	71.68	542.057	18.66
543.96	19.2561	310.96	1821	247.62	15.98	302.148	70.52	540.988	18.36
543.92	19.313	310.24	1784.5	247.61	15.98	301.235	69.09	539.654	18
543.83	19.4273	309.53	1748.6	247.61	15.98	300.098	67.34	537.992	17.56
543.66	19.6571	308.81	1713.3	247.6	15.98	298.212	64.52	535.232	16.84
543.46	19.9285	308.1	1678.7	247.59	15.97	295.871	61.13	531.802	15.98
543.26	20.2023	307.38	1644.6	247.57	15.96	293.514	57.86	527.565	14.97
543.05	20.4784	306.67	1611.2	247.55	15.95	291.175	54.75	523.361	14.01
542.84	20.7569	305.96	1578.3	247.52	15.94	288.855	51.78	519.191	13.11
542.63	21.0378	305.26	1546	247.49	15.92	286.553	48.96	515.054	12.27
542.42	21.3212	304.55	1514.3	247.46	15.91	284.27	46.28	510.95	11.47
542.21	21.6071	303.85	1483.1	247.42	15.89	282.005	43.72	506.879	10.71
541.99	21.8955	303.14	1452.5	247.38	15.87	279.758	41.3	502.84	10.01
541.78	22.1865	302.44	1422.3	247.33	15.85	277.529	38.99	498.833	9.34
541.56	22.48	301.74	1392.7	247.28	15.82	275.317	36.8	494.859	8.714
541.33	22.7762	300.35	1334.9	247.23	15.79	273.124	34.71	490.915	8.124
541.11	23.075	299.6	1304.6	247.17	15.77	270.947	32.73	487.004	7.57
540.88	23.3765	298.85	1274.7	247.11	15.74	268.788	30.85	483.123	7.05
540.65	23.6807	297.36	1216.6	247.05	15.7	266.647	29.07	479.274	6.562
540.42	23.9876	296.62	1188.3	246.94	15.65	264.522	27.38	475.455	6.103
540.19	24.2974	295.14	1133.3	246.8	15.58	262.414	25.77	471.666	5.673
539.95	24.61	294.4	1106.5	246.62	15.5	260.323	24.25	467.908	5.27
539.72	24.9254	292.93	1054.2	246.4	15.39	258.249	22.81	464.18	4.892
539.48	25.2438	292.2	1028.8	246.13	15.26	256.191	21.44	460.481	4.538
539.23	25.5651	290.75	979.25	245.79	15.1	254.15	20.14	456.812	4.206
538.99	25.8894	290.02	955.1	245.37	14.9	252.125	18.92	453.172	3.897
538.74	26.2167	288.57	908.04	244.84	14.65	250.116	17.75	449.561	3.607
538.49	26.5471	287.85	885.11	244.18	14.34	248.123	16.66	445.979	3.336
538.23	26.8805	286.42	840.4	243.35	13.97	246.146	15.62	442.425	3.083
537.98	27.2172	285.7	818.61	242.33	13.51	244.185	14.64	438.9	2.848
537.72	27.557	284.28	776.11	241.05	12.95	242.239	13.71	435.403	2.628
537.46	27.9	283.57	755.4	239.47	12.28	240.309	12.83	431.934	2.423
537.19	28.2463	282.15	714.99	237.5	11.49	238.394	12.01	428.492	2.232
536.92	28.596	281.45	695.29	235.14	10.58	236.494	11.23	425.078	2.055
536.65	28.949	280.04	656.86	232.8	9.726	234.61	10.49	421.691	1.89
536.38	29.3054	279.35	638.12	230.48	8.935	232.741	9.799	418.331	1.737
536.1	29.6653	277.95	601.55	228.19	8.198	230.886	9.146	414.997	1.594
535.82	30.0287	277.26	583.71	225.92	7.514	229.046	8.532	411.691	1.462
535.54	30.3957	275.88	548.9	223.67	6.879	227.221	7.954	408.41	1.34
535.25	30.7662	275.19	531.92	221.45	6.29	225.411	7.41	405.156	1.227
534.96	31.1405	273.81	498.77	219.24	5.745	223.615	6.899	401.928	1.122

534.67	31.5184	273.13	482.6	217.06	5.242	221.833	6.419	398.725	1.026
534.37	31.9001	271.77	451.04	214.9	4.777	220.065	5.969	395.548	0.9363
534.07	32.2856	271.09	435.64	212.76	4.348	218.312	5.546	392.396	0.8539
533.77	32.675	269.74	405.58	210.65	3.953	216.572	5.15	389.27	0.778
533.47	33.0683	269.06	390.9	208.55	3.589	214.847	4.779	386.168	0.7081
533.16	33.4656	267.72	362.26	206.48	3.255	213.135	4.431	383.091	0.6437
532.84	33.867	266.39	334.52	204.42	2.949	211.437	4.106	380.038	0.5846
532.52	34.2724	265.06	307.66	202.39	2.668	209.752	3.802	377.01	0.5304
532.2	34.682	263.74	281.65	200.37	2.411	208.08	3.517	374.006	0.4807
531.88	35.0958	262.42	256.46	198.38	2.175	206.422	3.252	371.026	0.4351
531.55	35.5139	261.11	232.06	196.41	1.961	204.778	3.004	368.07	0.3934
531.22	35.9364	259.81	208.42	194.45	1.765	203.146	2.773	365.137	0.3553
530.88	36.3632	258.51	185.53	192.52	1.586	201.527	2.558	362.227	0.3205
530.54	36.7945	257.22	163.36	190.6	1.424	199.922	2.358	359.341	0.2888
530.19	37.2304	255.94	141.89	188.7	1.276	198.329	2.171	356.478	0.2599
529.84	37.6708	254.66	121.09	186.83	1.143	196.748	1.998	353.637	0.2336
529.49	38.1159	253.39	100.94	184.97	1.021	195.181	1.837	350.82	0.2097
529.13	38.5658	252.13	81.428	183.13	0.9117	193.625	1.688	348.024	0.1881
528.77	39.0205	251.5	71.903	181.31	0.8127	192.082	1.549	345.251	0.1684
528.4	39.48	250.25	53.304	179.5	0.7233	190.552	1.42	342.5	0.1506
528.03	39.9445	249.62	44.225	177.72	0.6428	189.034	1.302	339.771	0.1346
527.65	40.4141	249.31	39.74	175.95	0.5704	187.527	1.192	337.064	0.12
527.27	40.8887	248.69	30.877	174.2	0.5054	186.033	1.09	334.378	0.1069
526.88	41.3685	248.38	26.499	172.46	0.447	184.551	0.9959	331.714	0.0952
526.49	41.8536	247.76	17.847	170.75	0.3948	183.08	0.9092	329.07	0.0845
526.09	42.344	247.62	15.987	169.05	0.3482	181.621	0.8294	326.448	0.075
525.69	42.8398			167.37	0.3065	180.174	0.7558	323.847	0.0665
525.28	43.3412			165.7	0.2694	178.739	0.6881	321.267	0.0588
524.87	43.8481			164.05	0.2364	177.314	0.6258	318.707	0.052
524.45	44.3606			162.42	0.2071	175.902	0.5687	316.167	0.0459
524.02	44.879			160.8	0.1811	174.5	0.5162	313.648	0.0404
523.59	45.4031			159.2	0.1581	173.11	0.4681	311.149	0.0355
523.16	45.9332			157.62	0.1377	171.73	0.4241	308.67	0.0312
522.72	46.4694			156.05	0.1198	170.362	0.3838	306.21	0.0274
522.27	47.0116			154.5	0.104	169.004	0.347	303.77	0.024
521.81	47.56			152.96	0.0902	167.658	0.3134	301.35	0.021
521.35	48.1148			151.44	0.078	166.322	0.2828	298.949	0.0183
520.88	48.6759			149.93	0.0674	164.997	0.2549	296.567	0.016
520.41	49.2435			148.44	0.0581	163.682	0.2294	294.204	0.0139
519.93	49.8177			146.96	0.05	162.378	0.2063	291.859	0.0121
519.44	50.3986			145.5	0.0429	161.084	0.1854	289.534	0.0105
518.94	50.9863			144.05	0.0368	159.8	0.1663	287.227	0.0091
518.44	51.5809			142.62	0.0314	158.527	0.1491	284.938	0.0079
517.93	52.1825			141.2	0.0268	157.264	0.1335	282.668	0.0068
517.41	52.7912			139.8	0.0229	156.011	0.1194	280.415	0.0059
516.88	53.4071			138.4	0.0194	154.768	0.1066	278.181	0.005
516.35	54.0303			137.03	0.0165	153.534	0.09515	275.964	0.0043
515.81	54.661			135.66	0.014	152.311	0.0848	273.766	0.0037
515.26	55.2992			134.31	0.0118	151.097	0.07548	271.584	0.0032
514.7	55.9451			132.98	0.0099	149.893	0.06711	269.42	0.0027

514.13	56.5987			131.65	0.0084	148.699	0.0596	267.273	0.0023
513.55	57.2602			130.34	0.007	147.514	0.05286	265.144	0.002
512.97	57.9298			129.05	0.0059	146.339	0.04682	263.031	0.0017
512.37	58.6074			127.76	0.0049	145.173	0.04143	260.935	0.0014
511.77	59.2933			126.49	0.0041	144.016	0.03661	258.856	0.0012
511.15	59.9875			125.23	0.0034	142.869	0.03231	256.793	0.001
510.53	60.6902			123.99	0.0028	141.73	0.02847	254.747	0.0009
509.89	61.4015			122.75	0.0023	140.601	0.02507	252.717	0.0007
509.25	62.1215			121.53	0.0019	139.48	0.02204	250.704	0.0006
508.59	62.8504			120.32	0.0016	138.369	0.01935	248.706	0.0005
507.92	63.5882			119.13	0.0013	137.267	0.01696	246.724	0.0004
507.24	64.3351			117.94	0.0011	136.173	0.01485	244.758	0.0004
506.55	65.0911			116.77	0.0009	135.088	0.01299	242.808	0.0003
505.85	65.8565			115.61	0.0007	134.011	0.01134	240.874	0.0003
505.14	66.6313			114.46	0.0006	132.944	0.00989	238.954	0.0002
504.41	67.4157			113.32	0.0005	131.884	0.00862	237.05	0.0002
503.67	68.2098			112.19	0.0004	130.833	0.00749	235.161	0.0001
502.92	69.0136			111.07	0.0003	129.791	0.00651	233.288	0.0001
502.15	69.8274			109.97	0.0003	128.757	0.00564	231.429	1E-04
501.37	70.6511			108.87	0.0002	127.731	0.00489	229.585	8E-05
500.58	71.485			107.79	0.0002	126.713	0.00423	227.755	7E-05
499.77	72.3291			106.72	0.0001	125.703	0.00365	225.941	5E-05
498.94	73.1835			105.66	0.0001	124.702	0.00315	224.14	4E-05
498.1	74.0483			104.6	8E-05	123.708	0.00271	222.354	4E-05
497.25	74.9237			103.56	6E-05	122.722	0.00233	220.583	3E-05
496.38	75.8097			102.53	5E-05	121.745	0.002	218.825	2E-05
495.49	76.7063			101.51	4E-05	120.774	0.00171	217.081	2E-05
494.58	77.6137			100.5	3E-05	119.812	0.00147	215.352	2E-05
493.66	78.5319			99.502	2E-05	118.857	0.00125	213.636	1E-05
492.72	79.461			98.512	2E-05	117.91	0.00107	211.933	1E-05
491.76	80.401			97.532	2E-05	116.971	0.00091	210.245	8E-06
490.78	81.3519			96.562	1E-05	116.039	0.00077	208.569	7E-06
489.78	82.3138			95.601	9E-06	115.114	0.00066	206.908	5E-06
488.77	83.2867			94.65	7E-06	114.197	0.00056	205.259	4E-06
487.73	84.2706			93.708	5E-06	113.287	0.00047	203.623	3E-06
486.67	85.2653			92.776	4E-06	112.384	0.0004	202.001	3E-06
485.58	86.271			91.852	3E-06	111.489	0.00034	200.391	2E-06
484.48	87.2875			90.938	2E-06	110.601	0.00028	198.795	2E-06
483.35	88.3147			90.034	2E-06	109.719	0.00024	197.211	1E-06
482.2	89.3525			89.138	1E-06	108.845	0.0002	195.639	1E-06
481.02	90.4007			88.251	1E-06	107.978	0.00017	194.08	8E-07
479.82	91.4592			87.373	8E-07	107.117	0.00014	192.534	6E-07
478.59	92.5278			86.503	6E-07	106.264	0.00012	191	5E-07
477.33	93.6062			85.643	4E-07	105.417	9.8E-05	189.478	4E-07
476.05	94.694			84.79	3E-07	104.577	8.1E-05	187.968	3E-07
474.73	95.791			83.947	2E-07	103.744	6.8E-05	186.47	2E-07
473.39	96.8968			83.111	2E-07	102.917	5.6E-05	184.984	2E-07
472.02	98.0108			82.284	1E-07	102.097	4.6E-05	183.511	1E-07
470.61	99.1326			81.466	1E-07	101.284	3.8E-05	182.048	1E-07
469.17	100.262			80.655	7E-08	100.477	3.2E-05	180.598	8E-08

336.88	100.811								
334.1	98.4336								
331.34	96.0452								
328.59	93.6412								
325.82	91.2148								
323	88.7594								
320.12	86.273								
317.15	83.7621								
314.11	81.2487								
311.01	78.7793								
307.94	76.4383								
305.02	74.3654								
304.39	73.9503								
304.3	73.8908								
304.21	73.83								

Table A2.2 Summary of the Phase Behavior Type

Type of phase behaviour predicted by the model for this system	2
Total number of Azeotropic End Points found	0
Pure Azeotropic End Points found	0
Critical Azeotropic End Points found	0
Heterogeneous Azeotropic End Points found	0

Appendix 3

KAPPA 1 OPTIMIZATION

3.1 Kappa 1 Optimization for Carbon dioxide

3.2 Kappa 1 Optimization for Hexamethyldisilazane

3.1 Kappa 1 Optimization for Carbon Dioxide

PROGRAM :KOPT: KAPPA-1 OPTIMIZATION FOR THE PRSV EQUATION
co2

KAPPA-1= .0807

T (K)	PEXP (BAR)	PCAL	AAD	VL (CM3/MOL)	VV
243.1500	14.2860	14.2860	.0001	39.7754	1190.3
253.1500	19.9300	19.7645	.8303	41.9498	849.4
263.1500	26.5400	26.6431	.3885	44.7273	613.1

PERCENT AAD (OVERALL), SUM (ABS (PEXP-PCAL) /PEXP) *100/NP: .406

3.2 Kappa 1 Optimization for Hexamethyldisilazane

PROGRAM :KOPT: KAPPA-1 OPTIMIZATION FOR THE PRSV EQUATION
hmde

KAPPA-1= .0517

T (K)	PEXP (BAR)	PCAL	AAD	VL (CM3/MOL)	VV
293.1500	.0120	.0120	.0026	209.1539	2027813.1
323.1500	.1030	.0613	40.4767	215.4815	435537.4

PERCENT AAD (OVERALL), SUM (ABS (PEXP-PCAL) /PEXP) *100/NP: 20.240

Appendix 4

PENG ROBINSON STRYJEK VERA EQUATION OF STATE RESULTS

4.1 Output for 298.75 K

4.2 Output for 313.45 K

4.3 Output for 327.65 K

4.4 Output for 341.95 K

4.1 298.75 K

PROGRAM: VDW - VAN DER WAALS MODEL(S), 1-PARAMETER
(CONVENTIONAL, 1PDW) OR
2-PARAMETER, 2PDW

K12= .0800 T(K)= 298.75

PHASE VOLUMES ARE IN CC/MOL, PRESSURE IS IN UNITS OF THE DATA.

X-EXP	P-EXP	P-CAL	Y-EXP	Y-CAL	VL-CAL
.2640	16.310	16.283	.99000	.99826	169.25 1382.3
.5320	33.990	34.460	.99000	.99844	128.24 567.0
.6280	40.790	40.971	.99000	.99831	113.88 447.0
.7850	50.730	50.497	.99000	.99799	91.38 321.4
.8810	55.290	55.264	.99000	.99783	79.08 271.0
.9480	59.640	59.144	.99000	.99792	72.42 233.0

AAD-Y= .821

AAD-P= .555

AAD=SUM[ABS(EXP-CAL)/EXP]*100/(NO. OF DATA POINTS)

4.2 313.45 K

PROGRAM: VDW - VAN DER WAALS MODEL(S), 1-PARAMETER
(CONVENTIONAL, 1PDW) OR
2-PARAMETER, 2PDW

K12= .0800 T(K)= 313.45

PHASE VOLUMES ARE IN CC/MOL, PRESSURE IS IN UNITS OF THE DATA.

X-EXP	P-EXP	P-CAL	Y-EXP	Y-CAL	VL-CAL	
.2520	18.350	18.595	.99000	.99649	174.26	1271.0
.4740	36.650	37.070	.99000	.99683	140.41	565.7
.6490	46.170	52.484	.99000	.99610	114.61	350.1
.7680	61.720	62.478	.99000	.99503	98.29	261.5
.8700	71.000	70.069	.99000	.99360	86.80	205.3
.9430	76.920	75.922	.99000	.99182	84.44	162.6

AAD-Y= .503

AAD-P= 3.332

AAD=SUM[ABS(EXP-CAL)/EXP]*100/(NO. OF DATA POINTS)

4.3 327.65 K

PROGRAM: VDW - VAN DER WAALS MODEL(S), 1-PARAMETER
(CONVENTIONAL, 1PDW) OR
2-PARAMETER, 2PDW

K12= .0800 T(K)= 327.65

PHASE VOLUMES ARE IN CC/MOL, PRESSURE IS IN UNITS OF THE DATA.

X-EXP	P-EXP	P-CAL	Y-EXP	Y-CAL	VL-CAL
.1860	15.630	15.630	.99000	.99265	187.79 1622.8
.4380	39.370	39.753	.99000	.99428	149.42 560.7
.5870	52.497	55.600	.99000	.99325	127.48 359.6
.7510	74.670	73.423	.99000	.99001	105.29 229.8
.8610	87.390	84.362	.99000	.98485	94.39 169.0
.9360	96.100	91.061	.99000	.97423	96.75 126.7

AAD-Y= .524

AAD-P= 2.877

AAD=SUM[ABS(EXP-CAL)/EXP]*100/(NO. OF DATA POINTS)

4.4 341.95 K

PROGRAM: VDW - VAN DER WAALS MODEL(S), 1-PARAMETER
(CONVENTIONAL, 1PDW) OR
2-PARAMETER, 2PDW

K12= .0800 T(K)= 341.95

PHASE VOLUMES ARE IN CC/MOL, PRESSURE IS IN UNITS OF THE DATA.

X-EXP	P-EXP	P-CAL	Y-EXP	Y-CAL	VL-CAL	
.1220	11.950	11.426	.99000	.98353	201.38	2373.3
.2930	28.140	28.878	.99000	.99000	175.21	872.0
.5410	58.010	57.974	.99000	.98912	138.39	372.6
.7350	84.540	83.118	.99000	.98268	112.52	214.2
.8450	100.930	96.609	.99000	.97190	102.63	154.8
.9310	111.270	105.620	.99000	.93573	107.66	109.5

AAD-Y= 1.465

AAD-P= 3.018

AAD=SUM[ABS(EXP-CAL)/EXP]*100/(NO. OF DATA POINTS)